Academic Year 2019-2020

Dissertation for Doctoral Degree

Smartphone enabled point of care medical diagnostics by optical tracking of the dynamics of magnetic particles

The University of Electro-Communications, Tokyo

Student ID	**1743005**
Name	**Jaiyam Sharma**
Department	**Department of Engineering Science**
Chief Advisor	**Professor Adarsh Sandhu**

March 2020

Smartphone enabled point of care medical diagnostics by optical tracking of the dynamics of magnetic particles

Doctoral thesis review committee

Professor Adarsh Sandhu (Department of Engineering Science)

Professor Hideo Isshiki (Department of Engineering Science)

Associate Professor Masumi Taki (Department of Engineering Science)

Assistant Professor Eriko Watanabe (Department of Engineering Science)

Professor Tsuyoshi Okuno (Department of Engineering Science)

Dissertation Summary in Japanese

Dissertation Title	磁性粒子のダイナミクスの光学追跡によるスマートフォン対応のポイントオブケア医療診断
Name	Jaiyam Sharma

臨床現場即時診断（Point Of Care Testing: POCT）は持ち運びが容易な機器や検査薬を用いて病気を検査する方法であり、被検者自ら簡単に、その場で、迅速な検査が可能である。そのため、革新的な医療診断手法の開発において大きな期待が寄せられている。スマートフォンは世界中で急速に普及しており、高解像度カメラと通信機能を有するため、POCTシステムへの導入において多くの利点が考えられる。磁性粒子は生体物質に対して最も広く利用される標識の１つであり、電磁気力によって制御が可能であり、スマートフォンによって撮像ができるなどPOCTへの応用において多くの利点が存在する。そこで、本論文では、溶液中の磁性粒子に磁場をかけた際の振る舞いに基づく、スマートフォン型の医療診断技術の開発を行った。初めに診断の感度を制限する非特異的相互作用の理論を紹介し、非特異を排除するために必要な技術を述べる。続いて、スマートフォンで使用されるイメージセンサーと、実際の溶液中の磁性粒子の画像認識の観点からの特性を示す。本研究では、溶液内の磁性粒子の画像認識に必要な要件を導き出し、約400㎚の解像度下、磁性粒子の光学追跡がスマートフォンにおいて可能となった。4つの診断プロトコルが開発し、1つは磁性粒子と画像認識に基づいており、他の3つは磁性粒子の光学追跡に基づいている。最後に、提案された診断プロトコルの実用化に関する問題と、これらの問題に対処するため、今後の研究の方向性について述べる。

Abstract

The United Nations has listed improving healthcare in developing countries as a major area of focus of its sustainable development goals, which, if met, will improve the quality of life of billions of people across the world. As of today, the healthcare systems in developing countries are crippled by the lack of availability of infrastructure in the form of hospitals as well as human resources in the form of doctors. Conventional medical diagnostics technologies, developed in the previous century, are unsuitable for use in resource constrained settings that these countries face. Success stories in the domains of financial services and e-governance, achieved on the back of rapidly proliferating mobile telecommunications technology has inspired the development of next generation 'point of care' medical diagnostics technologies (POCT).

In this thesis, I describe the development of smartphone based medical diagnostics systems based on magnetic particles as labels. While previous approaches in literature have tried to miniaturize conventional technologies to interface with a smartphone, I have adopted a different approach by designing diagnostics systems from the ground up, specifically to work with smartphones under the constraints found in the developing world.

I present an overview of the constraints on healthcare systems in a developing country and the reasons why conventional medical diagnostics technology is unable to meet these constraints. I introduce a new architecture to guide the development of point of care medical diagnostics systems which can successfully meet the requirements of modern medical diagnostics systems. Magnetic particles (MPs) are introduced and the properties of MPs used in this study are discussed. Fluorescent magnetic nanoparticles (f-MNPs) and their advantages over micrometer sized particles are discussed. I then describe the various forces acting on a magnetic particle in a liquid, analyze them quantitatively and explain the theoretical basis of non-specific interactions, which limit the sensitivity of several diagnostics protocols. Building upon this discussion, I propose the design of an actuator comprised of micrometer sized electrodes, which employs three dimensional electromagnetic forces to eliminate non-specific interactions and enhance the probability of specific interactions.

Subsequently, I discuss the details of the experimental setup used in this study. I then explain the need for automating data analysis in point of care diagnostics and introduce algorithms for automated detection and counting of magnetic particles from smartphone images with software. I then introduce an algorithm for optical tracking of MPs with sub-micron resolution in smartphone videos. The problem of optical tracking is introduced and various challenges in tracking a large number of MPs are discussed. I describe my solutions to these problems and the implementation details of the tracking software developed for this study.

I propose two POCT systems based on the methods of actuation and optical tracking discussed above. The first system is based on f-MNPs as labels and utilizes a smartphone camera for their fluorescent imaging. Images obtained from the smartphone are uploaded to a remote server and analyzed automatically, while the results are shared with various stakeholders. The second system is based on micrometer sized MPs and utilizes optical tracking to infer the concentration of biomolecules. Experimental results showing calibration curves and limits of detection of these protocols are presented. The advantages and limitations of each protocol is discussed.

Finally, I discuss directions for future work in this field of research in the near and long term and propose a new parameter for evaluating POCT technologies.

Contents

1. The problem: The ultimate goal of this research

1.1 Introduction

The research presented in this thesis concerns the development of medical diagnostics technologies. I have used the principles of physics, electronics and information science to develop the said technologies. In this chapter, I present the need for medical diagnostic technologies in developing countries. The inability of conventional technology to meet these requirements is discussed. Finally, the specific contributions of this research are summarized. This chapter is a self contained summary of the problem being solved, the limitations of existing technologies, an outline for the solution and my contribution.

1.2 Sustainable development goal #3

The United Nations World Health Organization (WHO) has outlined a set of 17 goals, called sustainable development goals (SDGs) to be achieved by 2030[1] in order to improve the lives of people all across the world. These include goals towards eliminating poverty, hunger and gender inequality while promoting quality education, sanitation and clean energy. The 17 SDGs are shown in figure 1-1.

Figure 1-1. The 17 sustainable development goals (SDGs) [2]

The third goal among these is:

Goal 3: Ensuring healthy lives and promote well-being for all at all ages

There are 13 specific targets to be achieved under this goal. The targets relevant to my research are[3]:

- **Target 3.2:** By 2030, end *preventable* deaths of newborns and children under 5 years of age.
- **Target 3.3:** By 2030, end the epidemics of AIDS, tuberculosis, malaria and neglected tropical diseases and combat hepatitis, water-borne diseases and other communicable diseases.
- **Target 3.8:** Achieve universal health coverage, including financial risk protection, access to quality essential health-care services and access to safe, effective, quality and affordable essential medicines and vaccines for all.
- **Target 3.D:** Strengthen the capacity of all countries, in particular developing countries, for early warning, risk reduction and management of national and global health risks.

It is clear from the above points that a major thrust for improving healthcare across the world is being focused on in developing countries and great emphasis is being given to prevent deaths of newborns and deaths due to 'global health risks' such as epidemics and communicable diseases. Rapid and accurate diagnosis is the first step in providing healthcare to diseased individuals. The research presented in this thesis can help in achieving the above outlined targets (3.2, 3.3, 3.8, 3.D) by enabling rapid, low-cost and accurate medical diagnosis during public health crises. Before explaining how next generation medical diagnostics can help in achieving these targets, I will first describe conventional medical diagnostics technologies and the challenges in achieving these targets in developing countries, taking the example of India.

1.3 Conventional medical diagnostics technologies

Here I discuss some conventional medical diagnostics technologies. The discussion is divided into two parts. First, commercially available technology called ELISA is described. Then, several alternative technologies have been described which have been proposed to replace ELISA.

1.3.1 Enzyme Linked ImmunoSorbent Assay (ELISA)

ELISA is a mature biosensing technology[4] which is commonly used for clinical diagnostics tests as well as in industrial settings for quality control.

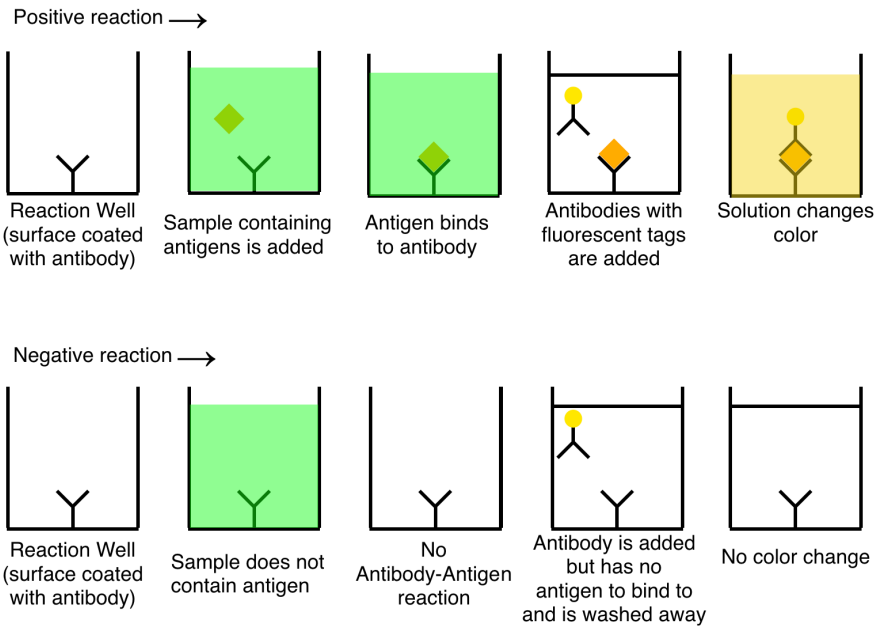

Figure 1-2. Schematic of key steps in ELISA

A schematic of the ELISA protocol is shown in figure 1-2. The setup consists of a reaction well, commonly on a 96-well plate. In the simplest form of ELISA, the surface of the reaction well is functionalized with antibodies and the sample containing antigens is introduced. An incubation time of several hours is required to allow the antibodies and antigens to interact with each other. After the incubation time, another set of antibodies with fluorescent enzymatic biological labels are added to the reaction well and the solution is allowed to incubate. After the second incubation step, the excess antibodies are washed away. Finally, detection is performed by exciting the surface of the reaction well with the appropriate citation wavelength (usually in the ultraviolet region). The fluorescence intensity from the residual captured enzymatic tags is measured by commercial plate readers, which are based on photomultiplier tubes (PMTs). More advanced variations of ELISA, based on magnetic particles and imaging have also been proposed [5].
ELISA machines are bulky, expensive and require a laboratory environment, electricity and a skilled operator to use the machine. Figure 1-3 (a) shows an ELISA plate reader recommended for medical diagnostics by United Nations International Children's Emergency Fund (UNICEF). UNICEF procures this machine at a cost of **8,000 US dollars**[6]. This is prohibitively expensive for use in rural areas of developing countries. For a comparison, the per capita GDP of India is only about **2,000 US dollars**. Although accurate estimates about rural GDP per capita are not available, considering the vast divide between urban and rural areas, the per capita GDP in rural India is likely to be 8-10 times less than the cost of an ELISA machine. This is why, as I will describe in later sections, such conventional technologies are not available in rural parts of India. Figure 1-3(b) shows a 96-well plate being loaded into the reader. A human hand is shown for

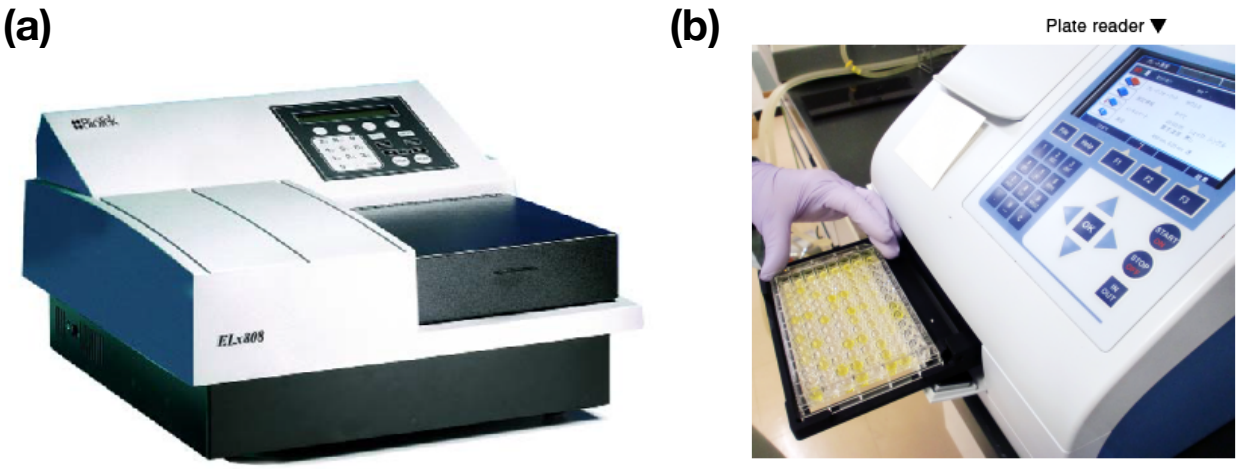

Figure 1-3. (a) A photograph of an ELISA plate reader recommended by UNICEF. This machine costs 8,000 USD[6] (b) A 96-well plate being loaded into a plate reader with human hand for scale.[7]

scale. It can be seen that not only is this device prohibitively expensive for use in rural areas of developing countries, but is bulky and cannot be taken out of the laboratory. Thus, it becomes necessary for poor people to travel to hospitals, which may be located **hundreds of kilometers** away.

The limitations of ELISA have been known for a long time and thus various alternative technologies have been proposed as alternatives. Next, I discuss a few of these newly proposed technologies.

1.3.2 Hall effect sensors for medical diagnostics

Magnetic particles are frequently used as labels for bio-receptors. Thus, several magnetic biosensors have been proposed for medical diagnostics. Our laboratory (Sandhu Laboratory) at Tokyo Institute of Technology proposed Hall effect based sensors for medical diagnostics.

When a conductor carrying an electric current is placed in a magnetic field perpendicular to the direction of the current, a transverse voltage develops in the conductor in a direction perpendicular to both the magnetic field as well as the current. This is due to the effect of Lorentz force experienced by the current carriers in the conductor. Since the Lorentz force is given by $\vec{F} = q(\vec{E} + \vec{v} \times \vec{B})$, where q is the charge of the carrier, $\vec{E}$ is the electric field which causes the current flow, $\vec{v}$ is the velocity of the carrier and $\vec{B}$ is the magnetic field This is known as the Hall effect and was discovered by Edwin Hall in 1879. Hall effect sensors are commonly used in auto motives, motors and smartphones.

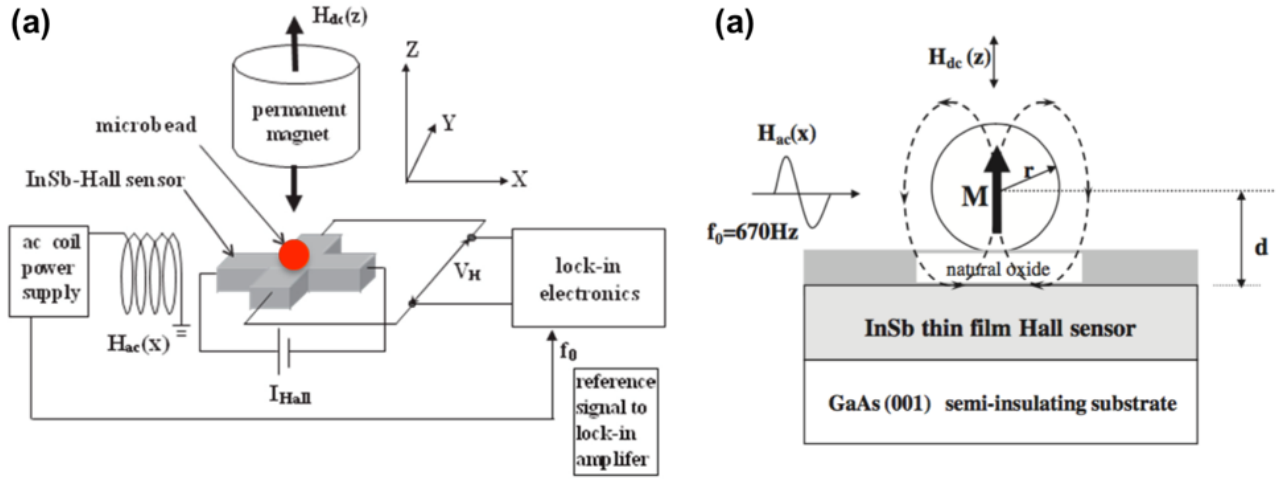

Figure 1-4. Schematic of magnetic particle detection by Hall sensors. (a) A permanent magnet is placed above the Hall element in z direction and an AC field $H_{ac}(x)$ is applied along x direction. A lock-in amplifier is used to measure the transverse voltage signal with the same phase as that of the applied field. (b) Schematic of the transduction mechanism. The vertical field induces a dipole moment in the bead in z direction. On application of the horizontal field, the magnetic moment vector oscillates about its mean position, thereby inducing a transverse voltage signal in the hall element. Source: [8]

Our laboratory[8] developed Indium-antimonide (InSb) micro-Hall sensors for the detection of magnetic micro and nanoparticles. As shown in figure 1-4, an alternating magnetic field was applied horizontally and a DC magnetic field was applied vertically (in z-direction). The Hall sensor achieved very high sensitivity and detection of a single 2.8 µm magnetic particle was possible with the proposed sensor. Although Hall sensors provide reliable detection of micro particles, they are unable to detect nanometer sized particles. This is due to the *intrinsic limitations* of the sensitivity of the Hall effect. Thus, more sensitive magnetic biosensors based on other magnetic phenomena have been proposed.

1.3.3 Giant magnetoresistance (GMR) based medical diagnostics

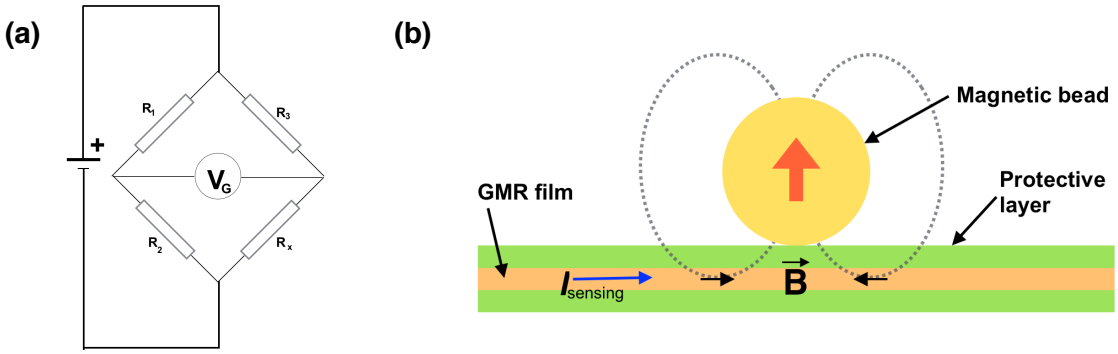

Figure 1-5. Principle of GMR biosensors (a) Wheatstone bridge configuration used by GMR sensors to cancel out noise and thermal drift effects. (b) Schematic of magnetic field induced in the sensor in proximity to a magnetic particle. This field decays rapidly as the distance from the sensor surface to particle increases.

The Magnetoresistive (MR) effect, discovered by W. Thompson in 1857, relates to the change in electrical resistance of a material in the presence of an external magnetic field. Albert Fert ad Peter Grunberg[9] discovered that in thin films of alternating ferromagnetic and non-magnetic layers, the electrical resistance changes significantly on application of magnetic field. This is called the giant magnetoresistance effect for which Fert and Grunberg were awarded the Nobel prize in physics in 2007. The GMR effect is more sensitive than the Hall effect in that smaller magnetic fields can be measured. Thus, nanometer sized particles which have significantly smaller magnetic field than micrometer sized particles are ideal candidates for detection via GMR sensors. Figure 1-5 shows a schematic of the principle of transduction in GMR biosensors. As shown in figure 1-5 (b), the magnetic field of the nanoparticle induces a field in the so-called 'sensing layer' of the GMR sensor. The induced magnetic field effects a change in the resistance of the sensing layer. A sensing current is applied across the sensing layer and the voltage is measured, which is the electrical signal of interest. It is noteworthy that GMR sensors in general suffer from various sources of noise such as thermal drift as well as some intrinsic noise such as pink noise. Thus, they are always used in a wheatstone bridge configuration as shown in figure 1-5 (a). As a result, the number of GMR sensors required for a single detection is at least four. In a multiplexed setup, the cost and complexity of fabrication of GMR sensors increases rapidly as four sensors are required for every detection.

GMR sensors have excellent sensitivity but have the following limitations:

- The cost of fabricating GMR sensor is quite high.
- GMR sensors suffer from large noise such as Johnson noise[10]
- These sensors can detect only magnetic signals. Thus, non-magnetic contaminants present in the sensing area cannot be detected.

Although GMR sensors for medical diagnostics have been proposed since 1998 [11], industrial efforts to bring them to the market has been very limited. In 2012, Nokia hosted the so called 'Nokia Sensing XChallenge'[12], a $2.25 million competition in which leading scientists from all around the world proposed next generation medical diagnostics

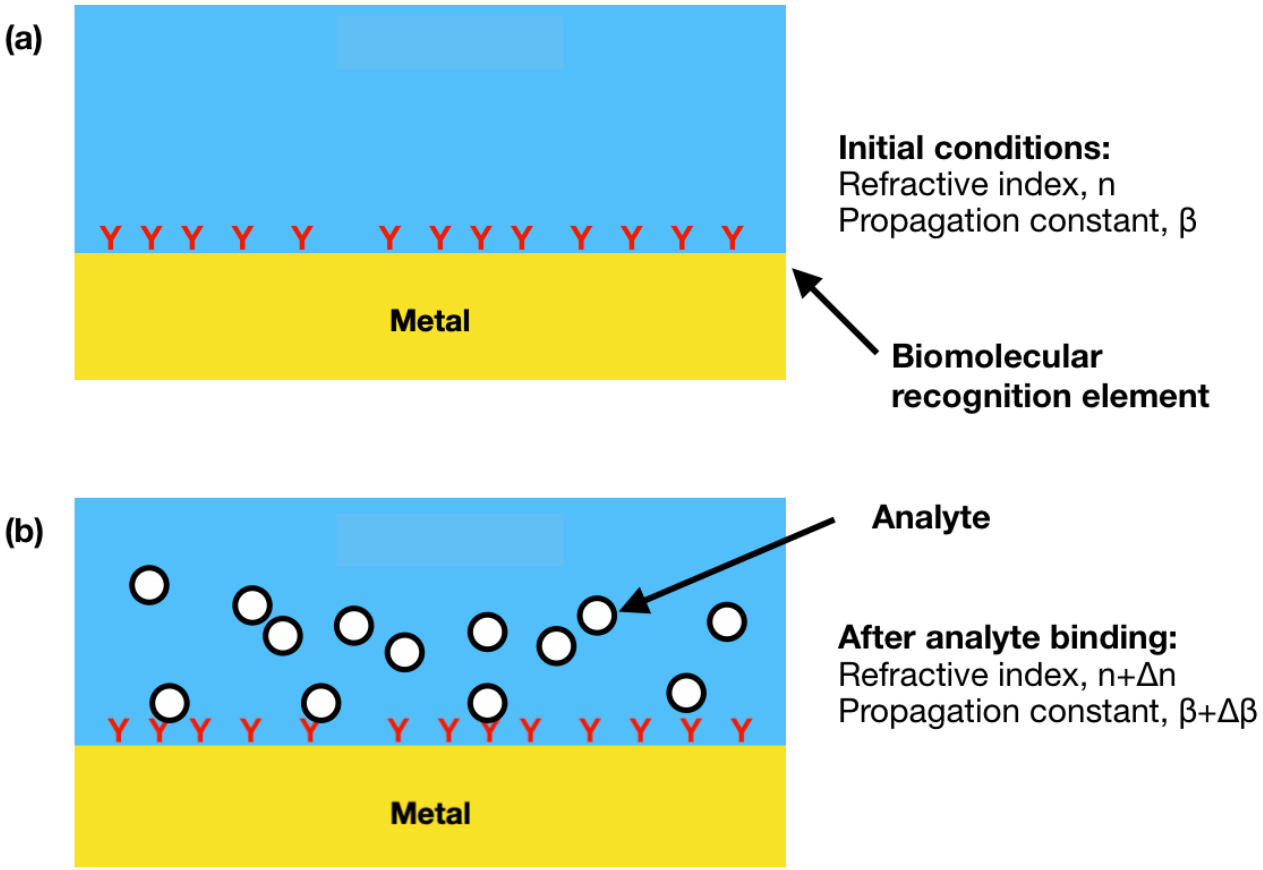

Figure 1-6. Principle of SPR biosensor. (a) Initially, the dielectric surface has a refractive index n and is functionalized with antibodies. (b) After the analyte is bound to the antibodies, the refractive index and hence the propagation instant of the SPW changes. This can be picked up via prism coupling, waveguide coupling or grating coupling.

Figure 1-7. A photograph of 'SPR-PLUS' platform for medial diagnostics from Xantec Bioanalytics [16]

technologies and produced prototypes for their ideas. A GMR based biosensor[13] was awarded one of the five 'Distinguished awards' of the competition. This is the closest that GMR sensors have come to adoption by the industry. Since the end of this competition, while more papers have been published using this device for research purposes[14], there is no indication that GMR sensors are being adopted by industry for clinical diagnostics.

1.3.4 Surface plasmon resonance

Surface plasmon resonance (SPR) biosensors exploit the electromagnetic phenomenon of surface plasmon polaritons to detect small variations in the properties of the sensing surface. A surface plasmon wave (SPW) is a transverse magnetic (TM) electromagnetic wave propagating along the boundary between a dielectric and a metal. Since the wave is TM, the magnetic vector is parallel to the interface whereas the electric vector is perpendicular to it. The propagation constant of a surface plasmon wave can be expressed as[15]:

$$\beta = \frac{\omega}{c}\sqrt{\frac{\epsilon_M \epsilon_D}{\epsilon_M + \epsilon_D}} \qquad (1.1)$$

where ω is the angular frequency, c is the speed of light, ϵ_M, ϵ_D are dielectric constants of the metal and dielectric respectively. Gold and glass are the most common metal and dielectric used for SPR biosensors.

Figure 1-6 shows the principle of SPR based transduction. In figure 1-6(a), initially the metal surface is functionalized with antibodies and the dielectric has an initial refractive index n and a propagation constant β. The analyte solution containing complimentary antigens are introduced into the solution and allowed to interact with the surface. The interaction of antibodies and antigens shifts the refractive index of the dielectric surface. Since the majority of the SPW intensity is concentrated within the dielectric, a change in its refractive index causes a large change in the propagation constant of the SPW. It can be shown that the change in propagation constant is proportional to the change in refractive index of the dielectric. Thus, the concentration of analyte in the solution has been transducer into an electrically measurable signal. The detection in SPR based biosensors is usually carried out via prism coupling, waveguide coupling or grating coupling.

In contrast to most of the methods discussed in this section, SPR biosensors have the advantage that they are label-free i.e. they do not use labels for detection of bio-receptors. However, SPR based diagnostic technology has inherent disadvantages as SPR sensors are bulky and expensive due to the requirement of a precise reference light source, liquid pumps to pump liquids with controlled velocity and personal computer to analyze the results. Thus, SPR based diagnosis devices are currently available for use in laboratories by trained professionals, but not for use in rural areas with no laboratories or access to electricity and running water. Figure 1-7 shows the photograph of a commercially available SPR sensing platform from Xantec Bioanalytics. This system requires electricity from a wall supply, is bulky and can only be operated by trained professionals.

1.3.5 Superconducting Quantum Interference Device (SQUID)

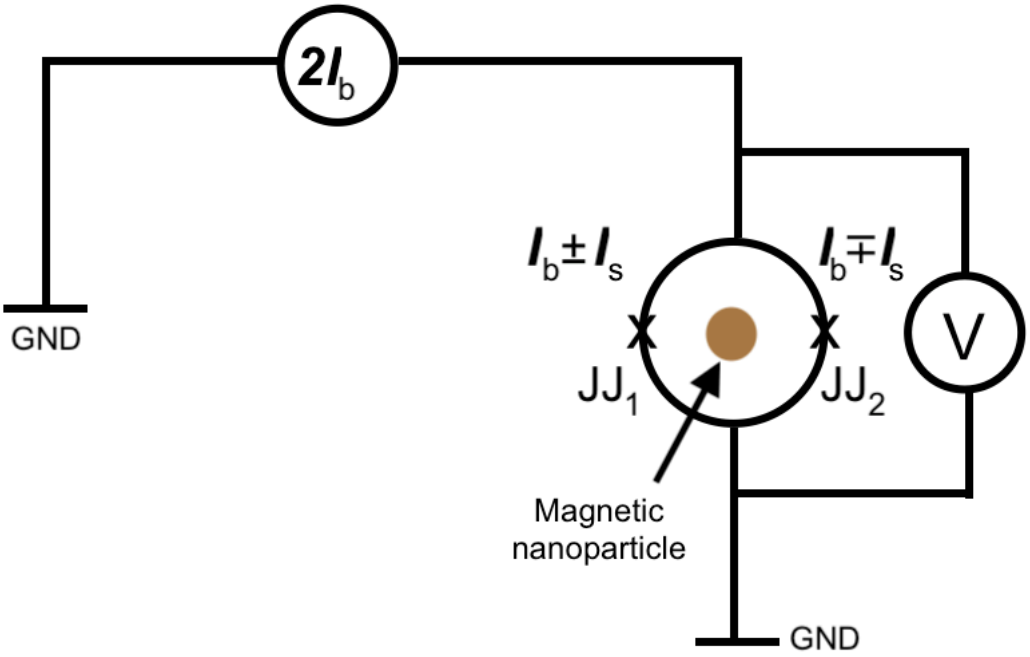

Figure 1-8. Schematic of a SQUID biosensor.

SQUID is one of the most sensitive magnetometers available today. The principle of operation of SQUID is based on superconducting loops containing Josephson junctions. The Josephson effect is a phenomenon by which Cooper pairs in superconducting materials can tunnel across a superconductor-insulator-superconductor interface. Figure 1-8 shows the schematic of the simplest variant of a SQIUD biosensor. The biosensor consists of a current source which produces a constant bias current of $2I_b$. The sensor has two Josephson junctions denoted by x's in the figure, across a superconducting coil. When no external magnetic field is present, the current is divided equally among the two halves of the SQUID sensor. However, when an external magnetic field is present due to a magnetic nanoparticle label, the currents in the two arms are not equal and a shielding current I_s is developed which tries to reduce or increase the magnetic flux passing through the coil so as to make it equal to an integer multiple of the magnetic flux quantum $\phi_0 (= h/2e)$, where h is the Planck's constant and e is the charge of a proton. The screening current induces a voltage across the input and output terminals of the superconducting loop which can be measured to infer the magnetic field. SQUID biosensors have been applied for extremely sensitive detections of magnetic nanoparticles[18]. While SQUID sensors are extremely sensitive to magnetic fields, they are constrained by the high cost, large size of the equipment as well as the requirement of cryogenic conditions and skilled personnel for operation of the equipment. Figure 1-9 shows a photograph of a SQUID system. Although SQUID is not a leading contender for medical diagnostics technology to be used in developing countries, I am mentioning it in this section to further underscore the fact that **conventional medical diagnostics technology is expensive, bulky and unsuitable for use in developing countries**.

Now that I have provided several examples of conventional medical diagnostics technologies in use and under development, I will next describe the state of healthcare in

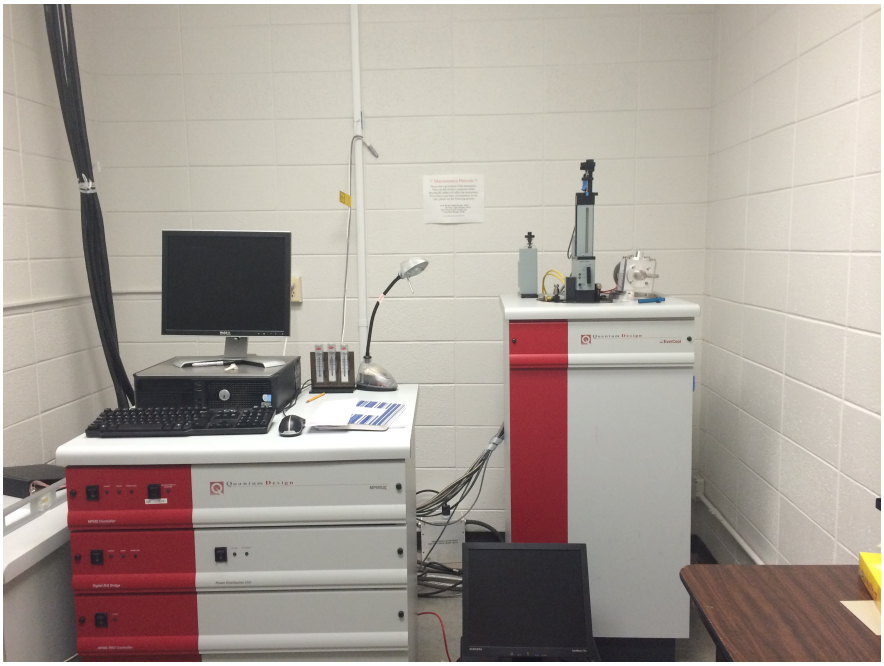

Figure 1-9 A photograph of a SQUID magnetometer system [17]

developing countries. Since any medical diagnostics technology has to be able to work under these real world conditions, this analysis will help the reader to understand the challenges that need to be overcome to achieve the vision of 'healthcare for all' described in SDG #3 by the UN. To keep this discussion realistic and fact based, I have chosen to describe the state of healthcare in my home country, India as I am quite familiar with the rural healthcare system in my country. India is the fifth largest economy in the world with a population of 1.27 billion people. The trends and lessons learnt from the example of India are applicable in many other developing countries across the world.

1.4 Healthcare in India

On one hand, the majority of growth in the world's population is taking place in the developing countries; and on the other the developed countries face the challenge of an ageing population. Thus, there is an acute need for making healthcare accessible to all in both: the developing and the developed countries. While the social and economic status of the people are very different across these two types of countries, there are remarkable similarities in the problems faced by the healthcare system. In this section, I will present the current status of healthcare system in India where I am from. In particular, I will focus on the challenges in achieving the targets outlined in SDG #3. Although, I am focusing on the example of India, yet the characteristics of the healthcare system presented are similar across the rest of the developing world.

1.4.1 Availability of hospitals

In public healthcare, the availability of medical facilities is measured by the number of hospital beds available, rather than the number of hospitals. The number of hospital beds available in public hospitals in India is approximately 740,000 as per the Ministry of Health and Family Welfare [19]. Accounting for the population of India this is just 0.56 beds per 1,000 people. The world average is 2.75 beds per 1,000 people while developed countries have multiple times the average (for example, Japan has 9 beds per 1,000

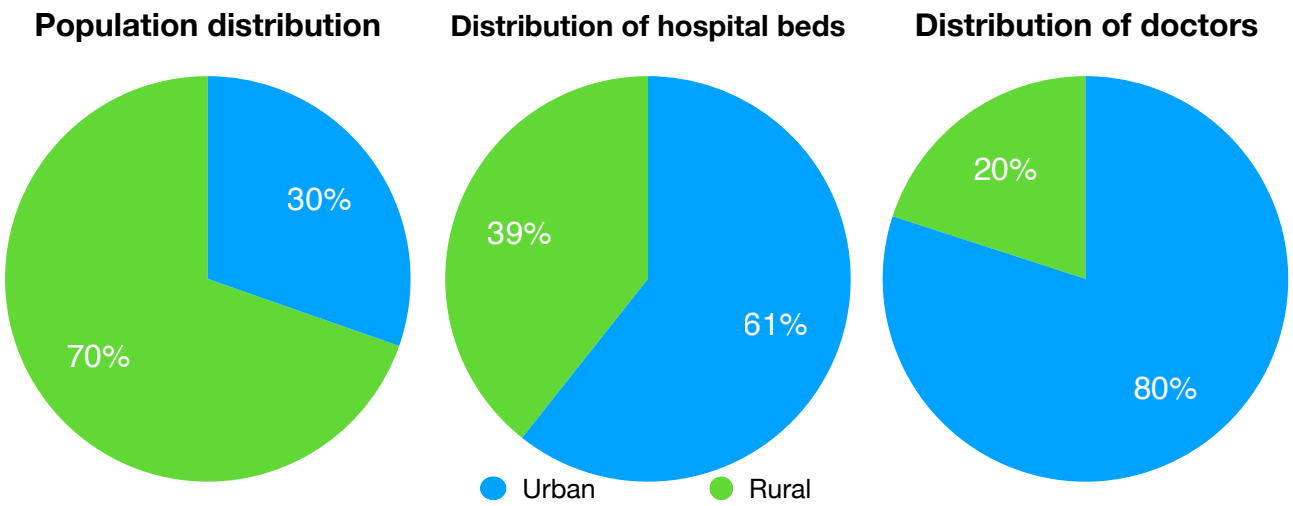

Figure 1-10. Urban rural divide in India. The 70% rural population is served by just 39% of hospital beds and 20% of doctors available in the country[19, 21].

people[20]). Not only is there a divide between developing and developed countries, even within a developing country such as India, there is a large divide between rural and urban healthcare systems. For example, among the 740,000 hospital beds available across the country, approximately two-thirds of them are in urban areas and only one third in rural areas[19]. This is in stark contrast to the demography of the country which is about two-thirds rural and one-third urban, as shown in figure 1-10. Thus, **rural people get access to roughly 4 times fewer hospital beds per person than urban people**. This presents a major challenge for public healthcare in India as a majority of the rural population has to travel to the closest available urban center in order to access even the most basic healthcare. This leads to the following problems:

- When infants get infected, they often go undiagnosed and untreated. This is because parents are unable to travel long distances to hospitals to get them diagnosed every time infants show symptoms of being unwell. For many of the poorest people who are inevitably employed in the informal economy (of course, without medical benefits), the long travel to hospitals requires at least a day's leave from work, which means loss of wages. Thus, the choice between lost wages and potential risks to a child's health is a tough one to make for many parents.
- Epidemics are not detected in time to contain their spread. If a large number of people get infected, only a few of them go to hospitals to get themselves diagnosed. Thus, public health officials who are themselves located far away from the centers of outbreak get incomplete, indirect and delayed information about the outbreak of epidemics and communicable diseases.

1.4.2 Availability of doctors

WHO recommends a minimum of 1 doctor for every 1000 people for a country in order to provide effective public healthcare. Due to the limited availability of quality education, the availability of doctors has been historically severely limited in India. In the last few years, improved availability of medical education has improved the number of qualified doctors available in the country. If alternate forms of medicine are excluded, the number of doctors in India is currently just about 1 million and the doctor to population ratio is about 0.77:1000, well below WHO recommendations. This ratio is not expected to reach the minimum recommended 1:1000 until 2024 [22]. Moreover, the urban-rural divide in

infrastructure discussed above is even more stark in the availability of personnel and staff. A majority of doctors (80%) of India live in urban areas[21], as shown in figure 1-10. Thus, only about 200,000 doctors serve about 900 million rural population of India i.e. only 0.22 doctors for every 1000 people. In fact, **rural people get access to roughly 9 times fewer doctors per person than urban people.** In developing countries such as India, educated people aspire to live in big cities since urban areas offer a better standard of living, also living in a big city is associated with upward social mobility. This leaves the rural population severely underserved. The few doctors who do live in rural areas, where they are in high demand, find it far more lucrative to operate private clinics. These private clinics often prioritize monetary profit over quality healthcare. Thus, healthcare from such clinics is not affordable.

The above discussion paints a very grim picture of healthcare in rural India. In order to combat the lack of trained medical professionals, people in India have depended on two alternatives. The first alternative is a vast public healthcare system staffed by uneducated and semi-literate public healthcare workers and the second alternative is traditional systems of medicine called *Ayurveda*, *Unani* and *Siddha*. A discussion on the traditional Indian medicine is beyond the scope of this thesis, but I explain the role of semi-literate public healthcare workers in rural India.

1.4.3 Health care (Anganwadi) centers

In 1970s, the condition of healthcare in India was even more grim than that presented above. Infant mortality, maternal deaths due to child delivery and malnutrition were very high. Against this backdrop, the Government of India decided to start public healthcare centers where rural women would provide basic public health services, primarily aimed at providing care to pregnant women, infants, vaccination to young children and pre-school education. These centers are known as *Anganwadi* centers (AWCs; the word anganwadi means a courtyard shelter in Indian languages). Each AWC is operated by three healthcare workers[23] who are all from the same neighborhood which they are serving. Thus, AWC workers have very close contacts with the people they serve and they understand the individual needs of their patients much better than a doctor does. Figure 1-11 (a) shows a photograph of an AWC near my home in Sikar district of Rajasthan state in India. Figure 1-11 (b) shows the six services provided by the AWC. These are:

1. Nutritious food to pre-school kids.

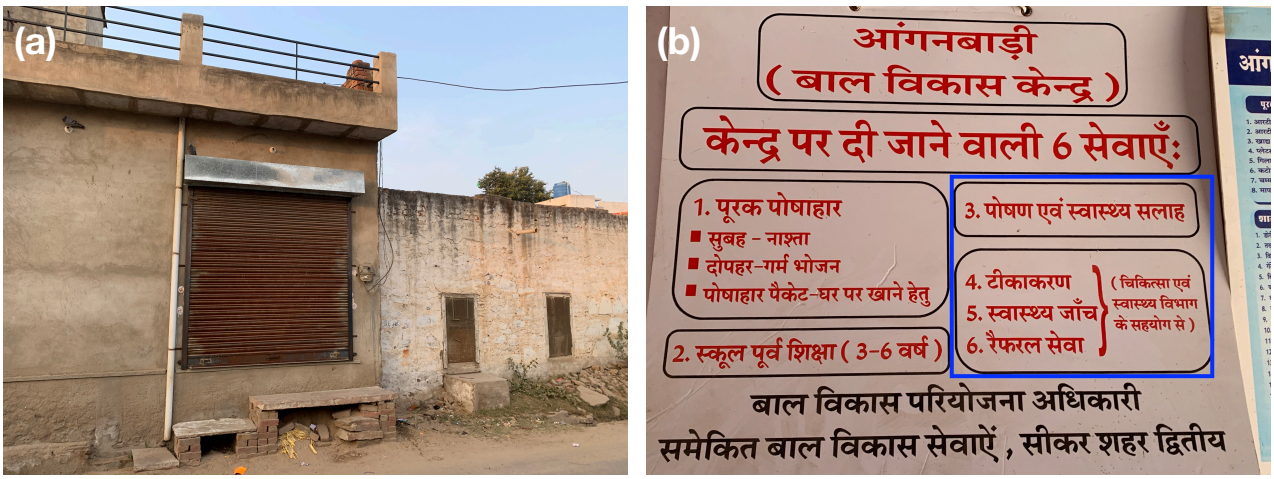

Figure 1-11 (a) Photograph of an AWC near my home in Sikar, Rajasthan, India. **(b)** A board outlining the six services offered at the AWC. Blue box indicates services 3 to 6 relevant to my research, which are related to healthcare.

2. Pre-school education
3. Nutrition and healthcare counseling
4. Vaccination
5. Health checkups
6. Referral to hospitals if the patient cannot be treated by the AWC.

There are 1.3 million such AWCs in operation in India today which are operated by approximately 4 million healthcare workers. Although AWC workers are themselves poor and often illiterate, they have played a large part in reducing maternal and infant mortality as well as successfully eliminating highly contagious diseases such as polio from India[24]. Thus, while most AWC workers lack the skills and knowledge of doctors and trained medical staff, they have proved themselves to be invaluable for providing targeted medical care for those most in need of it. It is also important to note that all of these 4 million AWC workers are already located in rural areas. Thus, **the number of AWC workers in rural India is 20 times that of doctors!** (4 million AWC workers v/s 0.2 million doctors) This research aims to empower these AWC workers to function as medical diagnosticians and provide healthcare in locations where hospitals are limited and doctors do not want to work.

1.5 Leapfrogging in telecommunications

In economics, the term leapfrogging refers to a fundamental shift in technology which enables progress that could not have been achieved with incremental improvements to conventional technology[25-27]. For example, in developing countries such as India landline telephones were accessible only to a small fraction of the population (primarily urban) as they were expensive to install. As a consequence, services like broadband internet were also accessible to a small fraction of the population. The fraction of Indian population with access to landline phones peaked at 4.4% in India in 2005 and have been falling ever since[28]. Several government policies during the 1980s and 1990s were focused on reducing the cost of landline telephones and making them available in rural areas. However, concerns about making landline phones available to rural areas became redundant with the advent of mobile telecommunications. With wireless communication technology, a single cell tower could serve up to tens of thousands of customers located in densely populated areas. Thus, economies of scale were leveraged by industry to make mobile communications much cheaper than landline communications had ever been. Mobile phones, especially smartphones equipped with camera, Wi-Fi and third and fourth generation (3G/4G) communication, allowed rural population of India to *leapfrog* from having no communication capabilities to having the latest mobile phone communications technology while skipping landline phone technology altogether. According to the latest data, the number of mobile connections in India is about 1.16 billion[29] which is a **penetration rate of 91%** (over 20 times the maximum fixed telephone penetration ever achieved). This has resulted in opening up a large market for telecommunication industry. The resulting economies of scale and market competition have transformed the landscape of communication in favor of end users and as a result, Indian customers enjoy the cheapest mobile data rates in the world at $0.26 (26 yen) per gigabyte, as shown in figure 1-12.

This revolution in telecommunications technology has further enabled leapfrogging in other areas like *financial services* (such as peer to peer money transactions without the use of banks, micro-credit loans to small businesses without a collateral), *e-commerce* (such as enabling rural artists to sell their art internationally and enabling people in rural areas to buy products from anywhere in the world) and *governance* (such as elimination of corruption in delivery of public services by making services available online in an entirely automated fashion, eliminating the need for interaction with government officials).

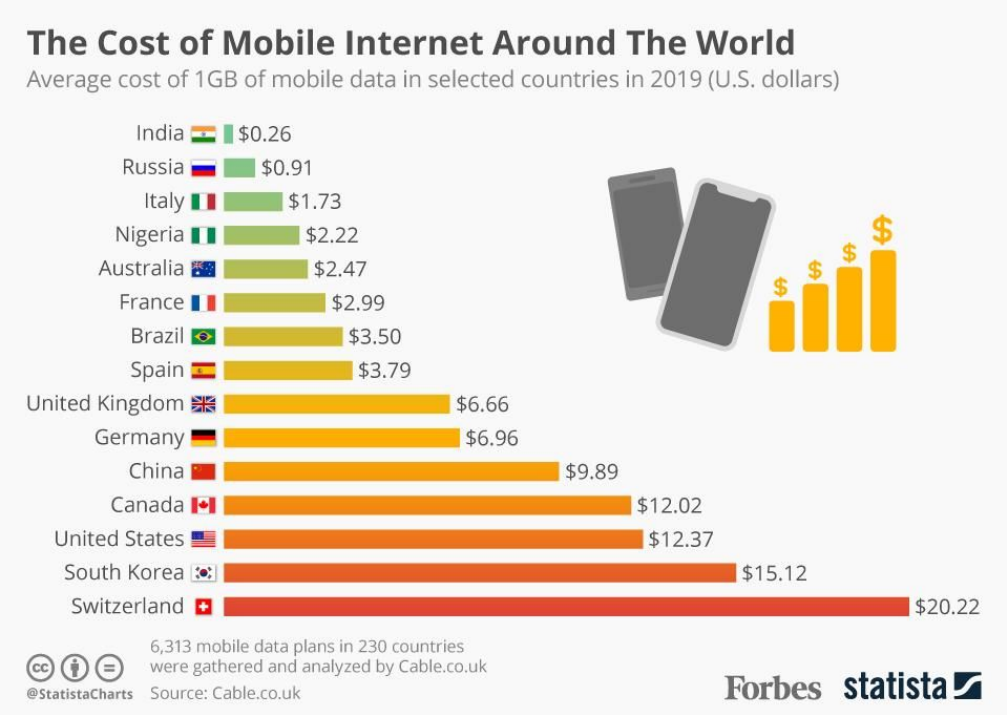

Figure 1-12. The cost of mobile data across the world. Source: cable.co.uk

The crux of my research is that smartphones can enable leapfrogging in medical diagnostics and serve orders of magnitude more people in developing countries than conventional medical diagnostics technologies. Experience in telecommunications, commerce, finance and governance in India shows that large strides in progress are achieved by fundamental shifts occurring due to new technology rather than incremental improvements in conventional technologies. It is expected that this trend will be replicated in the field of medical diagnostics. **Rapid improvements in medical diagnostics will be achieved by technologies which are designed from the ground up specifically for use with smartphones, rather than by miniaturizing conventional technologies like ELISA, GMR or SPR to interface with a smartphone.**

To this end, I will present two medical diagnostics systems based on smartphones in this thesis which are designed with this philosophy, take advantage of internet communication and can be used by anyone with minimal training. Thus, AWC workers can be trained to use the medical diagnostics systems which I will describe. The large number of public healthcare workers along with ready availability of smartphones can help India and other such developing countries to serve large parts of underserved populations. Although I have focused on India, similar public health institutions exist in several developing countries as does mobile phone connectivity. Thus, **this research can have a great impact in achieving the targets (3.2, 3.3, 3.8 and 3.D) outlined under SDG #3 on a global scale.**

1.6 An outline of the solution

The challenges faced by patients of conventional medical diagnostics systems are summarized in figure 1-13. The specific problems which impact the lives of millions of people are:

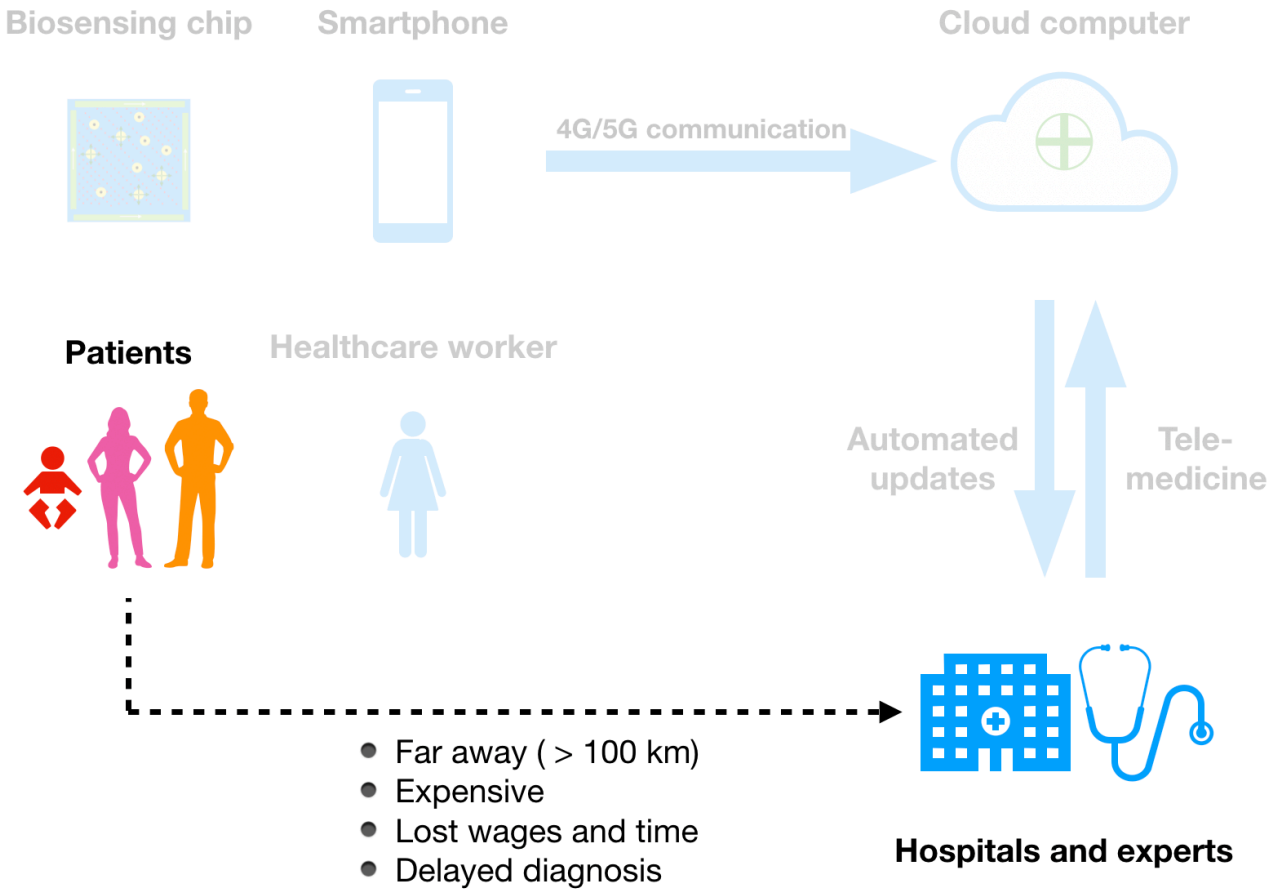

Figure 1-13 Challenges faced by patients under conventional healthcare system in developing countries.

- Hospitals are often located hundreds of kilometers away. Thus, a hospital visit requires one to travel long distances.
- Hospital visits are expensive for the poorest section of the population
- People in rural areas are employed informally and there are no provisions for healthcare or paid leaves. Thus, spending time away from work leads to loss of wages.
- Conventional medical diagnostics technologies require a long time (several days) to test the sample and deliver the results. Thus, there is a long delay in the diagnosis due to the time required to travel as well as to deliver the test results.

A mobile phone enabled medical diagnostics system contains the following essential components:

- A diagnostics chip where biomolecular reaction occurs.
- A smartphone equipped with a camera which can record photographs and videos.
- A cloud computer which can analyze results of a test and send the results to the patient as well as to public health officials.
- A public health worker who can perform the test as well as remotely located doctors who can act on the information provided by test results and make recommendations to the patient remotely.

A schematic of such a system is shown in figure 1-14. The benefits of this system for the patient are:

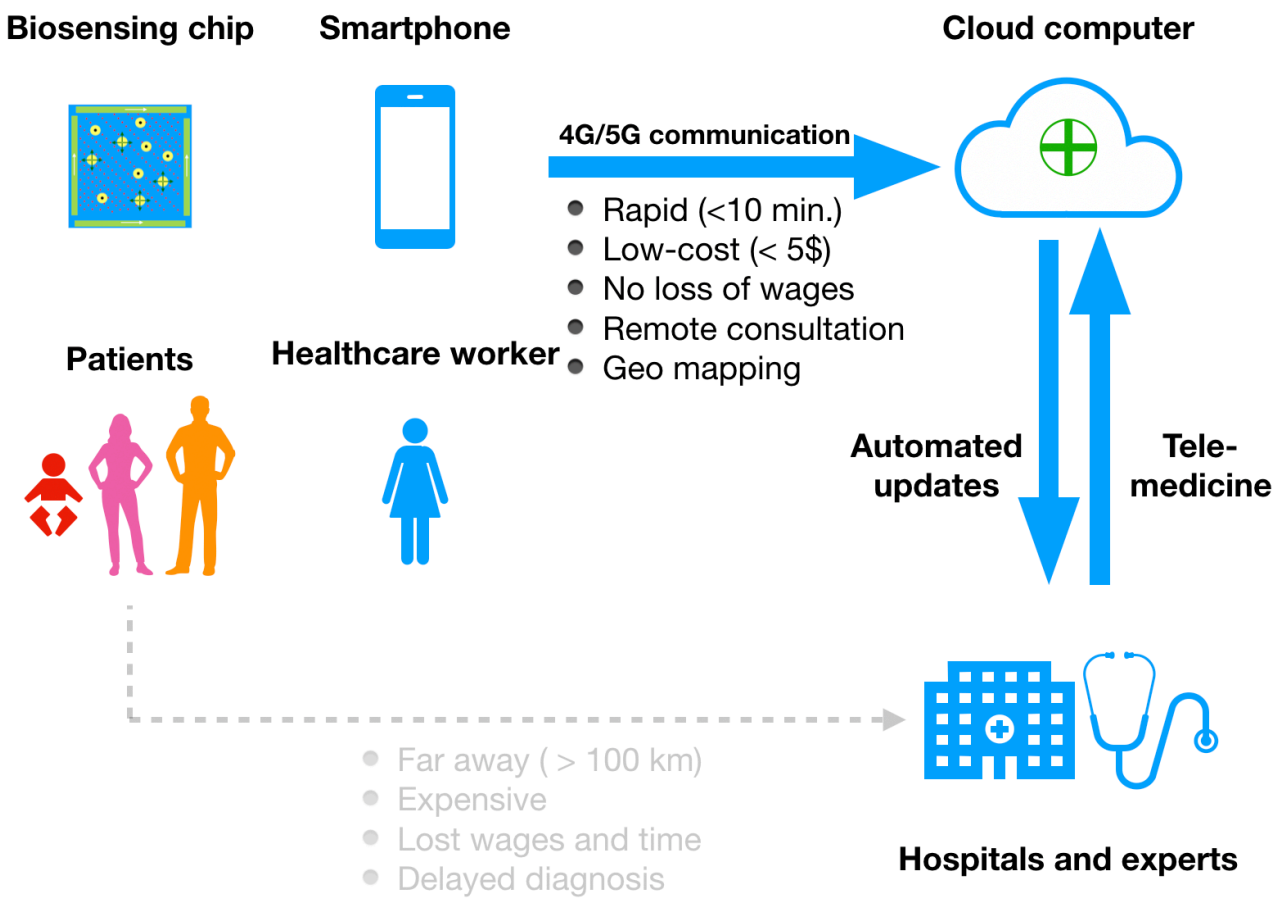

Figure 1-14. A schematic of a smartphone based medical diagnostics system comprising a diagnostics chip, internet connected smartphone, a public health worker, a cloud computing based data analysis system as well as remotely located doctors.

- Tests can be done without traveling to the hospital. Moreover, smartphone based diagnostics methods do not require a long time to perform he test. Thus, results are available in a few minutes, rather than days.
- Smartphone based tests can be administered at a lower cost than conventional tests. Since there is no need for the patient to travel, there are additional savings in cost.
- Public health workers such as AWC workers are located in every neighborhood, close to the patients. A visit to the AWC does not require one to take time off from work. Thus, there is no loss of wages to the poorest section of the people.
- Since the results of the tests are shared with doctors and health administrators, they can provide medical advice remotely.
- When public health authorities have access to the medical status of people in near real-time, public health risks such as an outbreak of epidemics and contagious diseases can be identified very quickly and action can be taken in time to prevent their spread and save lives.

The most important diseases which should be detectable by such a diagnostics system are common airborne, waterborne diseases as well as diseases caused by insects breeding in unsanitary environments. For example, in the case of India, the five most common diseases causing child mortality are[30, 31]:

- Pneumonia
- Diarrhea
- Cholera

- Malaria, and
- Typhoid

The most common diagnostics technology used to detect these diseases is ELISA[32, 33] and low-cost diagnostics tests are usually not available. In the absence of access to such diagnostics technology, sometimes inaccurate tests are used in developing countries which can lead to misdiagnosis and thus potentially cause harm to healthy individuals, For example, for typhoid, several low-cost tests such as typhidot, Widal and TUBEX tests have been in use in developing countries. However, these tests have been shown to have very low sensitivity and specificity for typhoid detection[34, 35]. The availability of low-cost and highly sensitive diagnostic tests would prevent premature deaths of children below the age of five, who remain the worst affected demographic due to these diseases.

Another scenario in which rapid diagnostics would be critical for public health is epidemics. As the world is getting more and more connected, epidemics originating in one part of the world spread extremely quickly to other parts. For the purposes of this discussion, I would like to classify epidemics into two categories: novel and recurring epidemics. A case of a novel epidemic is in the news recently. A new strain of virus, named as 2019 Novel Coronavirus (209-nCOV) has been the cause of a very recent epidemic originating in the city of Wuhan in China[36]. As of the time of writing, more than 800 people have been found to be infected with this disease in China alone, and the infection has already spread to U.S., Japan, Taiwan, Thailand, Singapore and Saudi Arabia[37]. Currently, diagnosis of this disease is being performed by isolating the virus from a blood sample, sequencing its DNA and comparing the sequence with that of 2019-nCOV provided by the Chinese public healthcare authorities.

If such a disease were to originate in a small remote village, rather than a big city, smartphone based medical diagnostics test *would not be able to diagnose it* since there is very little information about such an infection in the scientific community. Antibodies or biomarkers for such new diseases have to first be discovered and only then they can be used for conventional or smartphone based medical diagnosis.

The other type of epidemic is a recurring epidemic. A pertinent example of this kind of disease is the Ebola virus disease (EVD), which killed more than 11,000 people in Africa between 2013 and 2016[38]. Contrary of 2019-nCOV, EVD is a very old disease which has been known to the scientific community since the first outbreak of EVD in Democratic Republic of Congo in 1976[39]. Yet, about 40 years after this epidemic became known, the public healthcare systems in the north African countries were unable to prevent its spread when a new outbreak occurred in 2014, primarily because infected individuals were not diagnosed on time and continued to live and interact with healthy individuals, thereby spreading the disease. Since a vaccine or medicine for EVD is not known[40], the best course of action from a public health perspective is rapid diagnosis and isolation of infected patients. Smartphone based rapid, low-cost diagnostics tests can prevent the spread of epidemics by diagnosing infected individuals quickly and alerting public health officials about the outbreak through cloud computing based notification system.

1.7 Objectives of this research

I have discussed the key features of a smartphone based medical diagnostics system in very general terms until now. In closing this chapter, I mention the specific technical objectives and contributions of this research. Some technical terms used below will be introduced in later chapters. The specific objectives of my research were:

- **Development of smartphone based point of care medical diagnostics protocols**

Conventional medical diagnostics technologies require bulky equipment, skilled professionals and long time to provide results. My aim is to develop portable, rapid, low-cost and highly sensitive medical diagnostics protocols for quantitative detection of biomolecules. Diagnostics technologies with these features are called point of care testing (POCT) technologies. I aim to use smartphones as a platform to develop POCT technologies i.e. the protocol should take advantage of smartphone features such as camera, communication and processing to enable rapid diagnostics.

- **Development of fluorescent magnetic nanoparticle based POCT system for quantitative detection of biomolecules**

Fluorescent magnetic nanoparticles have several advantages as biomolecular labels. My aim is to develop a smartphone based POCT system which uses fluorescent magnetic nanoparticles as labels to enable highly sensitive quantitative detection of biomolecules.

- **Development of diagnostics protocols based on optical tracking of the dynamics of magnetic particles**

Studying the dynamics of magnetic particles on a surface can reveal information about the biomolecular interaction of the surface with the particles. This potential has not been effectively used in previous literature. I aim to develop a diagnostics protocol based on optical tracking of the dynamics of magnetic particles which can achieve rapid and highly sensitive quantitative detection of biomolecules with a smartphone.

1.8 Contributions of this research

Finally, I describe the contributions of my research. This makes this chapter a self contained introduction to the thesis, so that a reader can assess the problem being solved, an outline of the solution and originality of my research from this chapter alone.

In this work, I report the development of smartphone based point of care medical diagnostics systems utilizing magnetic particles as labels. My work takes advantage of the tremendous improvements in smartphone cameras over the past few years, driven by trends in consumer photography, which have made modern smartphones capable of detecting micrometer and nanometer sized particles via light microscopy and fluorescence microscopy respectively. I have built upon these capabilities of smartphones and developed methods for actuation of magnetic particles over a large area as well as for their detection and tracking with sub-micron resolution. I propose two types of POCT diagnostics systems:

1.8.1 Fluorescent magnetic particles based POCT system

Fluorescent magnetic nanoparticles (f-MNPs) are promising labels for biosensors due to their high surface area to volume ratio, magnetic and fluorescence properties. The POCT system based on f-MNPs as labels consists of three key components:

- A protocol for detection of prostate specific antigen (PSA) by fluorescent imaging of f-MNPs.
- A digital image processing algorithm for determining the concentration of PSA via fluorescent images of f-MNPs obtained with a smartphone.
- A shared ‘cloud server’ platform for performing the analysis and communicating the results to designated users.

The proposed method achieves a limit of detection of 100 pg/mL in 2.5 minutes (30 seconds for actuation, 1 minute for washing and 1 minute for data analysis). This is an

order of magnitude faster than previously reported methods for detection of PSA by a smartphone.

1.8.2 Magnetic micro particles based POCT system

Magnetic micro-particles are well resolved in images obtained by light microscopy. Thus a series of images of the substrate surface taken in quick succession (a video) contains information about the dynamics of each particle which can reveal information about the interaction of particles with the sensing area. I propose a POCT biosensing system based on magnetic micro-particles with two key components:

- A three dimensional actuation mechanism for magnetic particles which promotes specific interactions and inhibits non-specific interactions simultaneously. The actuator is based on application of dielectrophoretic forces on particles, due to which the particles exhibit harmonic oscillations.
- An algorithm for high resolution optical tracking of magnetic particles in a video taken from a smartphone. The optical tracking algorithm is based on template matching for spatial localization of particles and a Kalman filter based motion model for accurate temporal association of particle trajectories across the frames of a video.

The proposed method achieves a limit of detection of 1 nM for biotin in 9 minutes (2 minutes for actuation and 7 minutes for optical tracking). This is the first report of a smartphone based biosensing protocol using optical tracking of magnetic particles.

I have described that conventional medical diagnostics technologies are unsuitable for use in rural areas due to their large size (figures 1-3, 1-7 and 1-9) and cost (8,000 US dollars). To complete the discussion on the advantages of smartphone based medical diagnostics technologies in such areas, I am presenting the size and cost of the

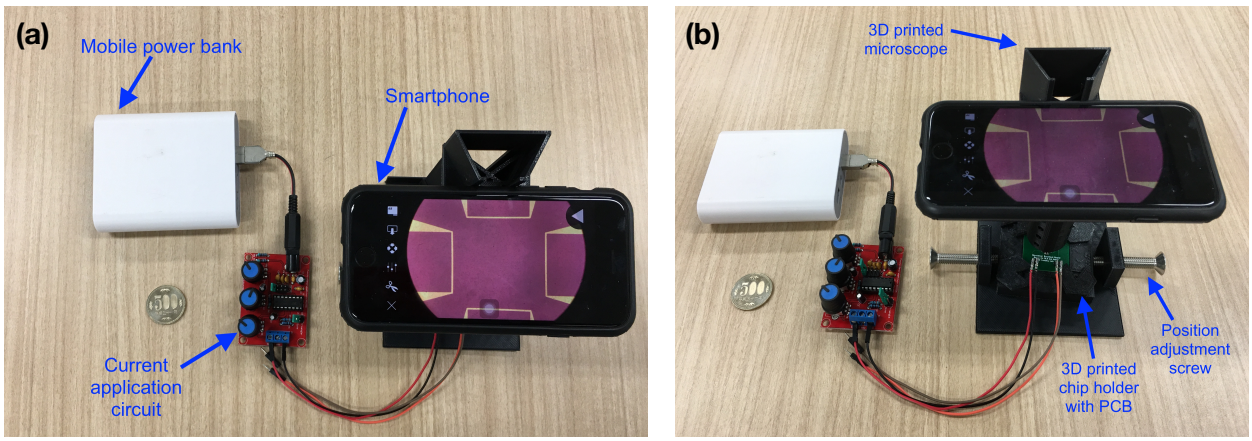

Figure 1-15 A prototype of the small medical diagnostics system developed in this study. A 500 yen coin is shown for scale. (a) The system is powered with a mobile power bank and consists of a current application circuit (b) A 3D printed microscope along with a smartphone is used to take 4K videos of the biosensing chip (not visible in these images). The video is then uploaded to a remote 'cloud' computer where they are analyzed and the results are sent back to the user.

smartphone based diagnostics system developed in my research. Figure 1-15 shows a prototype diagnostics system developed in this research. The proposed system is much smaller than a conventional diagnostics technologies and costs **about $20** excluding smartphone, battery and lens.

1.9 Organization of this thesis

This chapter was a non-technical introduction to the field of medical diagnostics. The remaining chapters of this thesis will be technical in nature and are organized as shown in figure 1-16.

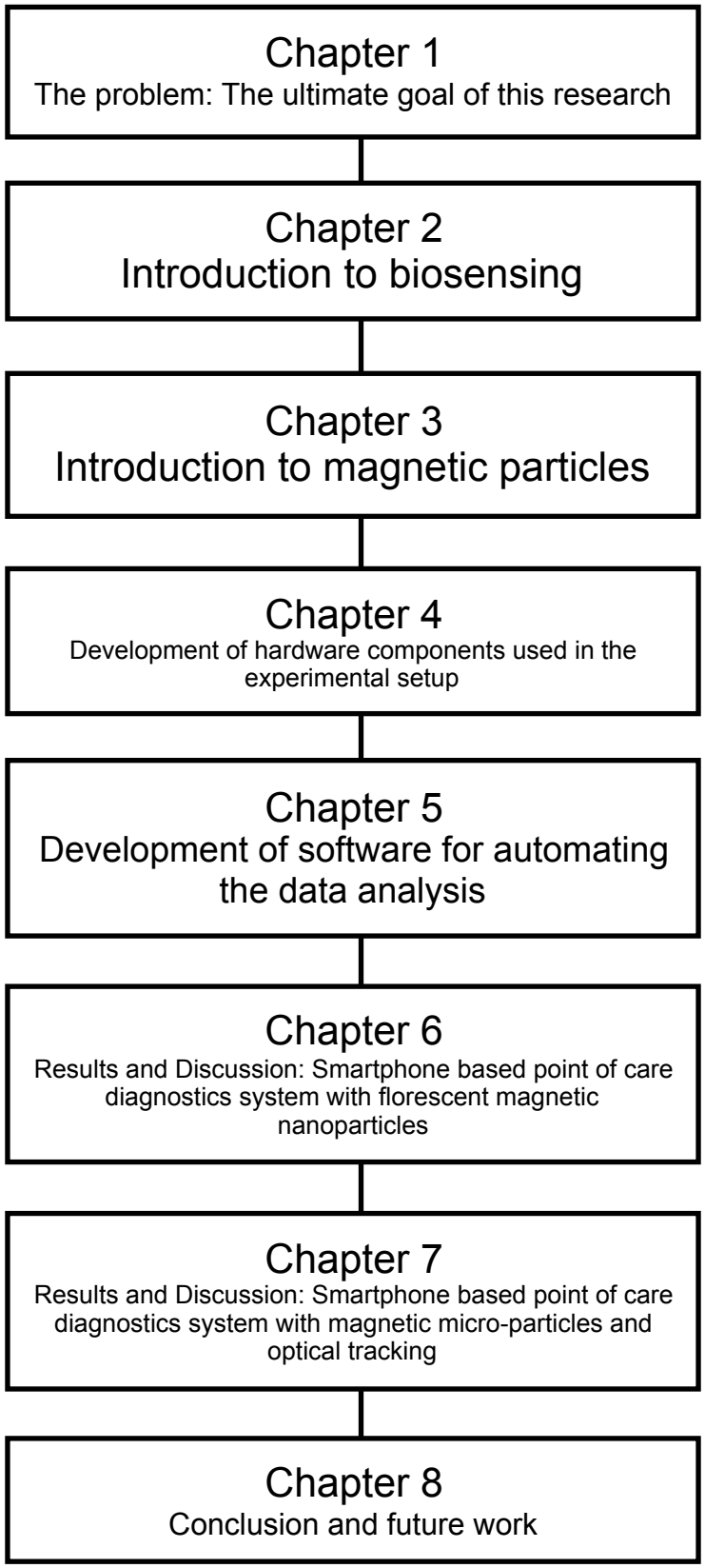

Figure 1-16. Organization of this thesis

1.10 References

[1] Sustainable Development Goals, https://www.un.org/sustainabledevelopment/

[2] ESA and the Sustainable Development Goals, http://www.esa.int/Enabling_Support/Preparing_for_the_Future/Space_for_Earth/ESA_and_the_Sustainable_Development_Goals

[3] Goal 3: Ensure healthy lives and promote well-being for all at all ages, https://www.un.org/sustainabledevelopment/health/

[4] Engvall, E. and Perlmann, P., 1972. Enzyme-linked immunosorbent assay, ELISA: III. Quantitation of specific antibodies by enzyme-labeled anti-immunoglobulin in antigen-coated tubes. *The Journal of Immunology*, *109*(1), pp.129-135.

[5] Holt, P.S., Gast, R.K. and Greene, C.R., 1995. Rapid detection of Salmonella enteritidis in pooled liquid egg samples using a magnetic bead-ELISA system. *Journal of food protection*, *58*(9), pp.967-972.

[6] ELISA, reader, 8 channel, https://supply.unicef.org/s0001312.html

[7] The principle and method of ELISA, https://ruo.mbl.co.jp/bio/e/support/method/elisa.html

[8] Sandhu, A., Sanbonsugi, H., Shibasaki, I., Abe, M. and Handa, H., 2004. High sensitivity InSb ultra-thin film micro-hall sensors for bioscreening applications. *Japanese journal of applied physics*, *43*(7A), p.L868.

[9] Binasch, G., Grünberg, P., Saurenbach, F. and Zinn, W., 1989. Enhanced magnetoresistance in layered magnetic structures with antiferromagnetic interlayer exchange. *Physical review B*, *39*(7), p.4828.

[10] Freitas, P.P., Ferreira, R. and Cardoso, S., 2016. Spintronic sensors. *Proceedings of the IEEE*, *104*(10), pp.1894-1918.

[11] Baselt, D.R., Lee, G.U., Natesan, M., Metzger, S.W., Sheehan, P.E. and Colton, R.J., 1998. A biosensor based on magnetoresistance technology. *Biosensors and Bioelectronics*, *13*(7-8), pp.731-739.

[12] Transforming Personal Health: The Nokia Sensing XChallenge, https://www.herox.com/blog/163-transforming-personal-health-the-nokia-sensing-xch

[13] Choi, J., Gani, A.W., Bechstein, D.J., Lee, J.R., Utz, P.J. and Wang, S.X., 2016. Portable, one-step, and rapid GMR biosensor platform with smartphone interface. *Biosensors and Bioelectronics*, *85*, pp.1-7.

[14] Ng, E., Yao, C., Shultz, T.O., Ross-Howe, S. and Wang, S.X., 2019. Magneto-nanosensor smartphone platform for the detection of HIV and leukocytosis at point-of-care. *Nanomedicine: Nanotechnology, Biology and Medicine*, *16*, pp.10-19.

[15] Elghanian, R., Storhoff, J.J., Mucic, R.C., Letsinger, R.L. and Mirkin, C.A., 1997. Selective colorimetric detection of polynucleotides based on the distance-dependent optical properties of gold nanoparticles. *Science*, *277*(5329), pp.1078-1081.

[16] SPR-PLUS, https://www.xantec.com/products/spr_biosensors/sprplus.php

[17] Superconducting Quantum Interference Device Magnetometer, https://physics.missouristate.edu/SQIDM.htm

[18] Oisjoen, F., Schneiderman, J.F., Zaborowska, M., Shunmugavel, K., Magnelind, P., Kalaboukhov, A., Petersson, K., Astalan, A.P., Johansson, C. and Winkler, D., 2009. Fast and sensitive measurement of specific antigen-antibody binding reactions with magnetic nanoparticles and HTS SQUID. *IEEE Transactions on Applied Superconductivity*, *19*(3), pp.848-852.

[19] Hospitals in the Country, https://pib.gov.in/PressReleasePage.aspx?PRID=1539877

[20] Hospital beds (per 1,000 people), https://data.worldbank.org/indicator/SH.MED.BEDS.ZS

[21] 80 per cent of Indian doctors located in urban areas, https://economictimes.indiatimes.com/industry/healthcare-biotech/80-per-cent-of-indian-doctors-located-in-urban-areas/articleshow/53774521.cms?from=mdr

[22] Kumar, R. and Pal, R., 2018. India achieves WHO recommended doctor population ratio: A call for paradigm shift in public health discourse!. *Journal of Family Medicine and Primary Care*, *7*(5), p.841.

[23] Anganwadi, https://en.wikipedia.org/wiki/Anganwadi

[24] The Role of the Anganwadi Worker in Polio Eradication in Bihar, India: From Awareness Generation to Service Delivery, https://www.researchgate.net/publication/282335896

[25] Leapfrogging, https://en.wikipedia.org/wiki/Leapfrogging

[26] Leapfrogging Tech Is Changing Millions of Lives. Here's How, https://singularityhub.com/2018/05/06/leapfrogging-tech-is-changing-millions-of-lives-heres-how/

[27] How leapfrogging can help developing countries surge ahead, https://www.centreforpublicimpact.org/cleared-for-take-off/

[28] Number of fixed telephone subscriptions per 100 inhabitants in India from 2000 to 2018, https://www.statista.com/statistics/733525/fixed-telephone-subscriptions-per-100-inhabitants-in-india/

[29] We Don't Have Enough Doctors in Rural India. That's Why We Need Telemedicine. http://bwdisrupt.businessworld.in/article/We-Don-t-Have-Enough-Doctors-in-Rural-India-That-s-Why-We-Need-Telemedicine-/14-06-2017-120121/

[30] Water-Borne Diseases in India, https://en.reset.org/blog/water-borne-diseases-india

[31] Rai, S.K., Kant, S., Srivastava, R., Gupta, P., Misra, P., Pandav, C.S. and Singh, A.K., 2017. Causes of and contributors to infant mortality in a rural community of North India: evidence from verbal and social autopsy. *BMJ open*, *7*(8), p.e012856.

[32] Laboratory Methods for the Diagnosis of Vibrio cholerae, Centers for Disease Control and Prevention, https://www.cdc.gov/cholera/pdf/Laboratory-Methods-for-the-Diagnosis-of-Vibrio-cholerae-chapter-7.pdf

[33] Spencer, H.C., Collins, W.E., Chin, W. and Skinner, J.C., 1979. The enzyme-linked immunosorbent assay (ELISA) for malaria. *The American journal of tropical medicine and hygiene*, *28*(6), pp.927-932.

[34] Keddy, K.H., Sooka, A., Letsoalo, M.E., Hoyland, G., Chaignat, C.L., Morrissey, A.B. and Crump, J.A., 2011. Sensitivity and specificity of typhoid fever rapid antibody tests for laboratory diagnosis at two sub-Saharan African sites. *Bulletin of the World Health Organization*, *89*, pp.640-647.

[35] Mehmood, K., Sundus, A., Naqvi, I.H., Ibrahim, M.F., Siddique, O. and Ibrahim, N.F., 2015. Typhidot-A blessing or a menace. *Pakistan journal of medical sciences*, *31*(2), p.439.

[36] Novel coronavirus (2019-nCoV), https://en.wikipedia.org/wiki/Novel_coronavirus_(2019-nCoV)

[37] 2019–20 Wuhan coronavirus outbreak, https://en.wikipedia.org/wiki/2019–20_Wuhan_coronavirus_outbreak

[38] Factbox: WHO international public health emergencies, https://www.reuters.com/article/us-china-health-who-emergency-factbox/factbox-who-international-public-health-emergencies-idUSKBN1ZL1S4

[39] Ebola virus disease, https://www.who.int/news-room/fact-sheets/detail/ebola-virus-disease

[40] Experimental therapies: growing interest in the use of whole blood or plasma from recovered Ebola patients (convalescent therapies). https://www.who.int/mediacentre/news/ebola/26-september-2014/en/

2. Introduction to biosensing

2.1 Introduction

The United Nations has identified ageing population across the planet as one of the most important issues in its 'Overview of Global Issues'[1]. Further, it is noteworthy that the number of people aged 65 or above exceeded the number of children under 5 years of age in 2018 for the first time in history[2]. These statistics underscore the fact that access to healthcare is expected to be one of the most important concerns for developing countries in the coming decades. This has motivated a large body of research in developing rapid, low cost and sensitive devices for medical diagnostics. In this chapter, I will introduce the concept of a biosensor and establish a terminology for discussing various aspects of the biosensing system. Building on the discussion in the previous chapter, I describe the need for point of care biosensors and introduce a new architecture for such biosensors. I then analyze the potential of smartphones for point of care biosensing and show that they are an attractive platform for development of next generation point of care biosensors. Finally, I perform a survey of previous research on smartphone based biosensors.

2.2 What is a biosensor?

A sensor is a device used to measure one or more properties of a system or environment of interest. For example, temperature sensors are used in automobiles to monitor the combustion process in the engine. When the system of interest is a biological system and the property of interest is the amount of certain types of biological markers, the sensor which enables these measurements is called a biosensor. Examples of biological systems includes cells, tissues, blood and saliva etc., while examples of biological markers include cell morphology, proteins or antibodies corresponding to specific diseases. In this work, we will restrict ourselves to using liquid systems and molecular biomarkers. Thus, cells and tissues and detection of their related properties are outside the scope of this study.

For a liquid biological sample where a molecule is the marker of interest, the components of a conventional biosensing system is given in figure 2-1.

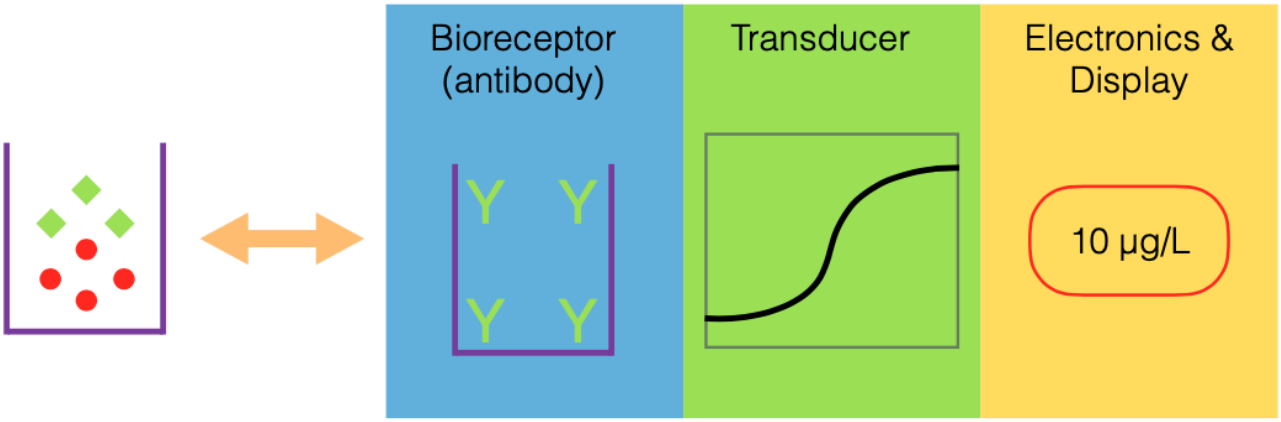

Figure 2-1. Components of a conventional biosensing system.

The bioreceptor (generally an antibody or antigen) is a complimentary molecule to the biomolecule of interest. The biological interaction between complimentary molecules is converted into an electronic signal by a transducer. Supporting electronic circuitry is used to reduce the noise in the readout of the transducer and the results are then displayed on

a screen. Some examples of each of the major components in the above figure are shown in Table 1.

Next, I will discuss these components in detail.

Table 1. Examples of components of a biosensing system

Bioreceptor	Transducer	Electronics
Antibodies	Magnetoresistive sensor	Wheatstone bridge
Antigens	Hall effect based sensor	Lock-in amplifier
Enzymes	optical imaging sensor	Analog front end

2.2.1 Bio-receptors and labels

A bio-receptor (say, A) is a molecule which can interact with the molecule of interest (say, B) and produces a signal which can be detected externally. Notably, the reaction of a bioreceptor is specific i.e. no other molecule (say, C) can interact with A to produce the signal. Bio-receptors on their own are insufficient for electronic detection of bimolecular interactions due to their small size. Thus, biomolecular labels are used to tag specific bio-receptors so that the presence of the bioreceptor can be detected by the presence of tags. Bio-receptors may thus be distinguished on the basis of their labels.

2.2.1.1 Bio-receptors

Antibodies (also known as immunoglobulins) are proteins produced by the human body in response to foreign agents. The function of an antibody is to bind to a specific type bacteria or virus and enable its destruction. Notably, the defining characteristic of an antibody is its specificity in binding to its complimentary molecule, called an antigen. Figure 2-2 shows the structure of an antibody. The structure of an antibody can be divided into two major parts: heavy chains (H-chains) and light chains (L- chains). The H-chains constitute the so-called ‘constant region’ of the antibody which is common in all types of antibodies. The front end of the H-chains consist of L-chains which varies among antibodies and is thus called variable region. The variable region forms the binding site where the antibody attaches to antigens. The specific structure of the variable region determines the binding properties of the antibody, forming the so called lock and key binding mechanism.

Table 2 lists various examples of antibodies and antigens. Among those listed, the Avidin-Biotin binding system and prostate specific antigen (PSA) and corresponding antibody anti-PSA are used in this work for verification of proposed medical diagnostics protocols. While strictly speaking, avidin and biotin are not antibody and antigen, their interaction is one of the strongest known non-covalent interactions found in nature. Thus, it is commonly used as a model for biological interactions.

Table 2. Examples of antibodies and antigens	
Antibody	**Antigen**
Immunoglobin G (IgG)[3]	Rabbit anti-mouse (RAM) IgG
anti-PSA [4]	Prostate specific antigen (PSA)
Avidin [5]	Biotin

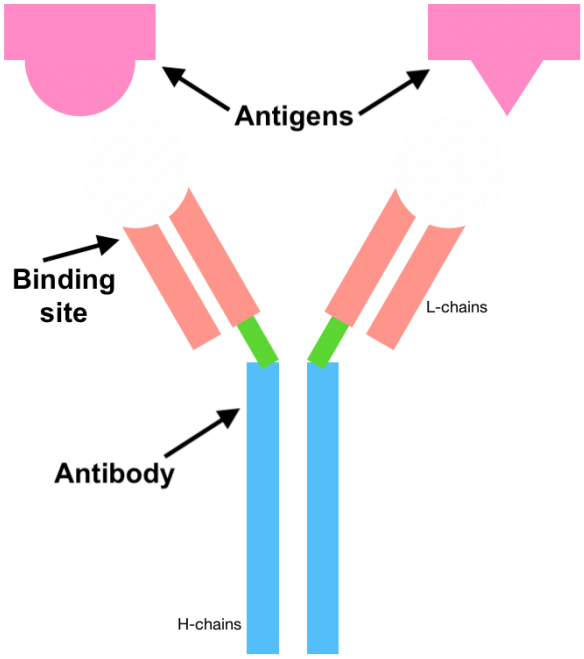

Figure 2-2. Structure of an antibody and its binding site.

2.2.1.2 Biological labels

The most commonly used labels for bio-receptors are radioisotopic labels, enzymes, fluorescent tags or nanoparticles. The most commonly used illogical labels are introduced briefly below:

- Enzymes are macromolecular biological catalysts which are most commonly used in Enzyme linked Immunosorbent Assay (ELISA). Enzymatic labels can interact with a substrate (a solution) such that the results of those interactions can be observed externally. In the most common form in ELISA, the enzyme causes a change in color of the solution which is observed with optical sensors.
- Fluorescent labels are most commonly used in the form of quantum dots (QDs). As the name suggests, the fluorescent labels attach selectively to antibodies and are detected in a fluorescent image. [6]
- Micro-particles composed of polymers are widely used as biological labels for bio-receptors. There are various types of particle based labels depending on their size, shape and magnetic properties:
  - **Size:** The size of the particles can vary over a wide range, from a few micro-meters to a few hundred nanometers. Smaller sized nanoparticles offer greater surface area to volume ratio for immobilization of biological receptors, but may require specialized transducers for sensing.

- **Magnetism:** Magnetic nano-particles can be encapsulated within larger polymeric particles, which imparts magnetic properties to the composite particle. Such composite 'magnetic particles' can be manipulated with the application of eternal magnetic fields.
- **Fluorescence:** Fluorescent chemical complexes can be encapsulated within polymer particles to produce fluorescent particles. Fluorescence is critical for detection of nanometer sized particles since they cannot be observed optically.

Magnetic particles form the mainstay of the work presented in this thesis and are discussed in detail in the next chapter.

2.2.1.3 Label free Biosensing

Although biological labels are commonly used along with bio-receptors, certain biosensing transducers allow direct detection of bio-receptors in a label-free fashion. Notable examples of label free detection methods include surface plasmon resonance (SPR) and guided mode resonance (GMR) biosensors.

2.2.2 Transducers

There are various types of transduction mechanisms which can be exploited for detection of biological labels:

- The change in color of the solution due to the interaction of an enzyme with its substrate can be observed with microplate readers.
- The change in electrical conductivity of the medium between fixed electrodes can be used to measure the concentration of bio-receptors provided conductive particles (such as gold) are used. [7]
- Direct observation of micro meter sized particles can be performed with optical microscopy.
- The scattering and absorption properties of nanoparticles can enable their detection[8].
- The change in refractive index of a substrate by nanoparticles can be observed by spectroscopic measurements.
- The change in optical properties of metal surface known as surface plasmon resonance (SPR) can be used to directly detect antibodies on the surface. This method is 'label free' in that no biological labels are required. As I will discuss, this has the advantage that non-specific interactions between label and sensing surface do not limit the sensitivity of the sensing method.

2.3 The need for point of care biosensors

In the previous section, I introduced the constituent elements of a conventional biosensor and provided examples of each. The paradigm for biosensing was conceived in the previous century when rapid advances were made in various medical diagnostics technologies and tests for previously undetectable diseases were discovered. This way of designing biosensors poses several limitations:

- Highly skilled personnel are necessary to operate conventional equipment such as 96-well plate readers of ELISA.
- The time required for performing the tests is very long. It typically takes several hours for a patient to receive the results of a conventional test such as ELISA.

- The cost of equipment such as incubation systems and plate readers is quite high thus, their availability is limited to hospitals and pathology laboratories. This presents a challenge as most of developing countries have limited infrastructure to support procurement and operation of conventional equipment.
- The results of the diagnostics test are not readily shared between patients and doctors. Access to information about the spread of a disease can be critical in case of outbreak of an epidemic in order to target the response to the most affected regions.

Thus, while **biosensors developed in the previous century had to address the problem of accurate and reliable detection, the next generation of biosensors will have to address the problem of scale as well as speed**. Thus, an ideal biosensor needs to have the following characteristics in order to address the healthcare needs of an ageing population in the 21st century:

- The biosensor should be **low cost**. This typically involves a disposable strip/substrate to be used in conjunction with a non-disposable analysis equipment.
- The biosensor should provide results quickly. For the best experience of patients, results should be available in **10 minutes or less**.
- The biosensor should be **easy to use** such that unskilled patients can perform their tests on their own and do not need to be trained.
- The biosensor should offer increased access to the patients by virtue of being integrated with existing technologies and devices commonly used by people across the world. For example, smartphones are ubiquitous across the world and are an attractive technology for integration with biosensors.

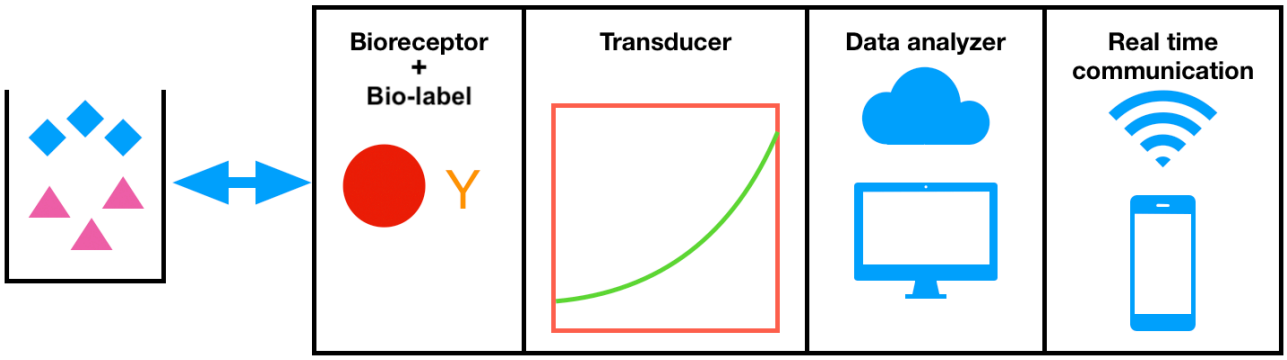

Figure 2-3. Overview of components of a POCT biosensor.

2.4 A new architecture for point of care biosensors

Biosensors designed with the above objectives in mind enable testing at the 'point of care' or bedside by the patient rather than in a laboratory by a technician. Thus, such types of biosensors are called point of care testing (POCT) biosensors. From the above discussion, it is clear that existing biosensing technologies cannot be modified retroactively to achieve the stated objectives and that next generation POCT biosensors should be designed from the ground up. Thus, I propose a **new architecture** for POCT biosensors to facilitate and guide the development of next generation of biosensors in figure 2-3. The proposed POCT biosensing system has two additional components compared to a conventional biosensor:

Data Analyzer: In addition to bio-receptors and transducers, the POCT biosensor requires a data analyzer module which can perform 'post-processing' of the data to extract valuable information from the collected data. Note that the data analyzer is in addition to any noise

reduction circuitry which forms a part of the biosensor. In particular, the noise reduction and processing circuitry described in figure 2-1 process the signals while the measurements are being carried out whereas the data analyzer performs analysis after the data has been collected (hence the term post-processing). This has a few advantages for biosensing:

- Post processing does not need to be performed in real-time and can be performed by at a remote location such as on a cloud server.
- With the rise of technologies such as big data mining and artificial intelligence it may be possible to extract information out of data which was not envisaged at the time of collection of the data. For example, scans of retinal images of patients have been shown to contain information about cardiovascular risk factors such as age, gender, smoking status and systolic blood pressure[9]. Such associations are surprising even to human experts and may be discovered by only big data mining, thereby allowing healthcare experts to offer new insights from existing data.
- Post-processing is necessarily performed in software. Thus, while the hardware of a biosensor cannot be modified once it has been introduced into the field, enhanced functionality can be introduced into a biosensor with a software update.

Real-time communication: The results of a diagnostic test need to be communicated among various stakeholders such as patients, doctors and policy makers in order to ensure rapid response by public healthcare system in the case of outbreak of an epidemic. Thus, next generation POCT sensors necessitate the integration of a real-time communication module. The communication module may work in conjunction with data analysis module when, for example, data obtained from the sensor needs to be uploaded to a remote server for analysis before the results are received back.

2.5 Smartphone as a biosensing platform

Smartphones have been a defining technology for the first two decades fo this century. The adoption of smartphones grew at more than 30% year on year during the early part of this decade and has now plateaued. As of 2018, among the top 50 countries with the most smartphone penetration about two-thirds are developing countries[10]. Smartphones enable three important functions which are suitable for biosensing:

- **Cameras:** Most smartphones are equipped with high resolution cameras. The complementary metal oxide semiconductor (CMOS) image sensors in smartphone cameras enable capturing of details under low light conditions. Moreover, users have access to raw image data as well as to compressed images and videos produced by the integrated image signal processor (ISP). Thus, both types of data could be used depending on the analysis method used. Notably, most modern smartphones are equipped with the ability to record 4K video streams (3840 pixels x 2160 pixels).
- **Communication:** Since the primary function of smartphones is communication, modern smartphones are equipped with latest communication technologies such as 4G long term evolution (LTE), Wi-Fi (802.11 a/b/g/n/ac/ax) and Bluetooth (Bluetooth 4.0, 5.0 and BLE). These high speed communication channels an be used to send raw data collected from the biosensor and receive information about the results of data analysis or vice versa.
- **Processing:** The most important component of an embedded computing device such as a smartphone is the power efficient reduced instruction set (RISC) processor. In addition to RISC processors, recent smartphones also contain several application specific domains such as graphics processing units (GPUs) to accelerate specific workloads such as massively parallel matrix multiplication which enables inference for neural

networks. Thus, data processing algorithms designed to take advantage of such specialized accelerators can perform previously infeasible data analysis locally on the smartphone.

Thus, it is clear that **smartphones are equipped with several features for development of POCT biosensors** as shown in table 3. Smartphone cameras can serve as low noise sensors, high speed processors can function as data analyzer and 4G/802.11 protocols can enable high speed communications.

Table 3. How smartphones can enable POCT biosensing

Requirement of POCT biosensor	Function in smartphone
Low noise transducer/sensor	High resolution (up to 4K) camera
Data analyzer	High speed processor with GPUs
Communication	4G, 802.11 ac, BLE

Thus, throughout the rest of this thesis I will focus on the development of smartphone based biosensors for POCT applications.

2.6 Previous literature on smartphone based biosensors

The potential of smartphones for medical diagnostics has long been recognized by researchers all across the world. Smartphone based biosensors developed in literature are primarily of two types:

- Conventional biosensors with a smartphone interface. These include well-known technologies such as surface plasmon resonance (SPR)[11], Enzyme linked immunosorbent assay (ELISA)[12], giant magnetoresistance (GMR)[13], which have been developed independently of smartphones but were then retroactively miniaturized and modified to interface with smartphones.
- Biosensors developed specifically for use with a smartphone. These are technologies which were developed from the beginning for use with smartphones. Examples of such technologies include breath analyzers for lung function testing and smartphone based urinalysis kit[14].

The biosensing methods most relevant to this research are SPR, ELISA and GMR. I have already described the miniaturization of GMR biosensor and their limitations in section 1.3.3. Here, I will describe research on smartphone based ELISA and SPR biosensors.

2.6.1 Smartphone based ELISA

The steps involved in an ELISA based test are described in section 1.3.1 (figure 1-2 and 1-3). At the end of an ELISA test, a 96-well plate reader is used to detect the intensity of fluorescent markers, and thus the concentration of biomarker of interest. Berg et. al.[12] at University of California, Los Angeles have demonstrated a miniaturized 96-well plate reader which integrates with a smartphone. A schematic of the plate reader is shown in figure 2-4. It consists of a 3D printed smartphone attachment which holds a 96 well plate and illuminates it with 24 blue LEDs. The light is transmitted via the wells and collected by an array of 96 individual optical fibers (one for each well). The optical fibers are bundled at one end into a 12x8 matrix which is then imaged with the camera of the smartphone. The

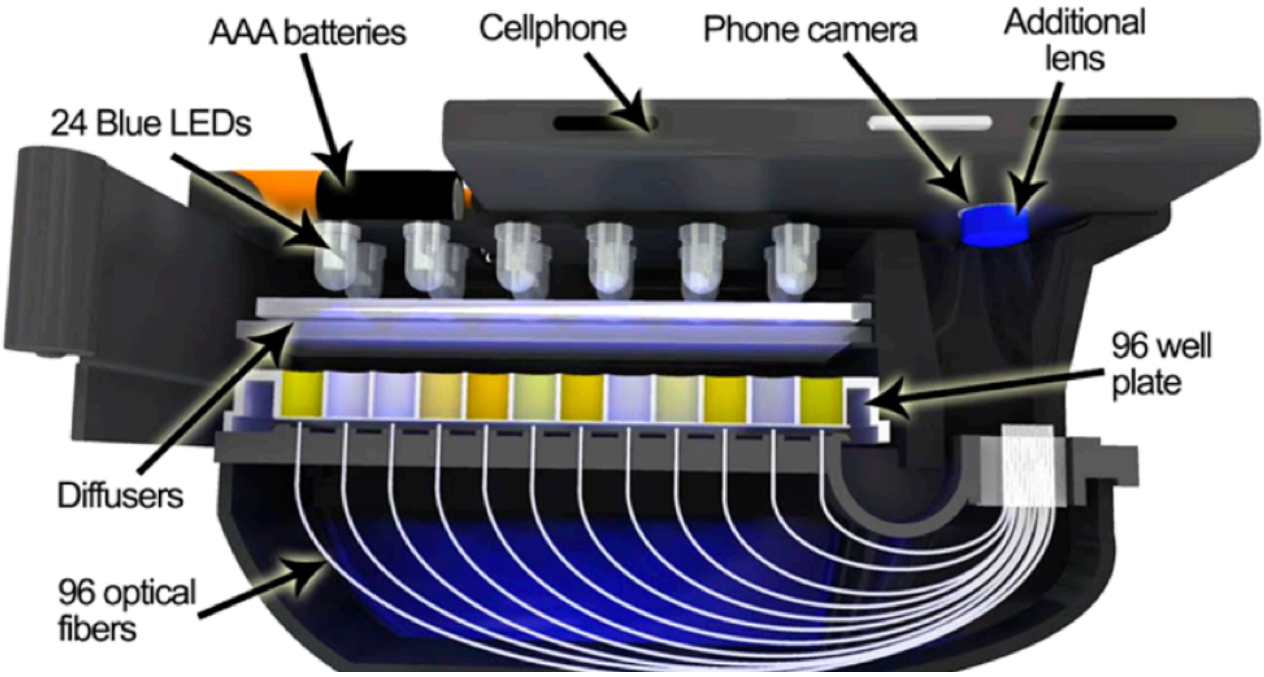

Figure 2-4. Schematic of smartphone based 96-well plate reader demonstrated by Berg et. al. Source: [12]

image is transmitted to a server and analyzed remotely. The results of the analysis are transmitted back to the user in about 1 minute. The researchers analyzed four types of biomarkers: mumps IgG, measles IgG, herpes simples IgG virus 1 and 2 (HSV-1 and HSV-2). The analysis consisted of qualitative classification i.e. whether a sample indicates disease or no disease, rather than quantitative analysis of the concentration of biomarkers. They obtained a classification accuracy of 99.6%, 98.6%, 99.4% and 99.4% for detection of mumps, measles, HSV-1 and HSV-2 respectively.

This study represents the potential of ELISA to be miniaturized and integrated with a smartphone. However, there are two specific limitations of this approach:

- One of the major limitations of ELISA is that a long time of 12-24 hours is required for incubation of sample for the biomolecular reaction to occur. Incubators are large and expensive equipment which are available only in laboratories. The plate reader is useful only after the incubation step is complete. While the proposed 96-well plate reader successfully miniaturizes the equipment for obtaining and analyzing ELISA plate images, from the point of view of practical use an incubator is still required. Thus, the proposed plate reader cannot successfully miniaturize ELISA tests unless further advances are made in miniaturizing biological incubators. The authors do not discuss the possibility of miniaturizing incubators.

- The image analysis software produces a binary output i.e. whether a disease is present or absent. This is often not enough for medical tests and for certain biomarkers, a quantitative measurement is necessary for the doctor to provide informed medical advice to patients. While the authors state that the proposed plate reader can obtain quantitative results, their experiments show that quantitative readout of the smartphone based plate reader can differ by as much as ±20% from a commercial spectrophotometer for all four biomarkers tested (figure 5 in the paper). Thus, the authors prefer to state qualitative results and do not show calibration curves or limits of detection of the biomarkers being studied.

2.6.2 Smartphone based SPR

SPR is one of the most sensitive methods of biomolecular detection available today. SPR biosensors are frequently used for extremely sensitive detections. Guner et. al. from Bilkent University, Turkey and Stanford School of Medicine, USA, have proposed a smartphone based SPR biosensor for rapid medical diagnostics. A schematic of the proposed biosensor setup is shown in figure 2-5. It consists of a 3D printed attachment which houses an LED light source and collimating optics. A sensor chip, containing a microfluidic channel is inserted into the smartphone attachment and the sample of interest is flowed at a rate of 50 µL/min through the channel for 5 minutes. The light from LED is incident on the sensor chip and the reflected light is imaged by the smartphone camera. The authors used this setup to detect mouse IgG and obtained a limit of detection (3σ) of 20 nM within 5 minutes.

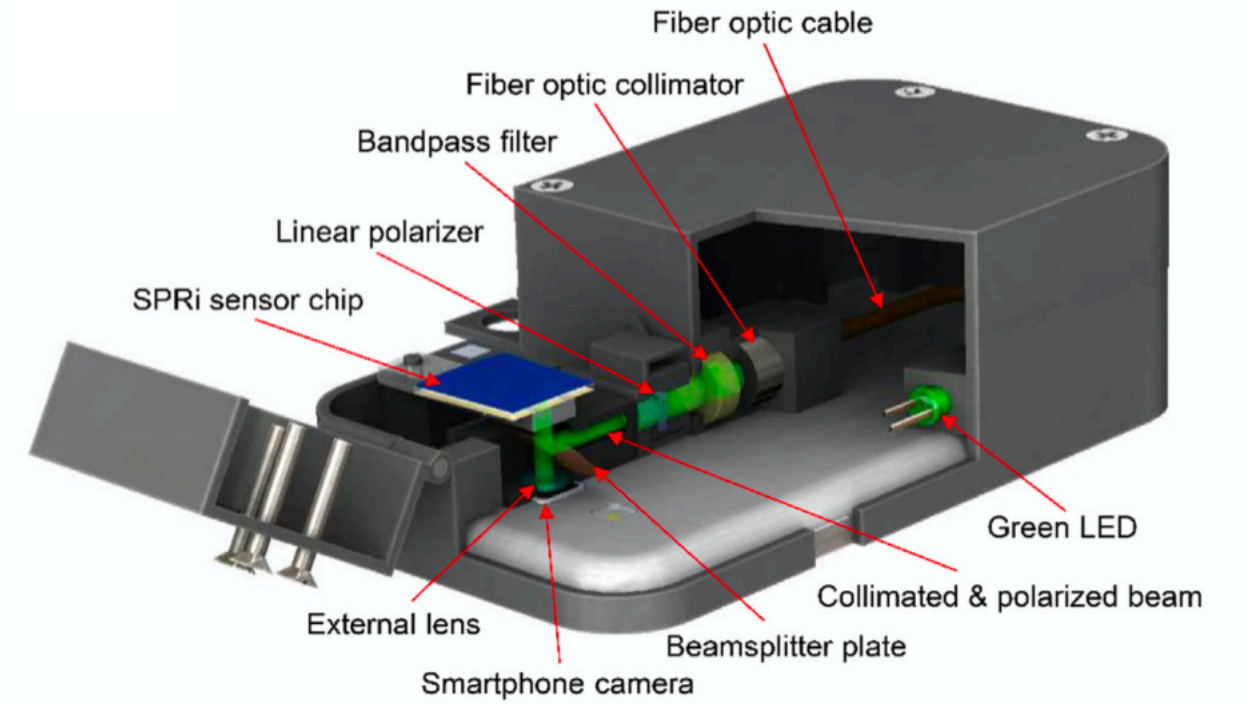

Figure 2-5. Schematic of smartphone based surface plasmon resonance biosensor by Guner et. al. Source: [11]

The results of this study are significant towards miniaturization of SPR biosensors. However, there are a few limitations of the proposed approach:

- The biosensor proposed in the study, as shown in figure 2-5 is not complete. An external peristaltic pump is used for controlled flow of liquids through the microfluidic channel. This presents a significant limitation for application of this biosensor for point of care since a pump for highly precise flow of sample is likely to be bulky and at the very least would require a walled power supply. The authors do not discuss the possibility of miniaturizing the pump.
- The sample volume required for conducting the test is quite large. It is estimated that the total sample volume required to carry out the test is 250 µL (50 µL/min for 5 minutes). The biosensing system I have developed can work with about two orders of magnitude less volume of sample.

It is important to note here that the limit of detection obtained is relatively large for an SPR based biosensor. The authors do not mention the limit of detection of IgG obtained. An analysis of figure 5(b) of the paper shows that the 3σ limit of detection of IgG would be about 20 nM. This shows that while sensitivities well into pico-molar ranges have been reported for SPR based biosensors, when an SPR biosensor is modified to work with a smartphone, the sensitivity of the sensor is reduced. Thus, one should be aware that smartphone based biosensors have inherent limitations due to the limits of the camera or miniaturized hardware and one should not expect state of the art biosensing systems to retain their sensitivity as they are integrated with smartphones.

I have described smartphone based biosensors most relevant to my research. These biosensors were obtained by miniaturizing well-known state of the art medical diagnostics technologies to interface with a smartphone. In both the examples discussed, key components of the biosensing pipeline were not miniaturized. For example, in ELISA a biological incubator was still required to complete the test, not to mention that the time required for incubation was also the same as conventional ELISA (typically 24 hours). In SPR, a peristaltic pump was required to flow the liquid through a channel at a precise rate. Thus, while certain components of the biosensing pipeline were miniaturized, the resulting systems were still not suitable to be used for real world applications.

As I will describe, starting from chapter 3, in this research I have adopted a different way of solving the problem. Rather than trying to miniaturize existing technologies, I have designed point of care biosensing systems which use new modalities of sensing and do not require any equipment other than what I explicitly state. In keeping with the spirit of leapfrogging, I expect that over the long term, this approach of solving the problem will be more successful than trying to make incremental changes to conventional technologies such as ELISA or SPR.

2.7 Summary

In this chapter, I have introduced the basics of biosensing. I began by introducing the constituent components of a biosensor i.e. bio-receptors, labels and transducers. The limitations of conventional biosensors were identified and key components of next generation biosensors were identified. I introduced a revised architecture to guide the development of next generation of biosensors. Specifically, the requirements of data analysis and communication were emphasized in order to realize the benefits of point of care testing. A clear view of these requirements allows us to identify smartphones as a promising platform for development of next generation POCT biosensors. I then reviewed existing literature on smartphone based biosensors which miniaturize existing technologies such as ELISA and SPR. I found that while parts of the sample processing pipeline are successfully miniaturized, vitally important components such as incubators and pumps are not. Therefore, this renders these technologies unsuitable for use in, say rural India, where they are needed the most.

2.8 References

[1] https://www.un.org/en/sections/issues-depth/global-issues-overview/index.html

[2] https://www.un.org/en/sections/issues-depth/ageing/index.html

[3] Tsugimura, K., Ohnuki, H., Endo, H., Tsuya, D. and Izumi, M., 2016. Protein-G-based human immunoglobulin G biosensing by electrochemical impedance spectroscopy. *Japanese Journal of Applied Physics*, *55*(2S), p.02BE06.

[4] Balk, S.P., Ko, Y.J. and Bubley, G.J., 2003. Biology of prostate-specific antigen. *Journal of clinical oncology*, *21*(2), pp.383-391.

[5] Green, N.M., 1975. Avidin. In *Advances in protein chemistry* (Vol. 29, pp. 85-133). Academic Press.

[6] Chan, W.C., Maxwell, D.J., Gao, X., Bailey, R.E., Han, M. and Nie, S., 2002. Luminescent quantum dots for multiplexed biological detection and imaging. *Current opinion in biotechnology*, *13*(1), pp.40-46.

[7] Park, S.J., Taton, T.A. and Mirkin, C.A., 2002. Array-based electrical detection of DNA with nanoparticle probes. *Science*, *295*(5559), pp.1503-1506.

[8] Elghanian, R., Storhoff, J.J., Mucic, R.C., Letsinger, R.L. and Mirkin, C.A., 1997. Selective colorimetric detection of polynucleotides based on the distance-dependent optical properties of gold nanoparticles. *Science*, *277*(5329), pp.1078-1081.

[9] Poplin, R., Varadarajan, A.V., Blumer, K., Liu, Y., McConnell, M.V., Corrado, G.S., Peng, L. and Webster, D.R., 2018. Prediction of cardiovascular risk factors from retinal fundus photographs via deep learning. *Nature Biomedical Engineering*, *2*(3), p.158.

[10] https://en.wikipedia.org/wiki/List_of_countries_by_smartphone_penetration

[11] Guner, H., Ozgur, E., Kokturk, G., Celik, M., Esen, E., Topal, A.E., Ayas, S., Uludag, Y., Elbuken, C. and Dana, A., 2017. A smartphone based surface plasmon resonance imaging (SPRi) platform for on-site biodetection. *Sensors and Actuators B: Chemical*, *239*, pp.571-577.

[12] Berg, B., Cortazar, B., Tseng, D., Ozkan, H., Feng, S., Wei, Q., Chan, R.Y.L., Burbano, J., Farooqui, Q., Lewinski, M. and Di Carlo, D., 2015. Cellphone-based hand-held microplate reader for point-of-care testing of enzyme-linked immunosorbent assays. *ACS nano*, *9*(8), pp.7857-7866.

[13] Choi, J., Gani, A.W., Bechstein, D.J., Lee, J.R., Utz, P.J. and Wang, S.X., 2016. Portable, one-step, and rapid GMR biosensor platform with smartphone interface. *Biosensors and Bioelectronics*, *85*, pp.1-7.

[14] Arumugam, S., Colburn, D.A. and Sia, S.K., 2019. Biosensors for Personal Mobile Health: A System Architecture Perspective. *Advanced Materials Technologies*, p.1900720.

3. Introduction to magnetic particles

3.1 Introduction

In the previous chapter, I discussed various aspects of a biosensor and identified micro and nanoparticles as one of the most suitable labels for biosensing. One of the major advantages of magnetic particles (MPs) is the ability to manipulate their motion with the application of external magnetic fields. Thus, a large body of work on MP based biosensing focuses on development of actuators for efficiently manipulating MPs. In this chapter, I begin with a brief overview of the particles used in this research. Their properties are discussed from the point of view of their manipulation as well as detection. I then discuss the physics of the motion of micro-meter sized particles suspended in a solution. This allows the reader to understand the theoretical basis for the problem of non-specific interactions which limit the sensitivity of biosensing protocols over and above the limitations imposed by sensor noise and experimental errors. I have developed an actuator for three dimensional electromagnetic actuation of particles based on the physics of motion of particles. Variations on the actuation scheme are discussed and various potential use cases are identified.

3.2 Introduction to magnetic particles

As discussed in the previous chapter, polymer micro particles have been in use as labels for bio-receptors. There are several types of polymer particles depending on their size magnetic and fluorescent properties as shown in table 1.

Table 1. Types of polymer particles

Property	Value/type
Size	≥ 1.0 μm or < 1.0 μm
Magnetism	Non-magnetic Ferro-magnetic Superparamagnetic
Fluorescence	Non fluorescent Fluorescent

These properties can be combined in various ways to synthesize different types of particles depending on the type of biosensor and transduction mechanism used for detection. Thus, the following types of particles can be synthesized:

- Superparamagnetic micro particle (MPs),
- Magnetic nanoparticles (MNPs),
- Fluorescent magnetic nanoparticles (f-MNPs),
- Fluorescent non-magnetic nanoparticles (f-NMPs).

In this research I have used all the above types of particles. However, I am mostly interested in magnetic micro-meter sized particles (MPs). The physical principles for manipulation and control of various types of particles are discussed in the next chapter. However, here I provide examples of all the types of particles used in this study.

3.2.1 Dynabeads M-280 Streptavidin

Dynabeads are well known magnetic particles in the literature and are one of the most common types of magnetic beads used for development of magnetic particles based biosensors. The M-280 Streptavidin variant of dynabeads are uniformly sized particles of size 2.8 µm each with superparamagnetic iron oxide nanoparticles of size 8-15 nm. These particles are categorized as magnetic micro-particles (MPs) as per the classification discussed above. These particles are readily observed by optical microscopy and can be easily imaged on a smartphone. Figure 3-1 shows a schematic of the structure of a dynabead as well as an SEM image showing the uniformity of their size and morphology.

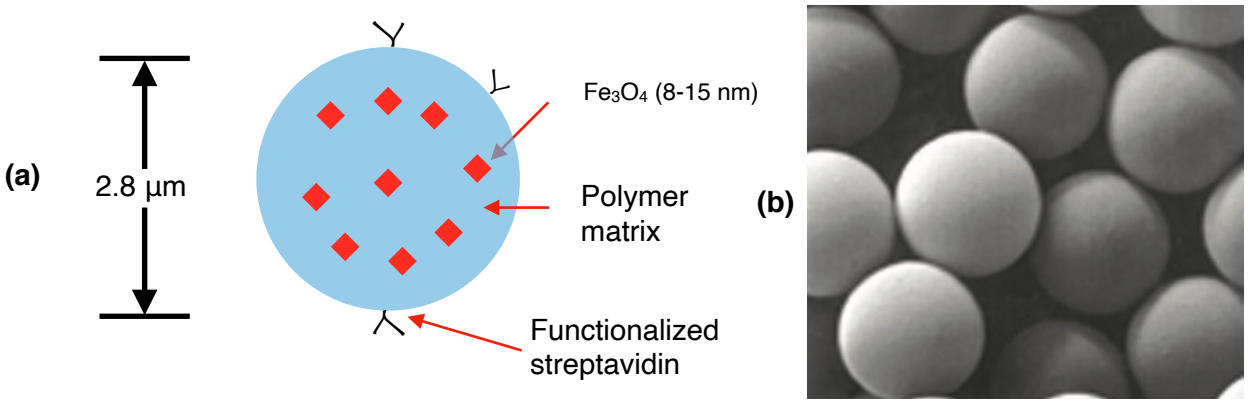

Figure 3-1 (a) Schematic of structure of a dynabead M-280. The structure consists of several superparamagnetic iron oxide nanoparticles embedded in a polymeric matrix. The surface of the polymer is functionalized with streptavidin. **(b)** A scanning electron microscope image of dynabeads provided by the manufacturer [1] showing the uniformity of size and surface morphology.

3.2.2 Dynabeads MyOne Streptavidin C1

The MyOne category of dynabeads are 1.0 µm in diameter and just like dynabeads M-280, consist of a polymer matrix in which superparamagnetic iron oxide nanoparticles are embedded. These particles are large enough to be observed by optical microscopy and can be imaged on a smartphone.

3.2.3 FG beads (prostate specific antigen)

FG beads derive their name from the polymer poly-(styrene-*co*-glycidyl methacrylate) (PGMA) which comprises them. They are 200 nm in diameter and are thus not observable with optical microscopes. Europium (Eu^{3+}) complexes embedded within the polymer matrix impart them fluorescent properties. The excitation wavelength is around 365 nm and the emission wavelength for fluorescence is around 615 nm. A detailed description of characterization of these particles is provided in [2]. Notably, these particles are ferromagnetic in nature since the iron oxide cores are approximately 40 nm in size. Thus, these particles tend to form clusters in the presence of magnetic fields. Figure 3-2 (a) shows the structure of the beads observed by transmission electron microscopy (TEM). Figure 3-2 (b) shows the fluorescence from FG beads under illumination from an ultraviolet light source. There were two types of FG beads used in this study. The first kind was functionalized with prostate specific antigen (PSA).

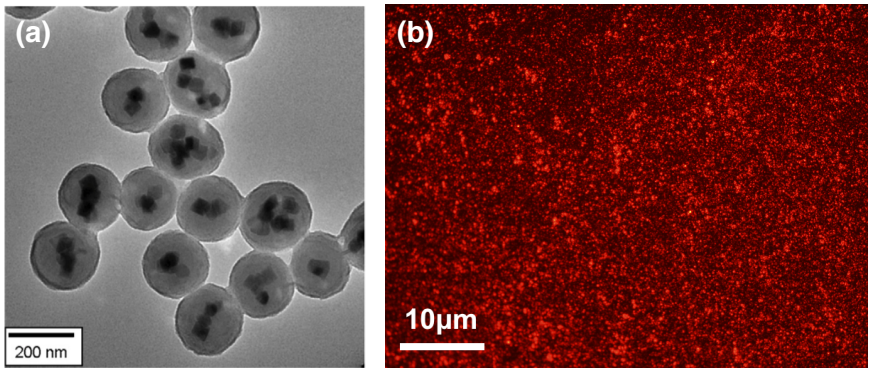

Figure. 3-2 (a) TEM image of FG beads [3], and (b) Fluorescence from FG beads under illumination from ultraviolet light

3.3 Forces on magnetic particles in a solution

Consider a micro sized particle suspended in a liquid just above a solid substrate. A AC or DC magnetic field is applied in an arbitrary direction such that it has components in all directions. Similarly, a AC electric field is applied in an arbitrary direction. The particle is in motion due to the applied forces. In this most general scenario, the particle experiences the following types of forces:

- Gravitational force
- Buoyancy force due to liquid
- Thermal/brownian force
- van der Waal's force
- Electrostatic force from the substrate
- Drag force due to resistance from liquid medium
- Magnetic force
- Electromagnetic force (Dielectrophoretic force)

We consider each of these forces in detail. The mathematical notation used in the rest of this section is as follows:

Radius of a particle is denoted by r or R.
Density of the particle is denoted by ρ followed by a subscript denoting the material.

3.3.1 Gravitational and buoyancy force

Polystyrene is the most commonly used polymer for synthesis of magnetic particles. The density of pure polystyrene is about 1.05 g/cm^3[4]. If the particles are magnetic, the iron oxide core introduces additional weight. The density if iron (III) oxide (Fe_2O_3) is 5.24 g/cm^3. Thus, a magnetic bead constituted out of a polymer of density ρ_{poly} which has an outer radius R and contains N magnetic cores, each of radius r and density ρ_{mag} is given by:

$$\rho_{MP} = \frac{\left(\frac{4\pi R^3}{3} - N\frac{4\pi r^3}{3}\right)\rho_{poly} + N\frac{4\pi r^3}{3}\rho_{mag}}{\frac{4\pi R^3}{3}} = \rho_{poly} + \frac{Nr^3}{R^3}(\rho_{mag} - \rho_{poly}) \qquad (3.1)$$

The above analysis ignores the contribution of surface functionalization to the density. Based on the data provided by the manufacturers, the densities of MPs used in this study is given below:

Table 2. Densities of particles used in this study

Name (size) of particle	Density, ρ_{MP} (g/cm^3)
Dynabeads M280 (2.8 μm)	1.3 [5]
Dynabeads MyOne (1.0 μm)	1.8 [6]
FG beads (180 nm)	1.28

The data regarding density of FG beads is not available from the manufacturer. Thus, the density stated in table 2 was calculated assuming that each nanoparticle contains an average of 5 iron oxide cores of size 40 nm each. This was deduced from an observation of the TEM images published by the manufacturer (figure 3-2(a) and [3]).

As is well known, the buoyancy force due to a liquid medium of density ρ_{med} on an object of volume V is given by $F_{buoyancy} = V\rho_{med}g$, where g is the gravitational constant. Thus, in the presence of only gravitational and buoyancy forces, the particle experiences a net downward force given by $F_{gravity} = V_{MP}(\rho_{MP} - \rho_{med})g$.

3.3.2 Brownian force

The well-known brownian motion was shown by Albert Einstein to be caused due to random motion of molecules of the liquid in which a particle is suspended. Brownian motion of particles is usually modeled as a random walk with equal probability of motion in all directions. However, a mathematically equivalent formulation of Brownian motion can be made in terms of Newtonian mechanics, where a stochastic force acts on a particle for a characteristic time scale[7]. Specifically, the random force can be stated as:

$$\overrightarrow{F_{BR}} = \vec{R}\sqrt{\frac{12\pi k_B T R\mu_f}{\Delta t}} \qquad (3.2)$$

where k_B is the Boltzmann constant, T is the temperature of the medium, R is the radius of the particle, μ_f is the dynamic viscosity of the liquid medium, $\vec{R}$ is a random vector drawn from a gaussian distribution with zero mean and unit variance, and Δt is the characteristic time scale. This formulation is very useful for performing Monte-Carlo simulations of the behavior of the system provided that the characteristic time scale is much smaller than the time scale over which the particle is simulated. For the purposes of biosensing, one is interested in time scales of a few seconds to tens of seconds. Thus, I have kept the characteristic time to be at least six orders of magnitude below this scale. Figure 3-3 shows a simulation of one dimensional browning motion performed for the three types of particles used in this research.

From the simulations it is observed that smaller particles have a tendency to exhibit larger drift from the mean position for the same amount of time. Thus, for example, in this simulation, the 200 nm FG beads have drifted away by more than ten micron from their initial positions, whereas the largest particles of 2.8 μm diameter have not drifted more than a few microns during the same time. This can also be understood by the fact that

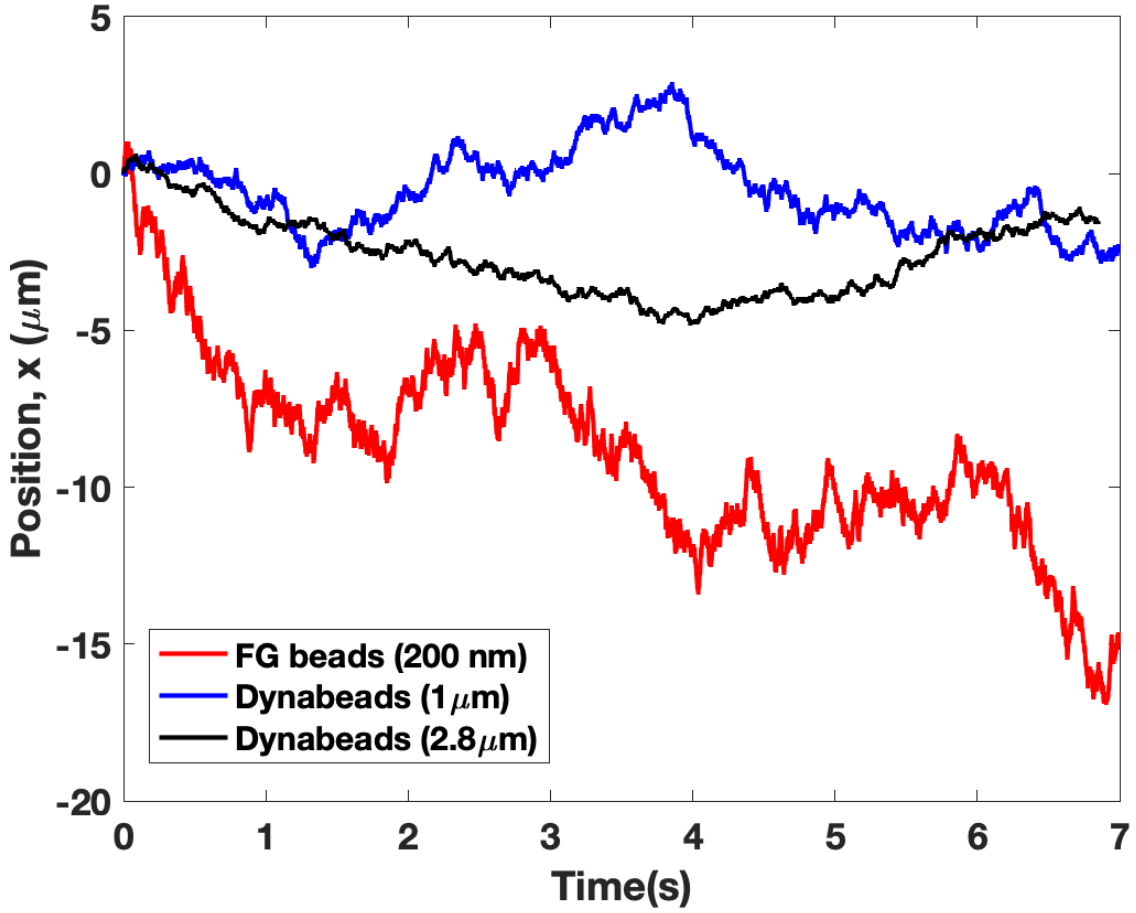

Figure 3-3. Simulation of one dimensional brownian motion for FG beads, dynabeads (1μm) and dynabeads (2.8 μm). A representative result of several runs of Monte Carlo simulations is shown.

similar thermal motion of surrounding molecules produce much larger amplitude of motion in smaller particles than in larger ones.

3.3.3 van der Waal's force

van der Waal's force is the name given to electromagnetic interaction between dipoles or induced dipoles of two atoms. If the atoms or groups of atoms belong to two different objects, it results in a net force of attraction or repulsion between the two objects. The van der Waals force between a spherical particle and a flat substrate can be calculated using Hamaker's formula given as[8]

$$F_{vdw} = -\frac{A_{132}R}{6z^3}\left[\frac{1}{1+14z/\lambda_{ret}}\right]\overrightarrow{e_z} \qquad (3.3)$$

where R is the radius of the particle, z is the vertical separation between the particle and the substrate, $\overrightarrow{e_z}$ is the unit vector along z direction. A_{132} is the Hammier constant of the particle of material 1 on a substrate of material 2 in a medium of material 3. λ_{ret} is the characteristic wavelength of interaction and is assumed to be 100 nm. For a particle with polystyrene surface on a substrate of silicon dioxide in water, the Hamaker constant is found to be 3.4×10^{-21} J. Since this interaction is electromagnetic (and thus conservative) in

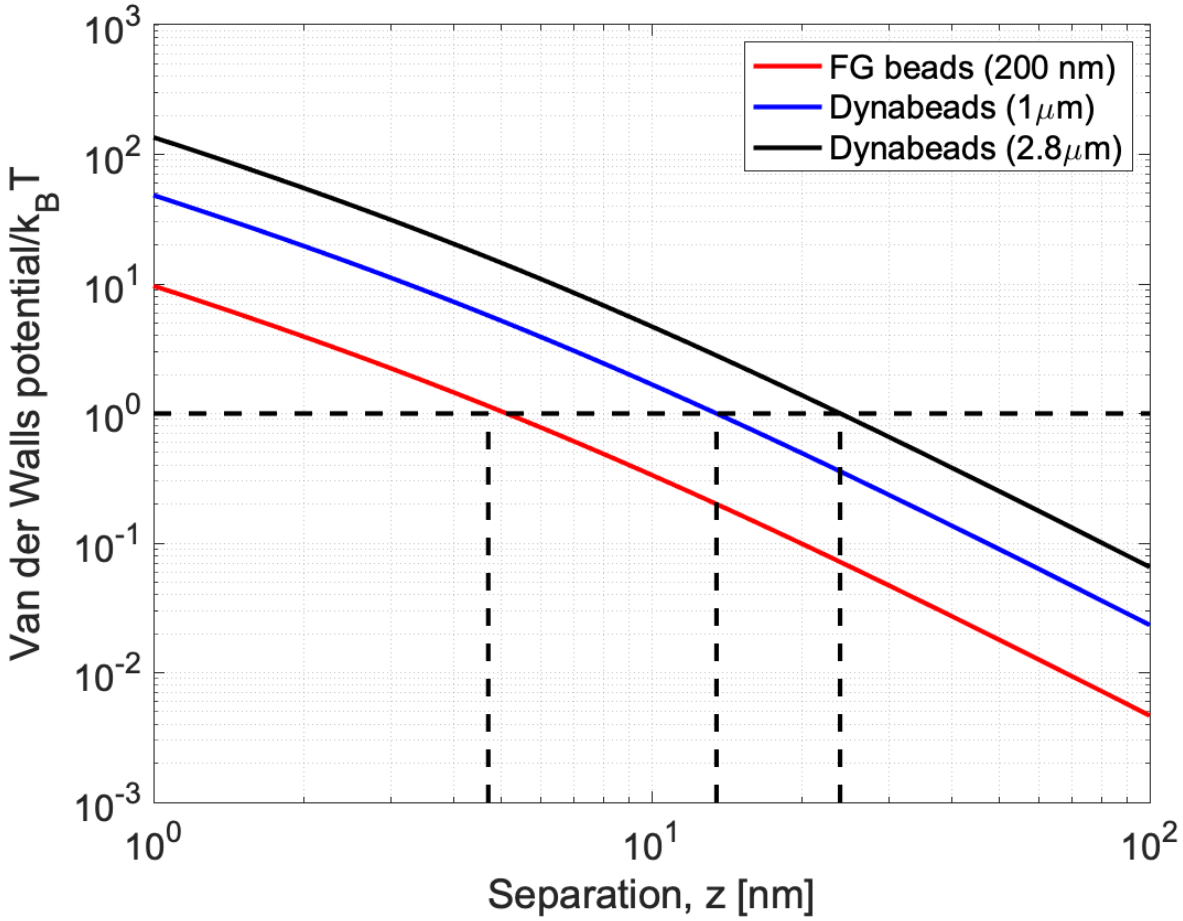

Figure 3-4. Simulation of potential of van der Waal's interaction between the various particles used in this study and a silicon dioxide substrate. Non-specific interactions become significant for particles at 24 nm (dynabeads, 2.8 μm), 13.5 nm (dynabeads 1 μm) and 4.7 nm (FG beads 200 nm).

nature, the corresponding energy potential due to van der Waal's interaction can be obtained as

$$U_{vdw} = \frac{A_{132}R}{6}\left[b\ln\left(\frac{1+bz}{bz}\right) - \frac{1}{z}\right] \qquad (3.4)$$

where $b = 14/\lambda_{ret}$. Since the Hamaker constant is positive, the van der Waal's force is attractive in nature. Thus, the particle tends to get attracted to the surface and can interact with the surface in spite of not having any specific chemical or biological agent of interaction. Thus, this kind of interaction is called **non-specific interaction**. This plays an important role in several biosensing systems as non-specific interactions introduce systemic noise in the biological system and limit the sensitivity of biosensors over and above the inherent limitations and noise present in any electronic sensor itself.

On its own the expression for the force due to van der Waal's interactions is difficult to interpret. However, the corresponding expression of potential energy allows us to predict when non-specific interactions assume important in a system. Generally, thermal forces tend to move the particle around, while van der Waal's forces tend to attract the particle towards the substrate. When the energy scale of interaction due to van der Waal's forces exceeds that due to thermal interactions ($\approx k_B T$), non-specific interactions become too

large to be ignored. Figure 3-4 shows a simulation of the potential of van der Waal's interaction between the various particles used in this study and a silicon dioxide substrate. As the separation between the particle and the substrate decreases, it is observed that van der Waal's interactions take over thermal ones. For the largest 2.8 μm particles, this transition occurs at about 24 nm, for 1 μm particles it occurs at 13.5 nm and for 200 nm particles it occurs at 4.7 nm. These calculations serve to show that non-specific interactions become significant at separations of the order of 100 nm.

3.3.4 Electrostatic force

The surface charges present on the substrate as well as the particle can induce attraction or repulsion among them. I have not considered this force in my calculations for the following two reasons:

- The substrates as well as particles used in our experiments were all functionalized with biomolecules, such as streptavidin, biotin or PSA. Thus, the charges due to the biomolecules are expected to be dominant over induced charges.
- Previous experimental studies have shown that the surface charges on particles at pH ranging from 5-7 are close to zero (figure 2 of [8]). Thus, the electrostatic force is not expected to play a significant role in the motion of magnetic particles.

3.3.5 Drag force due to resistance from the liquid

It is well known that a solid object moving through a fluid (liquid or gas) experiences a force due to the inertia of the medium. This force manifests itself as air resistance in fast moving everyday objects. In the context of biosensing, this force is important as it places a limitation on the speed of magnetic particles. The drag force on a particle of radius R, moving with a velocity v in water (of viscosity η) is given by[8]

$$\overrightarrow{F}_{drag} = -6\pi\eta R\overrightarrow{v} \qquad (3.5)$$

The drag force is thus, proportional to the velocity of the particle and opposite in direction.

3.3.6 Magnetic force

There are two important sources of external force which can be applied to manipulate the particles in a biosensing system. The first of these are magnetic forces. The magnetic force on a magnetic particle due to an external field is given by:

$$\overrightarrow{F}_m = V_b \chi_m \overrightarrow{\nabla}\left(\frac{|\overrightarrow{B}|^2}{2\mu_0}\right) \qquad (3.6)$$

where V_b is the volume of the bead, χ_m is its magnetic susceptibility, $\overrightarrow{B}$ is the external magnetic field and μ_0 is the permeability of free space. It is important to note that magnetic forces depend on the gradient of magnetic field, as well as its absolute value and thus High Gradient Magnetic separation Systems (HGMS) have attracted a lot of attention in literature [9]. Our laboratory has previously worked extensively on simulation and design of micro-current line patterns for manipulation of magnetic nanoparticles. I found that circular current coils were more effective in application of high gradient magnetic fields than the widely used linear current lines[10]. However, it is to be noted that magnetic fields on their own have a limited capture cross section a few tens of square microns. In the previously mentioned study, for example, I designed a high optimized current line pattern for biosensing with an effective capture cross section of 20 μm x 20 μm.

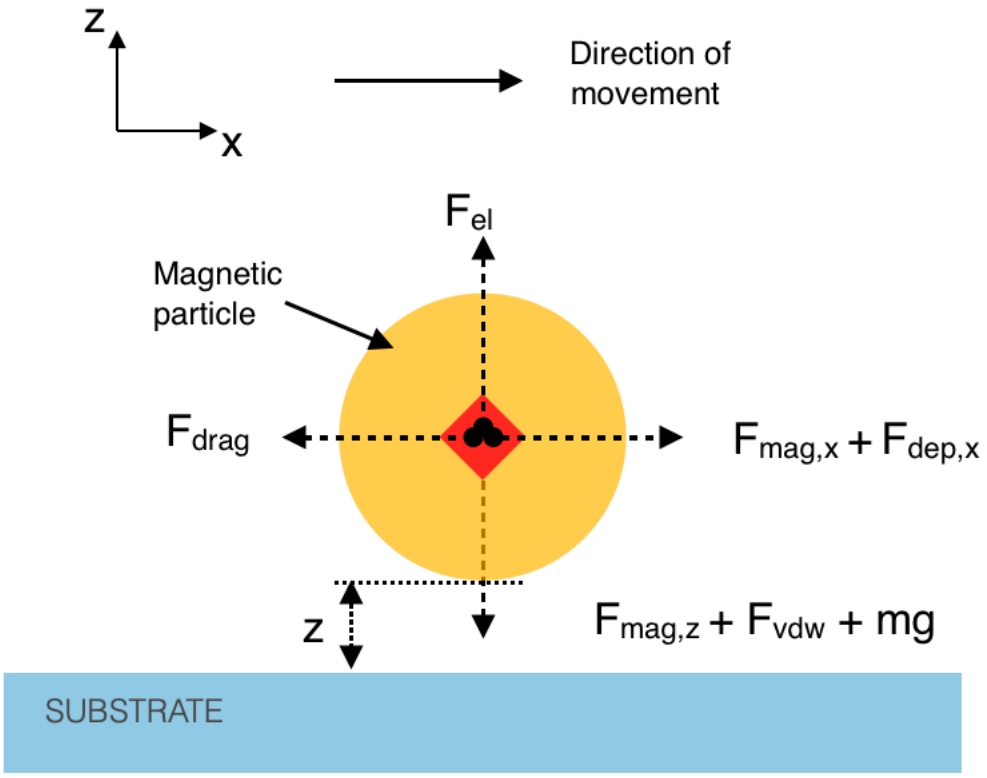

Figure 3-5. Free body diagram of a magnetic particle suspended in a liquid.

3.3.7 Dielectrophoretic forces

It is well known that an electric dipole in an electric field experiences a force proportional to the gradient of the electric field. If the field is strong enough, dipoles can be induced in an otherwise electrically neutral material which then experience a force as described above. This force is known as dielctrophoretic (DEP) force. The DEP force on a particle of radius R in an external AC electric field of frequency ω is given by[11, 12]

$$\overrightarrow{F}_{dep} = 2\pi R^3 CM(\omega)\overrightarrow{E}\cdot\overrightarrow{\nabla}\overrightarrow{E} \qquad (3.7)$$

where, $\overrightarrow{E}$ is the externally applied electric field and CM(ω) is the Clausius-Mossotti factor given as

$$CM(\omega) = \frac{\epsilon_m^* - \epsilon_p^*}{\epsilon_m^* + 2\epsilon_p^*} \qquad (3.8)$$

where ϵ_m is the relative permittivity of the medium (in this case, water), ϵ_p is the relative permittivity of the particle (in this case, polystyrene) and * denotes the complex conjugate. Please note that the expression $\overrightarrow{\nabla}\overrightarrow{E}$ in equation 3.7 is a tensor and the force (a vector) is the result of the dot product of a vector with a tensor. Similar to the expression for magnetic force, the dielectrophoretic force depends on the magnitude as well as the gradient of the electric field.

The above discussion allows us to construct a complete description of the various forces acting on a particle suspended in a liquid medium. Figure 3-5 shows a free body diagram of a particle in the liquid showing the directions of various forces described in this section.

3.4 Three dimensional electromagnetic actuation

The previous discussion has prepared us to discuss the first novel aspect of the biosensing scheme proposed in this work. Here, I will describe a novel scheme for three dimensional actuation of magnetic particles. To motivate our discussion, I recollect the following about forces on a magnetic particle:

- Removal of non-specific interactions requires reproducible can lead to erroneous output of a biosensor and limit its sensitivity.
- Magnetic forces can be used to externally manipulate magnetic particles but the capture cross-section of electromagnetic actuators is limited.
- Electro-static forces can be used to manipulate magnetic particles in addition to magnetic forces.

Several methods for the removal of non-specific interactions have been studied in biosensing literature ranging from mechanical washing[13] to automated washing by DC electric[14] and magnetic fields[15]. I note that previous studies have used either small sensing area and particles of large size or moment, so that one force is dominant in the system and thus the proposed scheme implicitly assumes such particles. For example, in a study by Luis et. al. [14], the authors have shown their results only on large 2.8 μm dynabeads. I have established in the previous section that such large particles show little brownian motion and are much denser than the surrounding medium. Thus, these particles readily sink to the surface of the substrate and hence, vertical forces are not necessary to bring them down. If the same study were to be conducted with 1 μm, 500 nm or 200 nm particles, the number of particles interacting with the surface would be markedly lower. Thus, the following constraints should be followed in designing an actuator for reducing non-specific interactions:

- The forces applied should be well-controlled and reproducible.
- The sensing area of the proposed scheme should be as large as possible.
- The proposed actuation scheme should allow for three dimensional actuation of particles, so that interactions can be induced as well as inhibited in all three dimensions.
- The proposed scheme should allow for tuning the forces depending on the size of the particle.

These objectives are achieved by a dual actuation scheme as described below:

3.4.1 Vertical magnetic actuation

As described earlier, magnetic forces are well understood and several biosensing protocols in literature have been developed to take advantage of high gradient magnetic field systems. Permanent magnets have been the mainstay of magnetic field based manipulation of magnetic particles. Although electromagnets based on current lines have been explored in literature, the small size of electromagnetic systems limits their capture cross-section. Thus, in the proposed actuation scheme, I use permanent magnet to create a weak magnetic field in order to draw small particles to the surface and enhance the interaction of magnetic particles with the surface. Specifically, I approximate the field of the permanent magnet with as a weakly varying magnetic field of near constant magnitude B_0 and gradient $\partial B_z/\partial z$. Thus, the expression for magnetic force reduces to

$$F_m = \frac{V_b \chi}{\mu_0} B_0 (\partial B/\partial z) \qquad (3.9)$$

This expression is valid for a given value of (z,B_0) provided the variation in z is much smaller than the dimension of the magnet. Typical bar magnets are the size of a few centimeters. I will use this approximation in a range of about 100 μm. Thus, within this

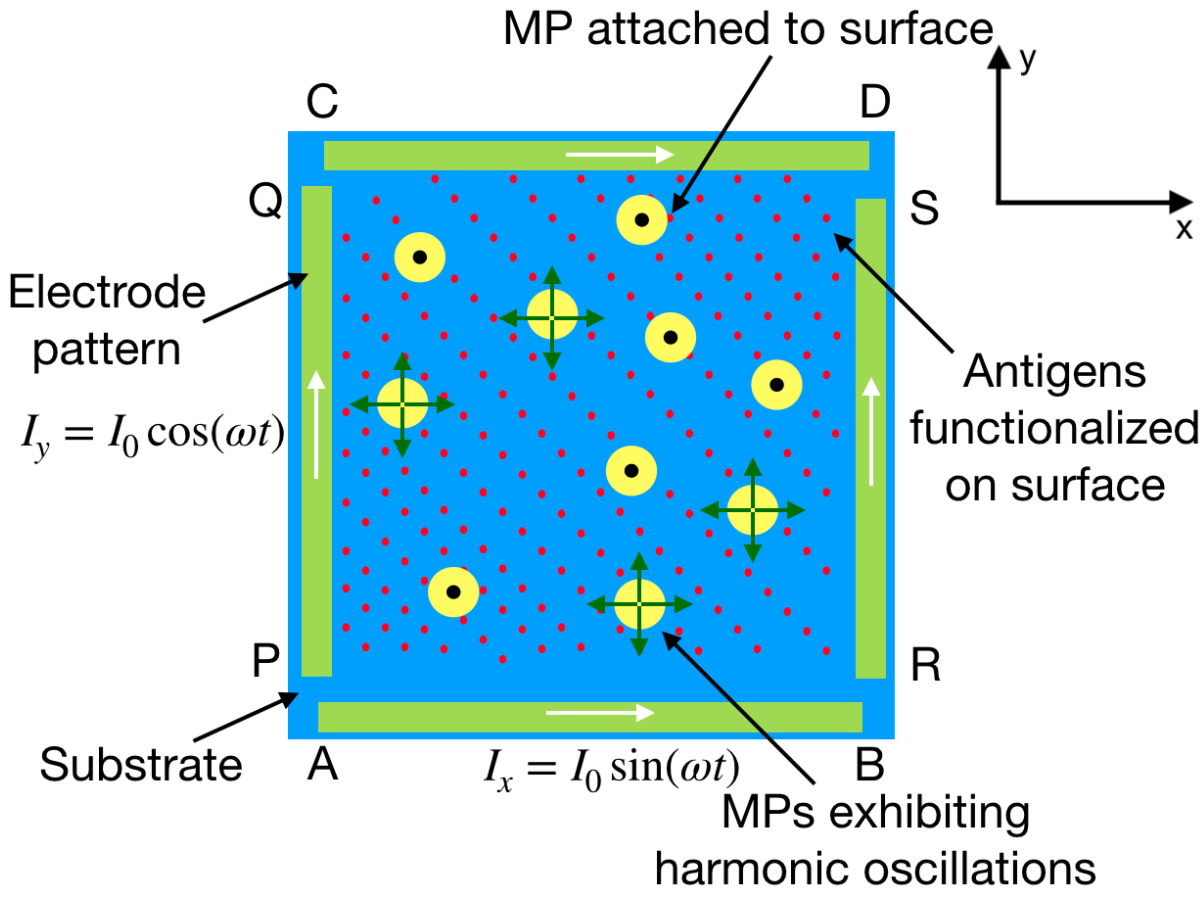

Figure 3-6. Schematic of the proposed DEP actuator. AB, CD, PQ and RS are micro-current lines, each 10 μm wide and 560 μm long. The points B and C are electrically connected. Similarly, Q and R are connected.

range, the magnet serves as a source of constant vertical force on the magnetic particle.

3.4.2 Horizontal dielectrophoretic actuation

Elementary electromagnetic theory tells us that for an electromagnetic plane wave propagating in free space, the magnitudes of electrical and magnetic fields are related as $|\vec{E}| = c|\vec{B}|$, where c is the speed of light. Thus, the magnitude of electric field is approximately eight orders of magnitude larger than that of the magnetic field. This motivates us that for the same amount of current, DEP forces, which are electric in nature are expected to create much higher forces for reducing non-specific interactions. This is the key observation which allows us to increase the sensing area by three orders of magnitude from magnetic force based actuation schemes. To take advantage of the DEP forces over a large area, I propose the design shown in figure 3-6. The design is simple as it contains four electrodes arranged in a square pattern. Each electrode is 560 μm long and 10 μm wide. The points B and C are electrically connected with cables of much smaller resistance than the electrodes. Thus, the points B and C are considered to be at the same electric potential. Similarly, points Q and R are connected. Thus, the electrodes form a pair of resistors, one in each direction x and y. Two sinusoidal currents of amplitude

I_0 and frequency ω, period T($= 2\pi/\omega$) is applied in both directions with a $\pi/2$ phase difference between the currents in the two directions.

On application of sinusoidal current, the electric and magnetic fields in the system are expected to be sinusoidal in time. Maxwell's equations for electromagnetic fields for this system acquire the form

$$\nabla \times \vec{E} = -\frac{\partial \vec{B}}{\partial t} = -i\omega\mu_0\vec{H} \qquad (3.10)$$

$$\nabla \times \vec{H} = \vec{J} + \frac{\partial \vec{D}}{\partial t} = \vec{J} + i\omega\epsilon_0\vec{E} \qquad (3.11)$$

$$\vec{\nabla} \cdot \vec{B} = 0 \qquad (3.12)$$

$$\nabla \cdot \vec{D} = \rho \implies \nabla \cdot \vec{E} = \rho/\epsilon_0 \qquad (3.13)$$

The quantities have usual meanings, and ρ which represents the surface charge density.

From equation 3.10, it can be seen that

$$\nabla \times \vec{E} = -i\omega\mu_0\vec{H} = -i\omega(\nabla \times \vec{A}) \qquad (3.14)$$

where A is the magnetic vector potential such that $\vec{B} = \vec{\nabla} \times \vec{A}$.
Thus,

$$\nabla \times (\vec{E} + i\omega\vec{A}) = 0 \qquad (3.15)$$

$$\implies \vec{E} + i\omega\vec{A} = -\nabla V \qquad (3.16)$$

for some scalar function V. Plugging this expression into 3.11, I get

$$\nabla \times \vec{H} = \vec{J} + i\omega\epsilon_0(-\nabla V - i\omega\vec{A}) = \vec{J} + \omega^2\epsilon_0\vec{A} - i\omega\epsilon_0\nabla V$$

Thus,

$$\nabla \times (\nabla \times \vec{A}) = \mu_0\vec{J} + \omega^2\mu_0\epsilon_0\vec{A} - i\omega\mu_0\epsilon_0\nabla V \qquad (3.17)$$

Since, $\nabla \times (\nabla \times \vec{A}) = \nabla(\nabla \cdot \vec{A}) - \nabla^2\vec{A}$, the above equation can be rearranged as

$$\nabla^2\vec{A} + \omega^2\mu_0\epsilon_0\vec{A} + \mu_0\vec{J} = \nabla(\nabla \cdot \vec{A} + i\omega\mu_0\epsilon_0 V) \qquad (3.18)$$

The above equations do not have unique solutions for $\vec{A}$ and V and given any solution ($\vec{A}$,V), the functions ($\vec{A'}$,V') are valid solutions to the above equations, provided

$$\vec{A'} = \vec{A} + \nabla\lambda$$

$$V' = V - \frac{\partial\lambda}{\partial t} = V - i\omega\lambda$$

for any scalar function λ.

Under Lorenz gauge, λ is chosen such that $\nabla \cdot \vec{A'} + i\omega\mu_0\epsilon_0 V' = 0$. Thus, taking the divergence of equation 3.16 on both sides and dropping the primed superscript, we get

$$\nabla \cdot \vec{E} + i\omega\nabla \cdot \vec{A} = -\nabla^2 V$$

$$\implies \nabla \cdot \vec{E} + i\omega(-i\omega\mu_0\epsilon_0 V) = -\nabla^2 V$$

$$\implies \nabla^2 V + \omega^2\mu_0\epsilon_0 V = -\nabla \cdot \vec{E} = -\rho/\epsilon_0$$

In the sensing area of the actuator there are no charge sources, thus $\rho = 0$. Thus,

$$\nabla^2 V + \frac{\omega^2}{c^2}V = 0 \qquad (3.19)$$

Here, I make the approximation that the frequency of interest is small, such that $c^2 >> \omega^2 V$. Hence, the equation 3.19 reduces to Laplace's equation

$$\nabla^2 V = 0 \qquad (3.20)$$

This can also be obtained by the equivalent assumption that magnitude of magnetic field is much smaller than that of the electric field. The boundary conditions for equation 3.20 are obtained as

$$V(x) = \frac{\rho x}{W.d} \qquad (3.21)$$

where ρ is the resistivity of the electrode material, W is the width of the electrode and d is the thickness (thus, $W.d$ is the area of cross section of the electrode). Solving the Laplace equation with these boundary conditions allows us to simulate the forces on magnetic particles in the sensing area.

Figure 3-7 shows a simulation of the potential energy of DEP forces. For simplification of illustration, I am showing only the case when current is applied along y direction (i.e. current along x direction is zero). It is found that when the current is positive along y direction, the potential energy surface has a gradient in the x direction. This

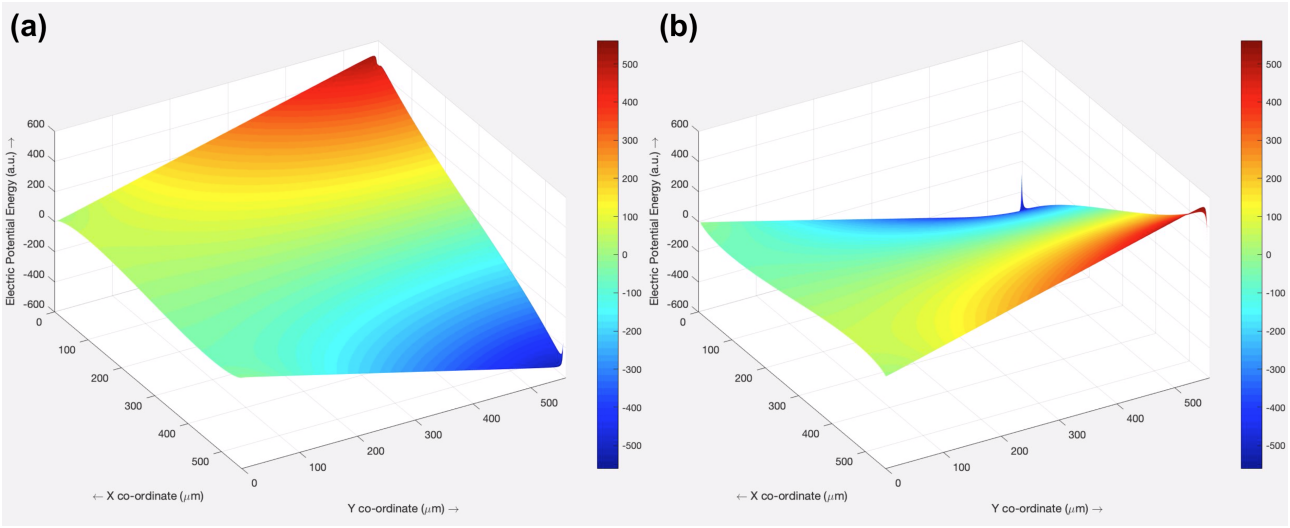

Figure 3-7. Simulation of electric potential energy in the sensing on application of currents. (a) When current is positive along y and (b) when current is negative along y direction.

implies that a force is present along the positive x direction. Any particles present in the sensing area will thus drift towards the positive x direction. On the other hand, when the direction of the current in the electrode changes during the second half of the sinusoidal period, the gradient in the potential energy surface changes direction, creating a force in the negative x direction and changing the drifting direction of the particles. Similarly, when currents are applied in x direction, forces are created in y directions. As a result, when both forces are simultaneously present in the system, the particles will exhibit harmonic oscillations in two dimensions. It is noteworthy that these DEP forces are primarily horizontal in the entire sensing area and acquire a non-trivial vertical component only near the electrodes themselves.

3.4.3 Combined motion

We have described previously how magnetic forces due to weak field of a permanent magnet act primarily in the vertical direction whereas those due to dielectrophoretic forces act primarily in the horizontal direction. When a magnetic particle is suspended in a medium and both types of forces are applied simultaneously, then

ignoring brownian motion, the particle will experience an average downward force as well as a horizontal harmonic force. The motion of the particle in such a case can be is a spiral as shown in figure 3-8. The vertical magnetic force, in addition to gravitational force, accelerates the interaction of the particle with the surface. This is especially necessary for smaller sized particles which would otherwise take a long time for interaction with the surface. After reaching the surface, horizontal forces prevent the particle from interacting non-specifically with the surface by constantly keeping the particle in motion. Any force

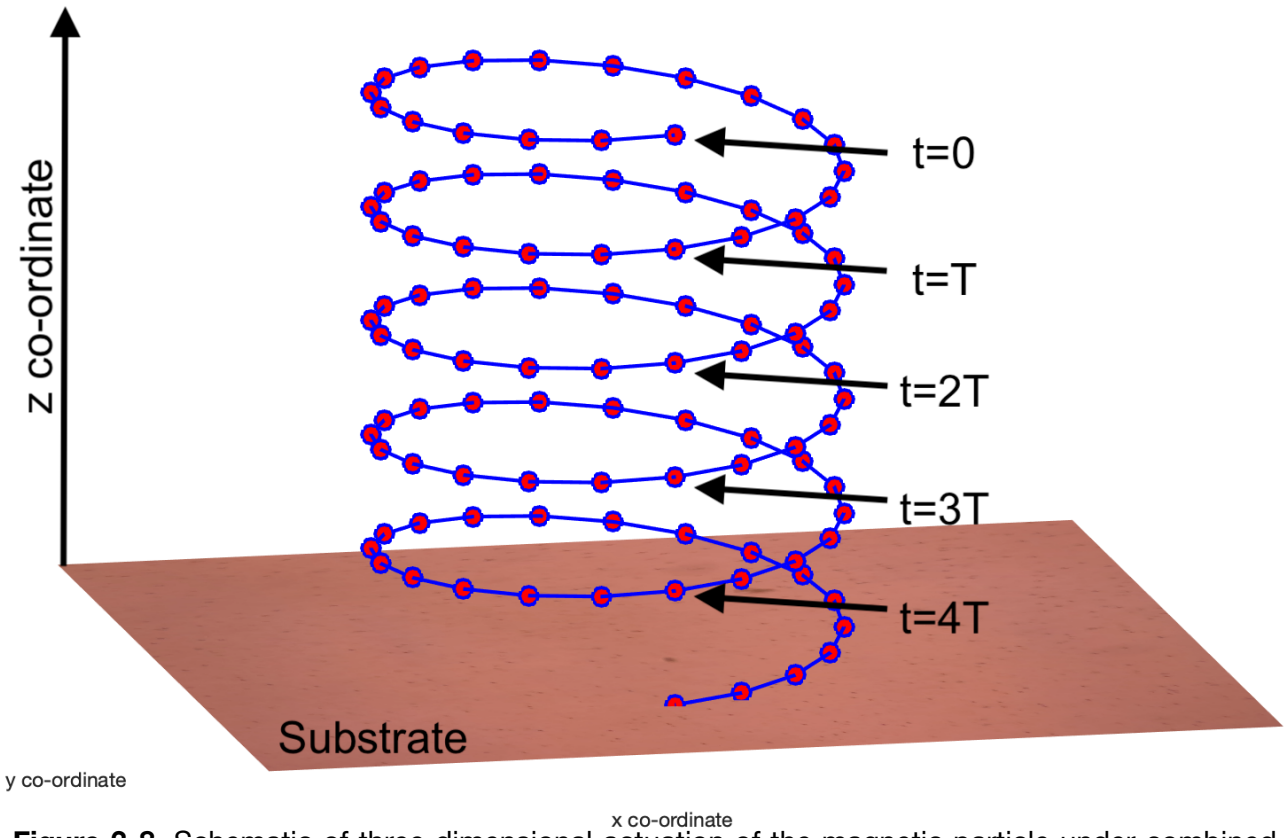

Figure 3-8. Schematic of three dimensional actuation of the magnetic particle under combined dieletrophoretic as well as magnetic forces. The red dots represent various locations of the particle. The vertical forces accelerate the interaction of the particle with the substrate, while the horizontal forces prevent the particle from non-specific interactions after it comes into contact with the surface.

required to stop the particle motion would necessarily have to be larger than the DEP force. Therefore, the DEP forces are applied such that they are greater than the estimated van der Waal's forces from equation 3.3. Here the motion has been exaggerated for ease of illustration.

For the sake of completeness, I would like to mention that the length of the electrodes was chosen to maximize the sensing area for the given field of view of the optical setup. I will show in Chapter 7, the sensing area achieved by this approach is about three orders of magnitude larger than that reported by purely magnetic forces.

3.4.4 The originality of this method of actuation

As stated before, several methods have been proposed in literature for actuation of magnetic particles such as mechanical washing[13], washing via DC electric[14] and magnetic forces[15]. The method closest to my method is the one proposed by Liu et. al in [14]. They used DC electric fields to move 2.8 μm magnetic particles across a sensing area defined by two electrodes and sensed the particles stuck in the sensing area with

spin valve magnetic sensors. The actuation method I have proposed is more suitable than their approach in the following ways:

- The method proposed in this thesis uses AC dielectrophoretic actuation whereas Liu et. al. have used DC dielectrophoretic actuation. DC actuation forces the particles to move across a sensing area over to the other side, whereas AC actuation makes the particles oscillate harmonically wherever they are, without moving them across the sensing area.
- As I will show in chapter 5, the harmonic dynamics of the particles is utilized for biosensing by optical tracking of the particles in a video, rather than just detecting the mere presence or absence of particles in an area.

- The actuation method used by Liu et. al. can actuate particles only in one direction (perpendicular to the linear electrodes), whereas my method can actuate the particles in all three dimensions.

- It should be further noted that the size of the particles used by Liu et. al. is very large (2.8 μm) and thus the particles precipitate immediately. Smaller particles do not precipitate quickly and thus would not be detectable by spin valve sensors embedded underneath the sensing surface. Thus their approach is applicable only to large particles whereas the actuation method presented in this section can work with nanometer as well as micrometer sized magnetic particles.

3.5 Summary

In this chapter, I discussed the properties of magnetic particles in detail. I began by providing an overview of the various types of particles used in this research which range from 200 nm fluorescent particles to 2.8 μm magnetic particles. Then, I described the various forces acting on a particle suspended in a medium in detail. I discussed gravitational and buoyancy force, brownian force, van der Waal's forces, electrostatic forces, magnetic forces as well as dielectrophoretic forces. A discussion of van der Waal's forces allows the reader to understand the theoretical origins of non-specific interactions which limit the sensitivity of biosensing systems. Finally, I describe the design of a novel actuator for three dimensional actuation of magnetic particles by combining both magnetic and dielectrophoretic forces. This actuation method achieves three orders of magnitude more sensing area than that achieved by purely magnetic forces.

3.6 References

[1] http://tools.thermofisher.com/content/sfs/brochures/dynabeads-streptavidin-manual-automated-brochure.pdf

[2] Hatakeyama, M., Mochizuki, Y., Kita, Y., Kishi, H., Nishio, K., Sakamoto, S., Abe, M. and Handa, H., 2009. Characterization of a magnetic carrier encapsulating europium and ferrite nanoparticles for biomolecular recognition and imaging. *Journal of Magnetism and Magnetic Materials*, *321*(10), pp.1364-1367.

[3] Nishio, K., Masaike, Y., Ikeda, M., Narimatsu, H., Gokon, N., Tsubouchi, S., Hatakeyama, M., Sakamoto, S., Hanyu, N., Sandhu, A. and Kawaguchi, H., 2008. Development of novel magnetic nano-carriers for high-performance affinity purification. *Colloids and Surfaces B: Biointerfaces*, *64*(2), pp.162-169.

[4] “Polymer Database”, https://polymerdatabase.com/polymers/polystyrene.html

[5] Raugel, P.J., 2012. Rapid food analysis and hygiene monitoring: Kits, Instruments and Systems. Springer Science & Business Media.

[6] “Dynabeads® MyOne™ Carboxylic Acid” https://www.thermofisher.com/jp/ja/home/references/protocols/proteins-expression-isolation-and-analysis/protein-isolation-protocol/dynabeads-myone-carboxylic-acid.html

[7] Michaelides, E.E., 2015. Brownian movement and thermophoresis of nanoparticles in liquids. *International Journal of Heat and Mass Transfer*, *81*, pp.179-187.

[8] Wirix-Speetjens, R., Fyen, W., Xu, K., De Boeck, J. and Borghs, G., 2005. A force study of on-chip magnetic particle transport based on tapered conductors. *IEEE transactions on magnetics*, *41*(10), pp.4128-4133.

[9] Hatch, G.P. and Stelter, R.E., 2001. Magnetic design considerations for devices and particles used for biological high-gradient magnetic separation (HGMS) systems. *Journal of Magnetism and Magnetic Materials*, *225*(1-2), pp.262-276.

[10] Sharma, J., Ishizawa, S., Yukino, R., Takamura, T., Hanyu, N., Yasuno, H., Handa, H. and Sandhu, A., 2016. Fast and sensitive medical diagnostic protocol based on integrating circular current lines for magnetic washing and optical detection of fluorescent magnetic nanobeads. *Sensing and bio-sensing research*, *9*, pp.7-12.

[11] R. E. Madrid, E. F. Treo, M. C. Herrera, and C. C. Mayorga Martinez, “Bioimpedance and Bioelectricity Basics” (Third edition), Chapter 7, pp. 179-254, ISBN: 978-0-12-411470-8, 2015.

[12] Houssin, T., Senez, V., “Waterborne Pathogens, Detection Methods and Applications”, Chapter 6, pp. 147-188, ISBN: 978- 0-444-59543-0, 2014.

[13] Pollet, J., Delport, F., Janssen, K.P., Jans, K., Maes, G., Pfeiffer, H., Wevers, M. and Lammertyn, J., 2009. Fiber optic SPR biosensing of DNA hybridization and DNA–protein interactions. *Biosensors and Bioelectronics*, *25*(4), pp.864-869.

[14] Liu, C., De Palma, R., Reekmans, G., Laureyn, W., Stakenborg, T. and Lagae, L., 2009. Discrimination of specific and non-specific bindings by dielectrophoretic repulsion in on-chip magnetic bio-assays. *Biosensors and Bioelectronics*, *24*(7), pp.2294-2297.

[15] Pamme, N., 2006. Magnetism and microfluidics. *Lab on a Chip*, *6*(1), pp.24-38.

4. Development of hardware components used in the experimental setup

4.1 Introduction

In the previous two chapters, I have established the importance of smartphones as a platform for development of point of care medical diagnostics systems and introduced a method for three dimensional actuation of magnetic particles suspended in a solution. In this chapter, I introduce the experimental setup used throughout this study. I will cover the motivations behind the design of the components used in the experiments and the improvements in reproducibility and reliability which result from these designs.

The experimental setup consisted of the following components:

- Substrate with micro fabricated current line pattern described in the previous chapter
- Reaction well fabricated from poly dimethyl siloxane (PDMS)
- Printed circuit board (PCB) for application of current
- Optical components for magnification
- Smartphone
- Current source

I now describe the design and fabrication of each component in detail below.

4.2 Micro fabricated current line pattern

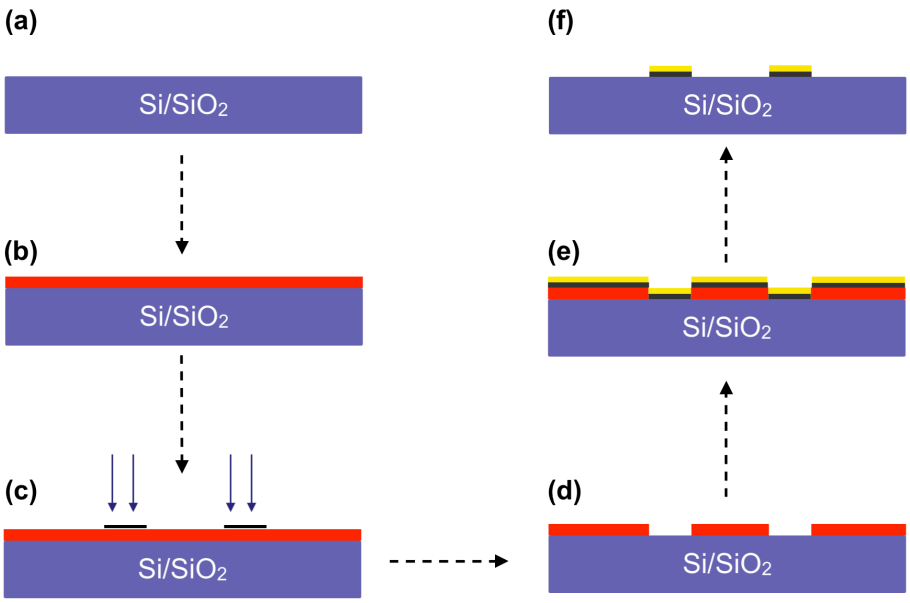

Figure 4-1. Schematic of fabrication of current line patterns with photolithography and electron beam deposition.

The current line pattern was fabricated with conventional photolithography followed by electron beam deposition of metals. I used Si/SiO_2 as well as Si_3N_4 substrates for the experiments reported, with identical fabrication protocol for both types of substrates. A schematic of the fabrication process is shown in figure 4-1. Negative photoresist (AZ5214-E) was spin coated on the substrate as shown in figure 4-1 (b). This was followed by photo exposure of the substrate under a mask with an ultra-violet light source (i-line, 365 nm) as shown in 4-1 (c). Development of the substrate leads to formation of ridges in the substrate where metal electrodes can be deposited. Electron beam deposition of titanium (thickness: 100 nm) and gold (thickness: 100 nm) is performed next as shown in figure 4-1 (e). Finally, lift off is performed for removal of excess photoresist and metal. This results in the fabrication of electrodes 200 nm in thickness.

4.3 PDMS reaction well

Polydimethyl siloxane (PDMS) is a well known polymer used in contact lenses and medical devices. In our experimental setup, the reaction well for containing the sample under analysis was fabricated with PDMS. The steps required for fabrication of the reaction well are:

- Commercially available PDMS (Silpot 184) and its hardening agent were mixed in a ratio of 10:1 (5 mL: 0.5 mL).
- The resulting viscous fluid was de-gassed in a vacuum chamber for 3 minutes.
- The degassed fluid was poured over a clean acrylic substrate of size 70 mm x 70 mm.
- The acrylic substrate was placed on a hot plate and heated at 120℃ for 10 minutes to allow solidification of the PDMS.
- The solidified PDMS was transferred along with the acrylic substrate onto a commercially available laser cutter where square reaction wells of outer side 4 mm and inner side 2 mm were cut into the solid PDMS.

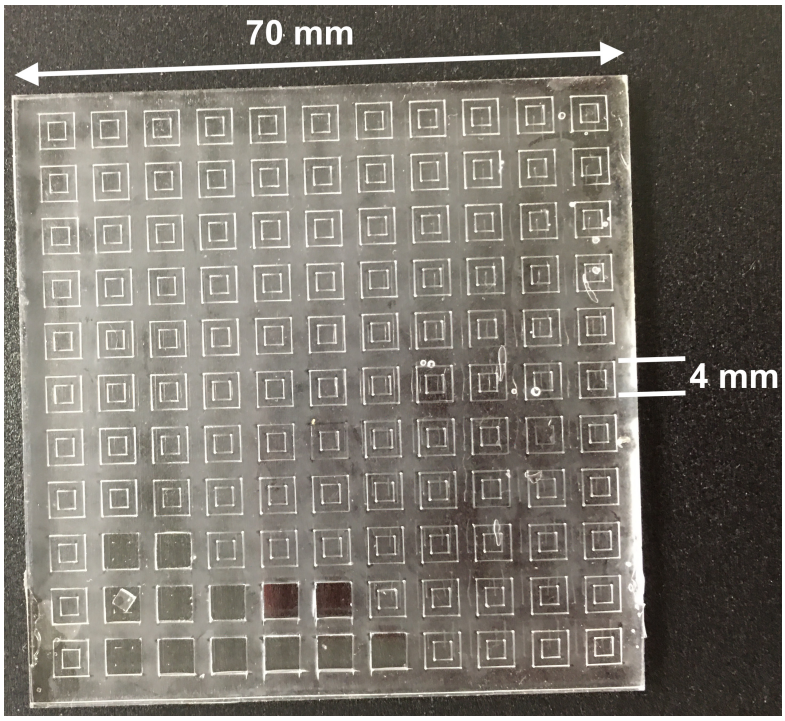

Figure 4-2. A photograph of solidified PDMS with an array of 11x11 (total of 121) reaction wells cut into it. Some reaction wells have been removed.

The laser cutter contains a 40 W continuous CO_2 laser and operates with pulse width modulation at a pulse frequency of 1000 Hz, duty cycle 50% and head travel speed of 10 mm/s. Once the reaction wells have been cut into the PDMS, individual reaction wells can be removed and attached onto the silicon dioxide substrates.

Figure 4-2 shows a photograph of 121 reaction wells cut into solidified PDMS on the 70 mm x 70 mm substrate. Some wells have been removed. The thickness of the PDMS was measured to be 0.75 mm and the volume of the reaction well was found to be 3.0 µL. Thus, the PDMS reaction well ensures that a constant volume of approximately 3 µL is under analysis. Figure 4-3 shows a photograph of the substrate after the attachment of the reaction well.

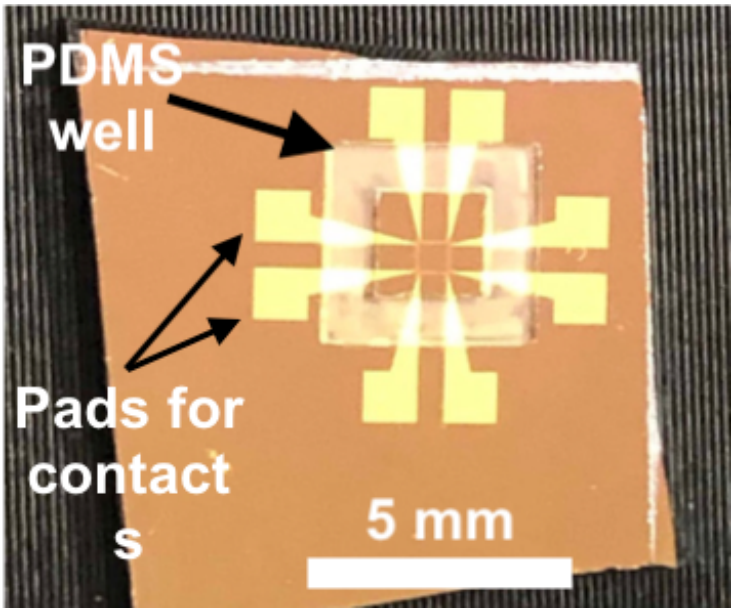

Figure 4-3. A photograph of the actuator after attachment of the reaction well.

While large scale fabrication of regularly shaped reaction wells is not a scientific achievement on its own, it is a critical step for making the biosensor easy to use and ensuring reproducibility of results. Thus, it is a **minor originality** of this research.

4.4 PCB for current application

In figure 4-3, the eight exposed gold pads for making contacts with other circuits are visible. Each pad is approximately 1 mm x 1.5 mm in size. In electronics, contacts between integrated circuits and external circuits is often performed via soldering. Soldering is a well known and mature technology by which two or more metals are joined together by a filler metal (called solder). This technique is highly dependent on the materials involved with the most commonly used materials being alloys of copper, zinc or aluminum. However, gold is not compatible with soldering materials and thus, soldering cannot be used to connect the actuator with the current source.

To solve this problem, in academic research, silver paste is commonly used for making contacts along with a conductive material such as copper tape. I found that this method of making contacts was

(a) unreliable,
(b) time consuming as it took approximately 30 minutes to an hour to create contacts, and
(c) often resulted in mechanically weak connections which would break during the experiment, thus wasting time and materials.

To solve this problem, I developed a method for making contacts which
(a) does not use a consumable item such as silver paste,
(b) is fast (takes 1minute or less), and
(c) results in mechanically robust contacts.

Our method consists of two parts a printed circuit board and a 3D printed mechanical holder. The PCB is 30mm x 30 mm, consists of two layers and its design is shown in figure 4-4.

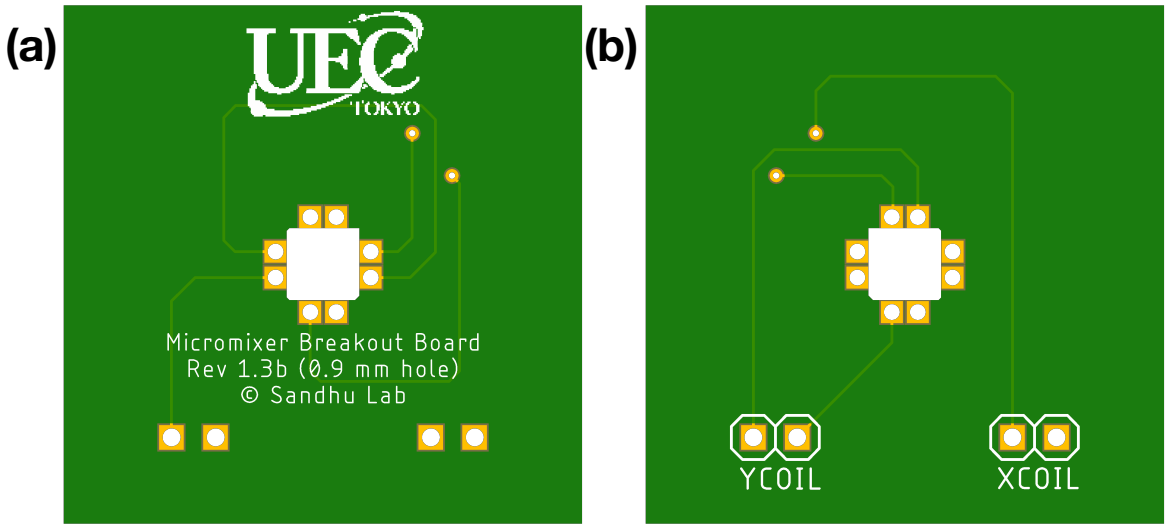

Figure 4-4. Design of the two layer PCB used for making contacts with the actuator. (a) top side, and (b) bottom side.

This design contains eight vias for connecting spring loaded pogo pins. The area corresponding to reaction well in the middle of the pattern is milled out during the manufacturing process, creating a window for observation of the sample. Using the notation introduced in figure 3-6, the vias corresponding to points B and C are connected internally within the PCB. Similarly, the vias corresponding to points Q and R are connected. Thus, the PCB receives current from four terminals (labelled as 'XCOIL' and 'YCOIL') and distributes it to the eight terminals. It should be noted that the X and Y branches of the PCB are independent of each other, and thus currents can be applied to the two axes of the actuator independently of each other.

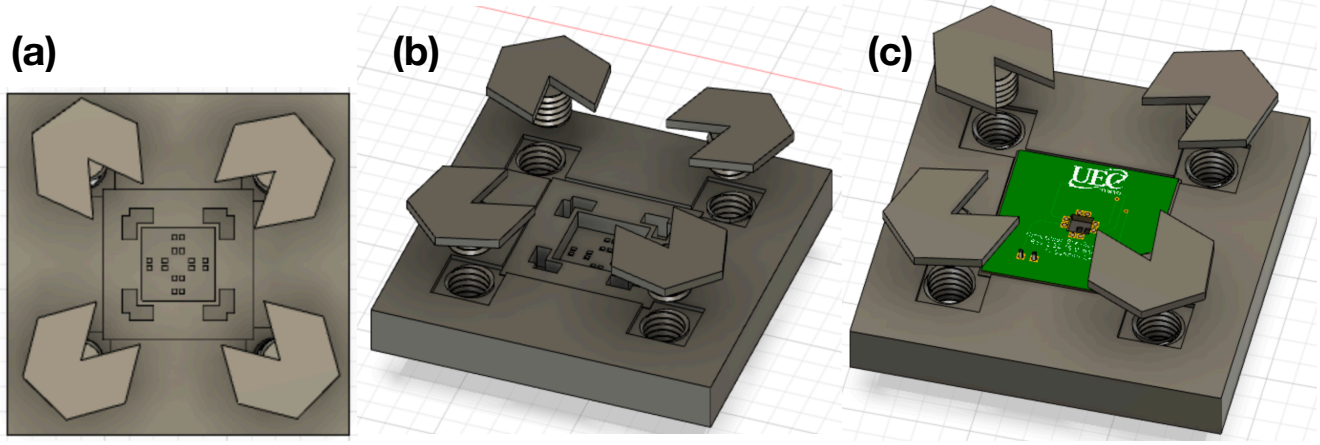

Figure 4-5. Schematic render of the 3D printed holder for mechanical alignment of the substrate with the PCB. (a) Top view of the holder with four notched, wide base screws, (b) Perspective view of the holder, and (c) Mechanical arrangement of the holder with the PCB described above.

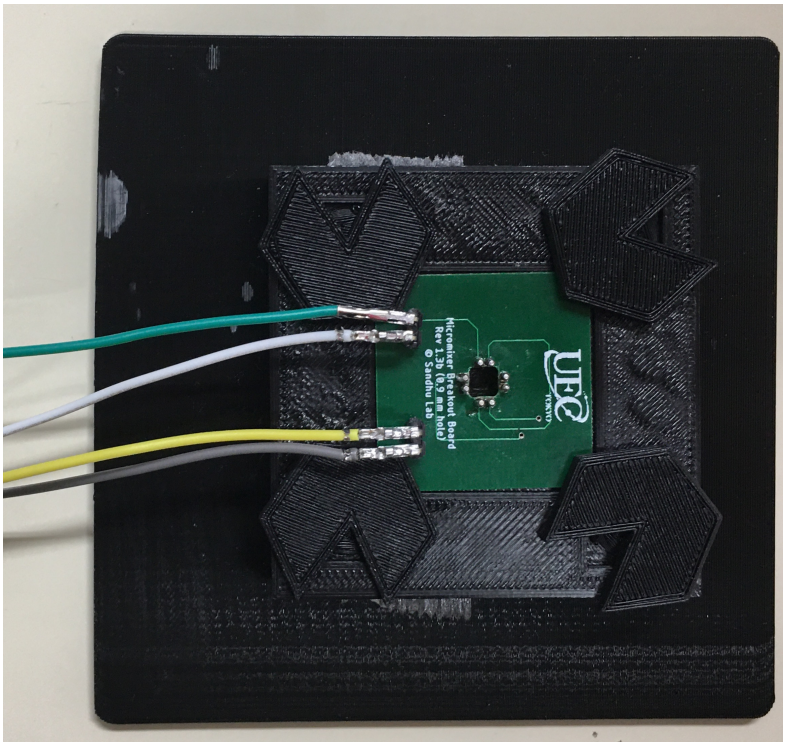

Figure 4-6. A photograph of the current application assembly. The PCB is mounted on a holder which also houses the substrate. Four 90° jumper pins are soldered onto the PCB and wires are drawn from each to be connected to the current source.

The second part of the contact assembly consists of a 3D printed holder. The design of the holder is shown in figure 4-5. The holder consists of a central well with alignment markers for alignment of the actuator pads with the PCB as shown in figure 4-5 (a). The holder is designed to house the PCB and the substrate within it as shown in figure 4-5 (c). Four screws printed with the holder are used to apply light pressure on to the PCB so that the spring loaded pogo pins are under tension and the contact of the pins with the substrate is robust. The screws contain a notch for insertion and removal of the PCB.

Figure 4-6 shows a photograph of the current application setup. The PCB and holder are lightly pressed against each other by four screws. Creating contacts requires placing the substrate inside the substrate well and aligning the pads of the substrate with alignment markers. The PCB is then inserted into the slot meant to house it. The screws are tightened in order to apply light pressure. This setup allowed us to create robust contacts between the actuator and the power supply within 1 minute. The design of the PCB was performed in AutoDesk Eagle[1] software whereas the design of the holder was performed in AutoDesk Fusion 360[2] CAD software.

As with the fabrication of PDMS wells, fabrication of 3D printed chip holder and PCB is not a new scientific result but it is extremely important step to make this method practical for use in real world applications. The design I have come up with has the advantage that there are no consumable items as in the case of silver paste contacts or soldering. The holder and PCB are reusable and the pogo pins used are rated for use at least 200,000 times. While I have not tested it so many times, the same holder and PCB have been used about 500 times in our lab and do not show any signs of wear or tear. Thus, this is an extremely robust setup for making contacts and is also a **minor originality** of my research.

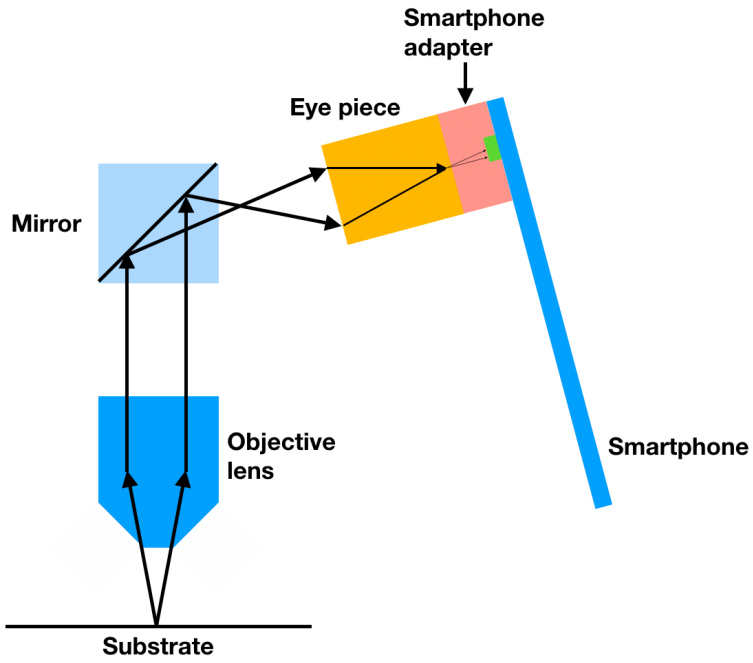

Figure 4-7. Schematic of the optical setup for observation with a smartphone.

4.5 Optical setup

All the optical measurements reported in this study were obtained by a smartphone mounted on the eye piece of a microscope (Olympus BX-51). Thus, the objective lens of the microscope was used but the high resolution microscope cameras (such as Olympus DP 71, also available on the microscope) were not used. The optical setup thus, consists of an objective lens (20x magnification, numerical aperture 0.45), an eyepiece (10x) and the smartphone. The limit of resolution of the system is determined by the objective lens and is calculated as

$$\Delta x = \frac{0.61\lambda}{NA} = \frac{0.61 \times 0.40}{0.45} \approx 0.54\mu m \qquad (4.1)$$

assuming a minimum wavelength of 400 nm for observation. Thus, single fluorescent particles of diameter 200 nm were not observable with optical measurements. A schematic of the optical setup is shown in figure 4-7. The substrate is imaged with an objective lens and the light is reflected by a mirror into the eye piece. The eye piece focuses the light a few millimeters from the surface of the lens. An adapter is mounted on the eyepiece which can adjust the separation between the camera and the eye piece. The separation is adjusted before start of the experiment to obtain a good focus.

4.6 Smartphone

The smartphone used in this study was an iPhone 6S Plus (Apple Inc.). The smartphone features a camera with a 4K image sensor (2160 x 3840 pixels). Videos were recorded by a commercially available application called ‘Filmic Pro’. All the videos were recorded at 24 frames per second. Thus, the measurements reported do not require any features other than a 4K camera. The per-pixel spatial resolution of the videos obtained was 0.4 µm i.e. each pixel in the video represented a square area of 0.4 µm x 0.4 µm on the substrate.

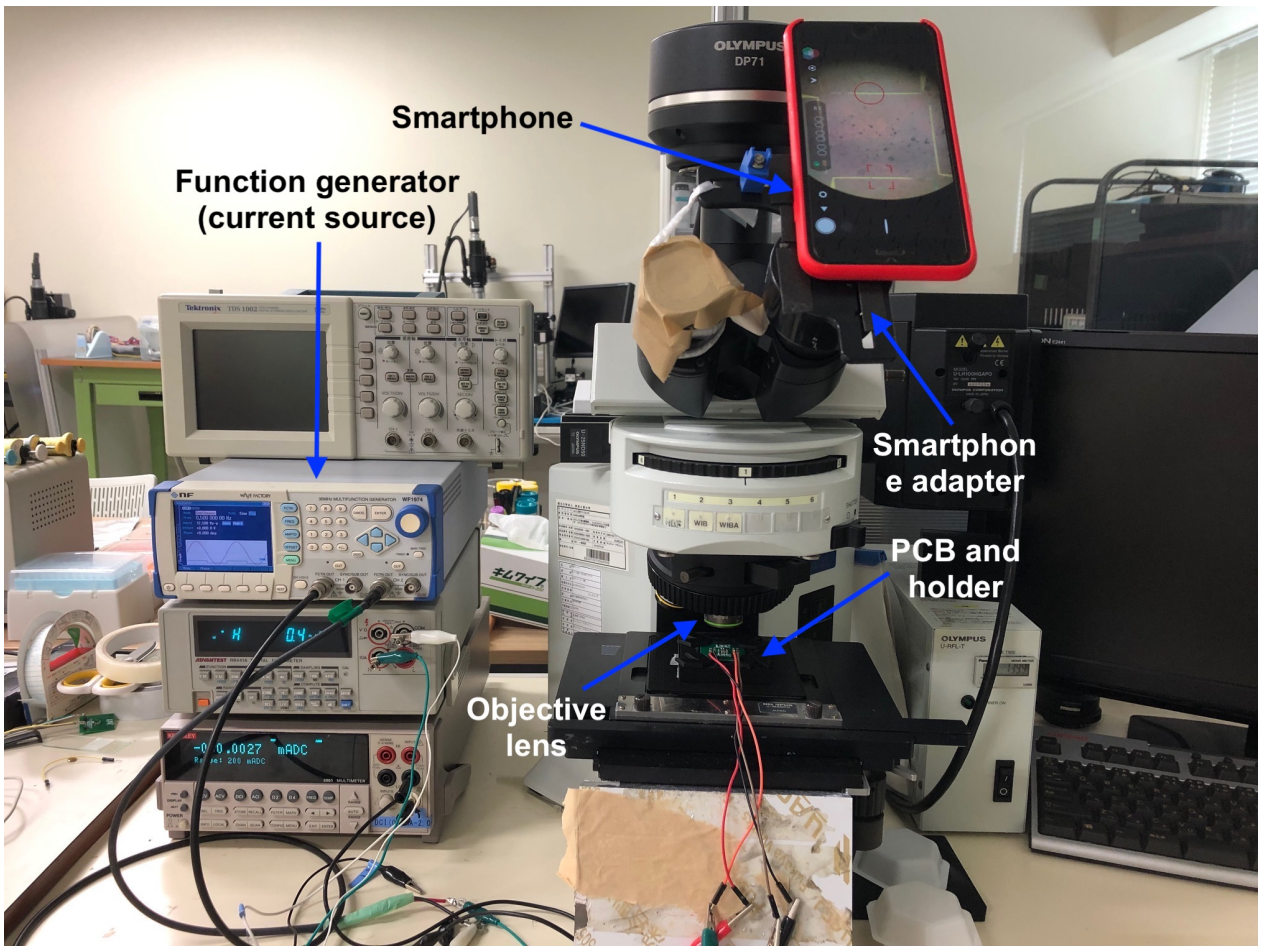

Figure 4-8. A photograph of the complete experimental setup.

4.7 Current source

We used a two channel programmable function generator (WF1974, NF Corporation) as the current source. The two channels of the function generator were used to apply currents in x and y directions respectively. The frequency was kept at 0.5 Hz in all measurements (unless otherwise mentioned) and the amplitude of the sinusoidal voltage was adjusted to obtain a current with amplitude 30 mA (peak to peak amplitude 60 mA).

A photograph of the complete experimental setup with the above components is shown in figure 4-8. One of the eye pieces of the microscope was covered with tape to reduce the effect of ambient light on our measurements.

4.8 A portable experimental setup

The results presented throughout this thesis are based on the experimental setup described in previous sections and shown in figure 4-8. However, towards the end of my research, I have worked to miniaturize the experimental setup. Here I will present some preliminary results of a miniaturized experimental setup.

Figure 4-9 shows a 3D CAD design of a miniaturized experimental setup, consisting of a small microscope. The microscope allows adjusting the focus by moving the dial in vertical direction. A tube containing a magnifying lens fits into the annular ring (not shown in figure 4-9 to avoid excessively cluttering the figure). The chip holder and PCB assembly described in section 4.4 fits onto a base which contains a mechanism based on nuts and

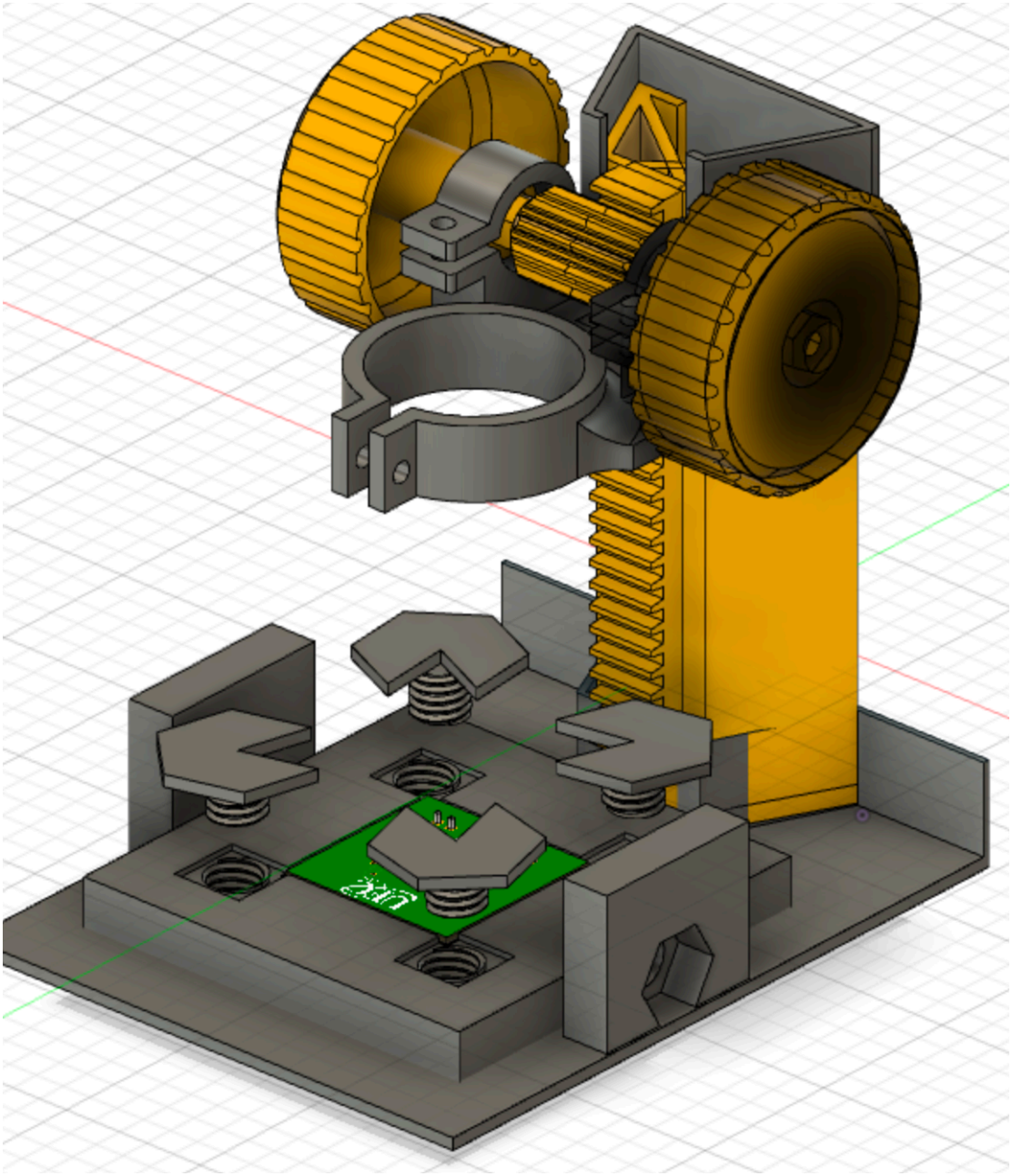

Figure 4-9. A CAD design of the miniaturized optical setup. The 3D printed chip holder described in section 4.4 as well as the PCB are placed on the stage of a 3D printed microscope. The setup allows adjustment of the focus as well as adjustments to the position of the chip holder with a hexagonal but and bolt mechanism.

bolts (not shown) to adjust the position of the chip. The design shown is partly based on an open source microscope design from [3].

Similar to the microscope, the function generator for application of current can also be miniaturized. In fact, several low-cost function generators are available off the shelf. The current prototype uses a low cost function generator based on XR-2206 function generator chip[4].

A complete prototype of the small, portable point of care diagnostics system is shown in figure 4-10. The cost of this experimental setup is estimated to be about 2000 yen ($20) when assembled in a laboratory. This does not include the cost of the smartphone, mobile power bank or lens. This cost is expected to come down as more units are manufactured after commercial adoption of the biosensor.

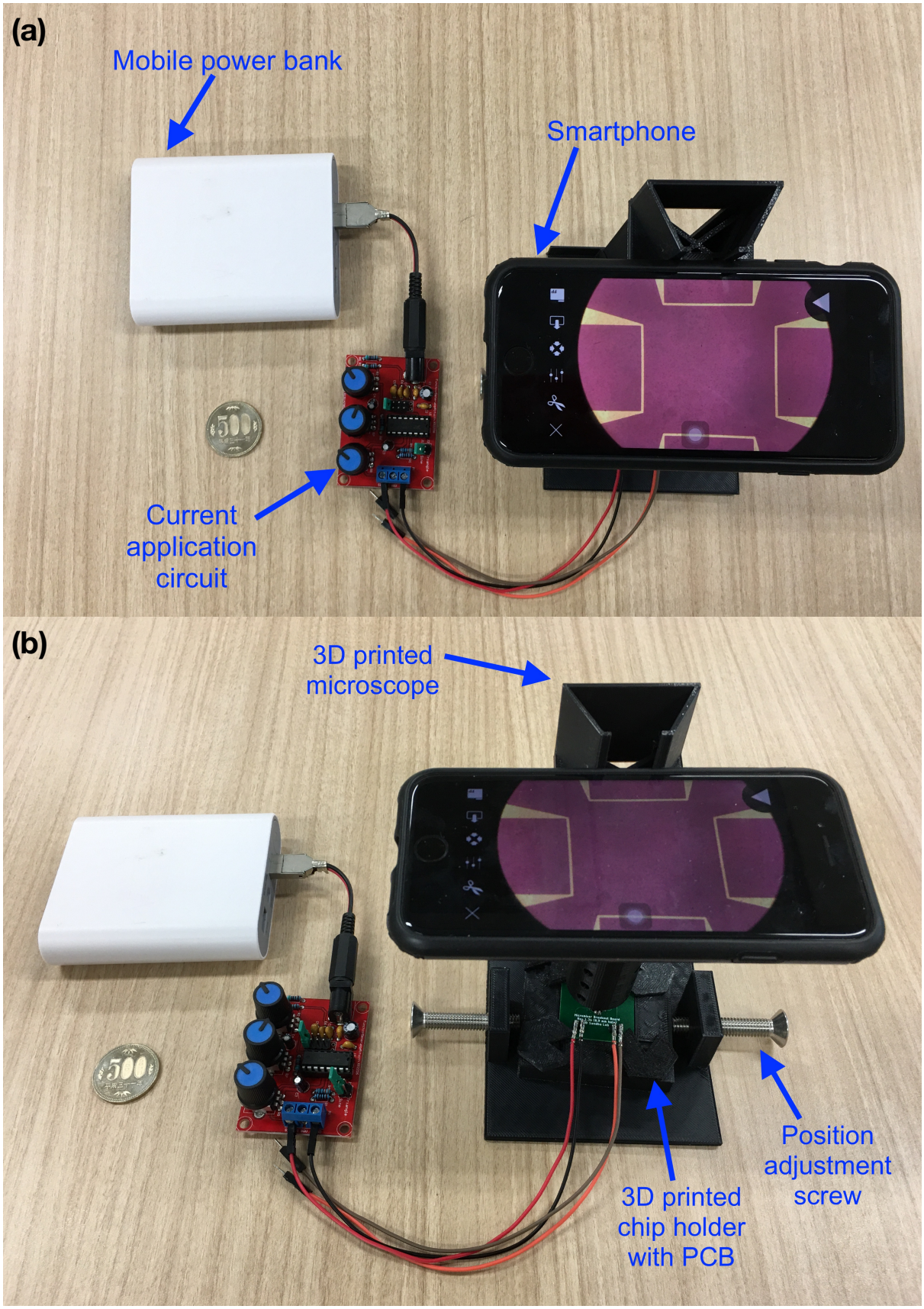

Figure 4-10 A prototype of the portable medical diagnostics system. A 500 yen coin is shown for scale. (a) The system is powered with a mobile power bank and consists of a current application circuit (b) A smartphone mounted on a 3D printed microscope is used to take 4K videos of the biosensing chip (not visible in these images). The video is then uploaded to a remote 'cloud' computer where they are analyzed and the results are sent back to the user.

4.9 Summary

In this chapter, I introduced the experimental setup used in this research. I began by explaining the method for micro-fabrication of current line. In order to reduce variability in experimental conditions and ensure reproducibility, I fabricated PDMS reaction wells and a printed circuit board for creating robust contacts quickly. The optical setup used in this study has a diffraction limited resolution of 0.54 μm. Finally, I presented preliminary results of a miniaturized portable experimental setup.

4.10 References

[1] Eagle PCB Design Software, https://www.autodesk.com/products/eagle/overview

[2] Fusion 360, https://www.autodesk.com/products/fusion-360/overview

[3] USB microscope Focus stack, https://www.thingiverse.com/thing:2945251

[4] XR-2206 Datasheet, https://www.sparkfun.com/datasheets/Kits/XR2206_104_020808.pdf

5. Development of software for automating the data analysis

5.1 Introduction

This chapter focuses on methods for automated optical detection of magnetic beads in smartphone camera images with software. I first introduce the need for automating data analysis in the context of point of care diagnostics. The methods for optical detection are classified into two types: (a) detection of micrometer sized magnetic particles, and (b) detection of nanometer sized fluorescent magnetic nanoparticles (FG beads, 200 nm). A method for accurate detection of beads in images allows us to sequentially analyze several frames in a video and track the positions of the particles in each frame. I explain the limitations of previous approaches particle tracking methods and my solutions. I also show experimental results of tracking of particles in a smartphone video. While position tracking algorithms have been developed in many areas of engineering, I use the algorithm developed in this chapter to demonstrate for the first time a point of care biosensing protocol based on tracking of magnetic particles in smartphone videos.

5.2 The need for automating data analysis

In the first chapter, I showed that the number of public health workers in a developing country is much more than the number of doctors. For example, in the case of India, the number of public health workers is 20 times that of professional doctors. The objective of 'healthcare for all' laid out under sustainable development goal (SDG #3) can be achieved only if these public health workers are enabled to operate as diagnosticians. Previous experience has shown that when trained well, these workers are quite effective in successfully executing stated policy objectives like eradication of polio virus. However, public health workers have their own sets of challenges which may not be readily apparent to scientists developing next generation medical diagnostics technologies:

- Public health workers are often extremely busy as they serve several hundred children and patients every day.
- Workers are often uneducated. Some workers are even illiterate, meaning that they are unable to read or write their *own name*, never mind anything else.
- Public health workers have several duties apart from administering tests and providing medicines.
- In a public health emergency such as the outbreak of an epidemic, several hundred patients may need to be tested in a short span of time.

Thus, any steps that can be adopted to reduce the workload of these workers should be adopted in the very design of the biosensing technology. Two specific steps which can go a long way towards reducing the workload of public health workers are:

- The data analysis should be completely automated. The workers will not understand even the basics of magnetic particles and their significance. Thus, they should not be involved in obtaining actionable information once raw sensor data has been collected.
- The data collected as well as test results should be available as soon as possible to various stakeholders involving not only patients but also doctors and public health officials located far away.

I have implemented both these steps in the design of the biosensing systems that I am going to describe in the coming chapters. Specifically, I have used image and video processing algorithms to automate data analysis with software. Moreover, I have developed a system which integrates the smartphone with a remote ‘cloud’ computer. The data obtained by the smartphone is automatically uploaded to the remote computer, which triggers an automatic analysis of the raw data. The results obtained are shared with the patients, doctors and public health officials. This is performed automatically in software without the healthcare worker needing to even press an ‘upload' button.

In the rest of this chapter, I will describe the algorithmic details of automated data analysis methods I have developed. This will include automated detection of micrometer sized particles in an image, automated detection of fluorescent particles in an image as well as optical tracking of particles in a video.

5.3 Detection of micrometer sized particles

Consider an image of magnetic particles taken from a smartphone camera as shown in figure 5-1. In this example, 2.8 μm beads are imaged. A small part of the full 4K video frame is shown for ease of illustration. There are four steps required to accurately detect positions of magnetic particles in the image in an automated way as described below.

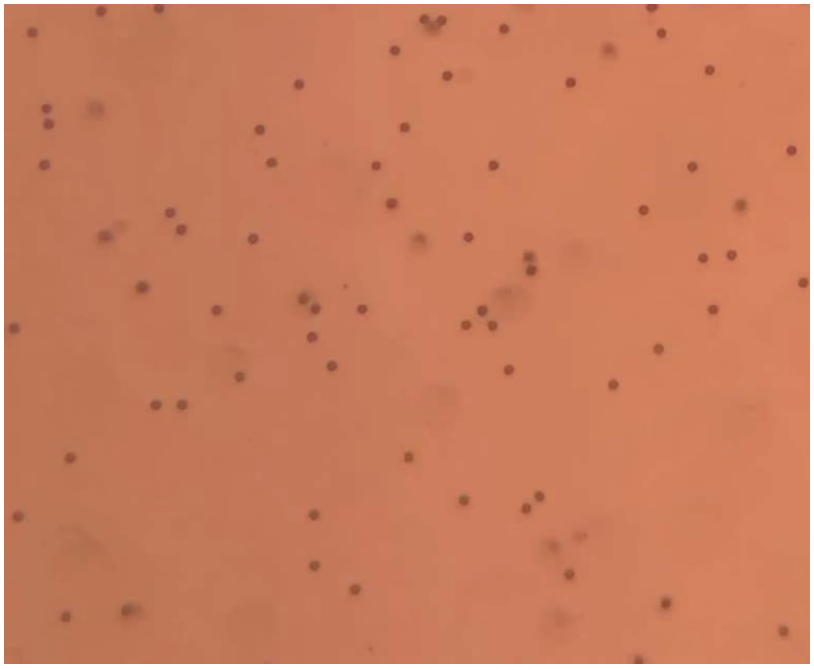

Figure 5-1. An image of 2.8 μm particles taken from a smartphone. This image will be used to illustrate the steps for detection of particles in smartphone images. Scale bar for this image is not drawn as the image processing is demonstrated on the image and scale bar will act as noise.

5.3.1 Grayscale conversion

The first step is to convert the color image into a gray scale image which shows the intensity of light at each point and discards the color information. The result of conversion of the above image into grayscale is shown in figure 5-2.

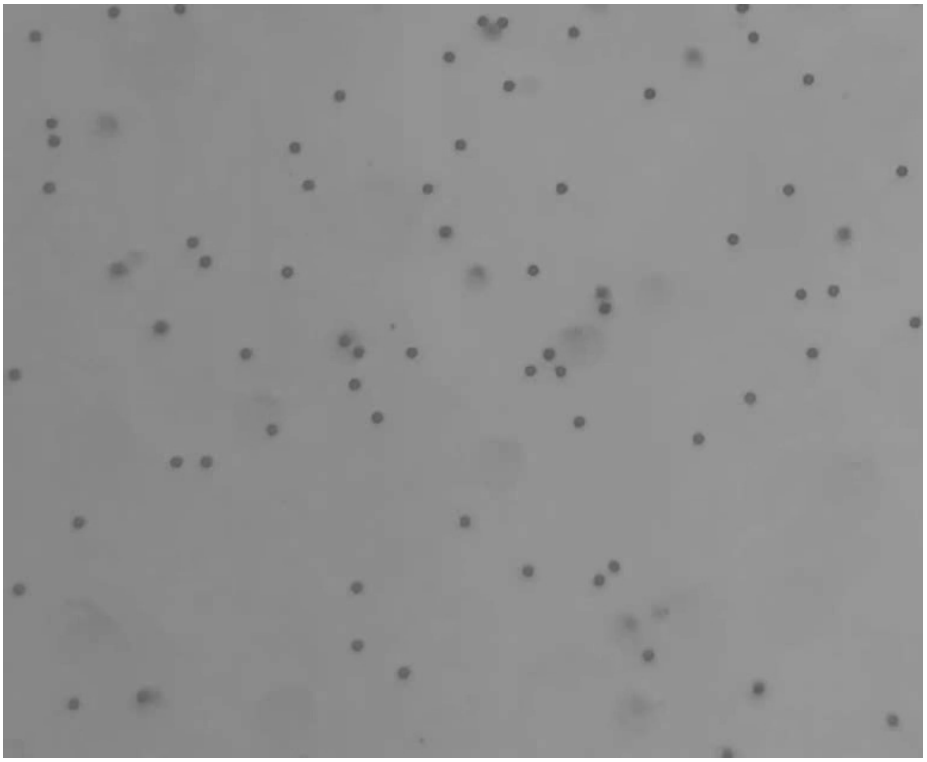

Figure 5-2. Grayscale of the above image.

5.3.2 Template matching

From the original image as well as the grayscale image, it is clear that the magnetic particles are well resolved and the sizes and shapes of all the particles are uniformly similar. This allows us to perform template matching with a known photograph (a template) of the particle we want to detect. Mathematically, template matching is equivalent to a

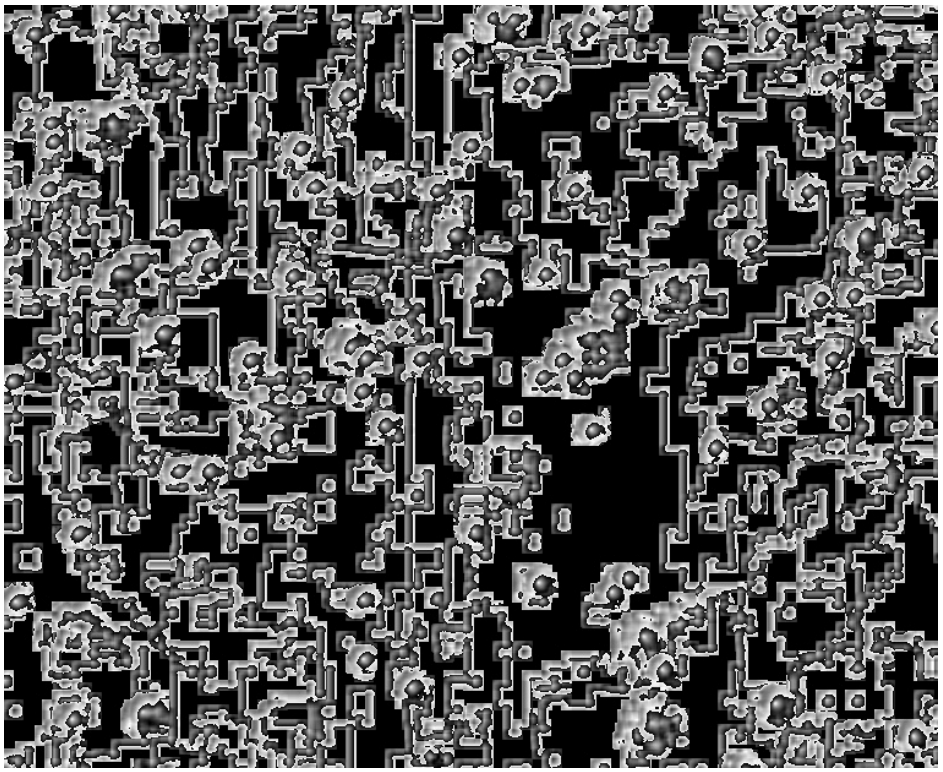

Figure 5-3. Results of template matching in the above image.

convolution or cross-correlation with a kernel specified by the template[1]. Locations where the pattern being matched is present will have a higher cross-correlation with the template , resulting in a high output whereas empty locations will have a very small or no correlation with the template, resulting in low output. After performing the convolution, the result is normalized to lie between 0 and 1. Thus, the cross-correlation results can be interpreted as the probability that a particle is present at the given location. The result of matching the above image with a template of the particle is shown in figure 5-3.

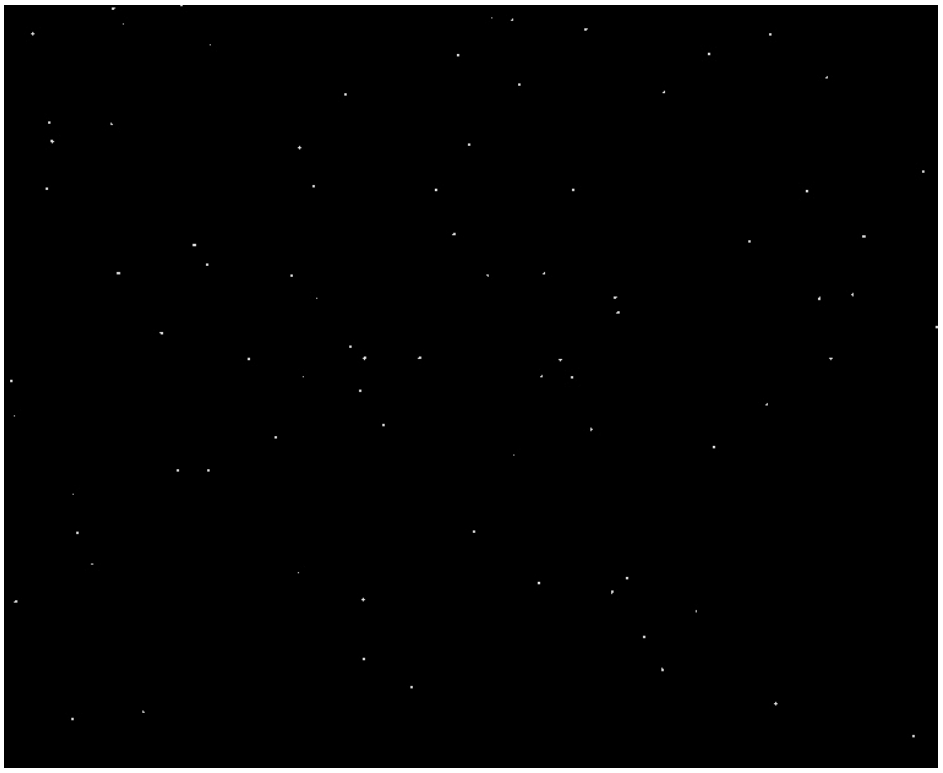

Figure 5-4. Result of thresholding the above output and choosing locations where the output is greater than 0.8 (probability > 80%).

5.3.3 Thresholding

As can be observed in figure 5-3, the results of template matching contain a lot of noise. This is expected and can be mitigated by choosing only the locations where the probability of finding a particle is very high. For example, I chose a threshold of 0.8 and choose locations where the probability of finding a particle is at least equal to the threshold. The results of the thresholding operation are shown in figure 5-4.

5.3.4 Non-maximal suppression (NMS)

The result obtained in the previous step contains very little or no noise and the locations of the particles are clearly identified. However, it may contain false positives. This can be understood from the fact that while the pixel corresponding to the center of a particle is likely to have a high output, pixels just adjacent to the center may also show a big output. This can lead to a single bead being counted multiple times during detection. To avoid this, non-maximal suppression (NMS) is used. The NMS algorithm divides the positions obtained after thresholding and discards locations which have a smaller output than their immediate neighbors within the radius of the particle. Thus, only points with the maximal outputs are identified and non-maxima are suppressed. In the example above, after thresholding 307 pixels were identified as containing beads. However, only 80

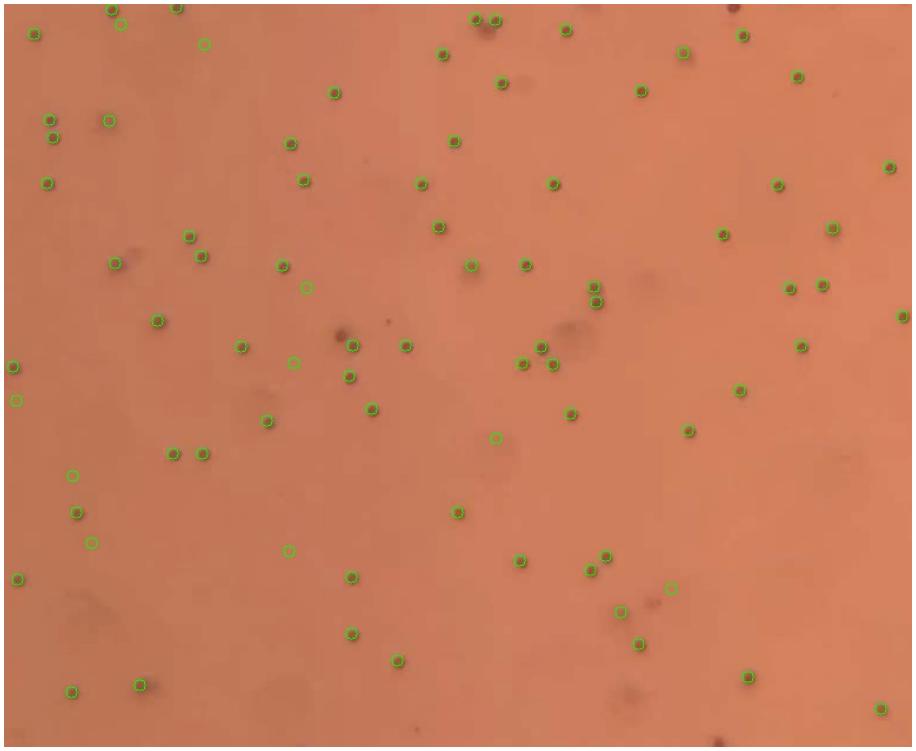

Figure 5-5. Locations of parties identified after non maximal suppression, shown with green circles.

candidates remained after non-maximal suppression. This example illustrates that NMS plays an important role in accurate detection and counting of particles in an image. The results obtained after non-maximal suppression are shown in figure 5-5. Green circles have been drawn around the centers of the beads identified. It can be seen that the method accurately detects almost all the particles present in the image. The false negatives occur for beads which are out of focus and thus have a low cross-correlation output.

Although the method was illustrated for 2.8μm sized particles, the algorithm for detection of 1 μm sized particles is the same with the appropriate choice of template.

5.4 Detection of fluorescent nanoparticles

As compared to micro-meter sized particles, the images of fluorescent nanoparticles are markedly different. The sizes as well as luminosity of the particles are not uniform for all the particles. Thus, template matching cannot be used to estimate the locations of particles in the image. Figure 5-6 shows an example of image of fluorescent magnetic nanoparticles (f-MNPs) captured with a smartphone. It can be seen that the illumination from the light source is not uniform across the image. While this can be improved with better experimental setup, in practice the illumination of the substrate is never uniform enough to ensure equal luminosity and apparent size of fluorescing particles. Thus, the algorithm for automated detection and counting of f-MNPs is slightly different from the one described earlier. The detection method contains two steps.

5.4.1 Estimation and removal of background

In the first step, the distribution of background illumination from the light source is estimated. This estimated background is subtracted from the original image. The steps are summarized as follows:

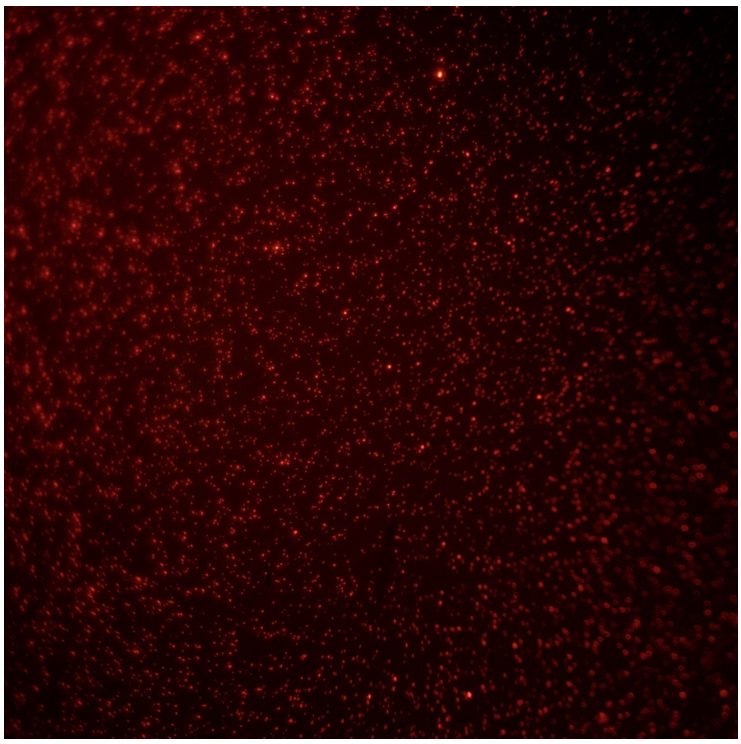

Figure 5-6. An image of fluorescent magnetic nanoparticles taken with a smartphone. Similar to figure 5-1, a scale bar is not being shown for this image.

- Morphological erosion of the image with a kernel, K.
- Morphological dilation of the image with the same kernel, K. The output of this operation is the estimated background.
- Subtraction of the background from the original image to obtain an image with near uniform background illumination.

Mathematically, the grayscale erosion of an image I with a kernel K is defined as[2]

$$(I \ominus K)(x) = \min_{y \in K}[I(x+y) - K(y)] \qquad (5.1)$$

Here the minimum is taken over all positions y where K is defined.

Similarly, the dilation of an image I with a kernel K is defined as

$$(I \oplus K)(x) = \max_{y \in K}[I(y) + K(x-y)] \qquad (5.2)$$

Thus, the background B is estimated to be

$$B = (I \ominus K) \oplus K \qquad (5.3)$$

The erosion step suppresses the edges of small objects[3] in the image such as f-MNPs but large structures, such as the background illumination are left unchanged. However, since the erosion step chooses the minimum of the intensity in a neighborhood around each pixel, the output of the erosion step has a lower intensity than that of the original image. The next step of dilation restores the intensity of the estimated background to that in the image. Although the equations 5.1 and 5.2 are defined only for grayscale images, in software implementation, I have performed this step for all three channels of the image. Thus, the estimated background is a full color (RGB) image.

The process described by equation 5.3 is also called morphological opening of the image[2]. The choice of the kernel K is important to get a good estimation of the background. The size of the kernel should be significantly larger than the size of a fluorescent particle. However, it should be significantly smaller than the size of the image so as to be able to capture variations in the background illumination which occur at those

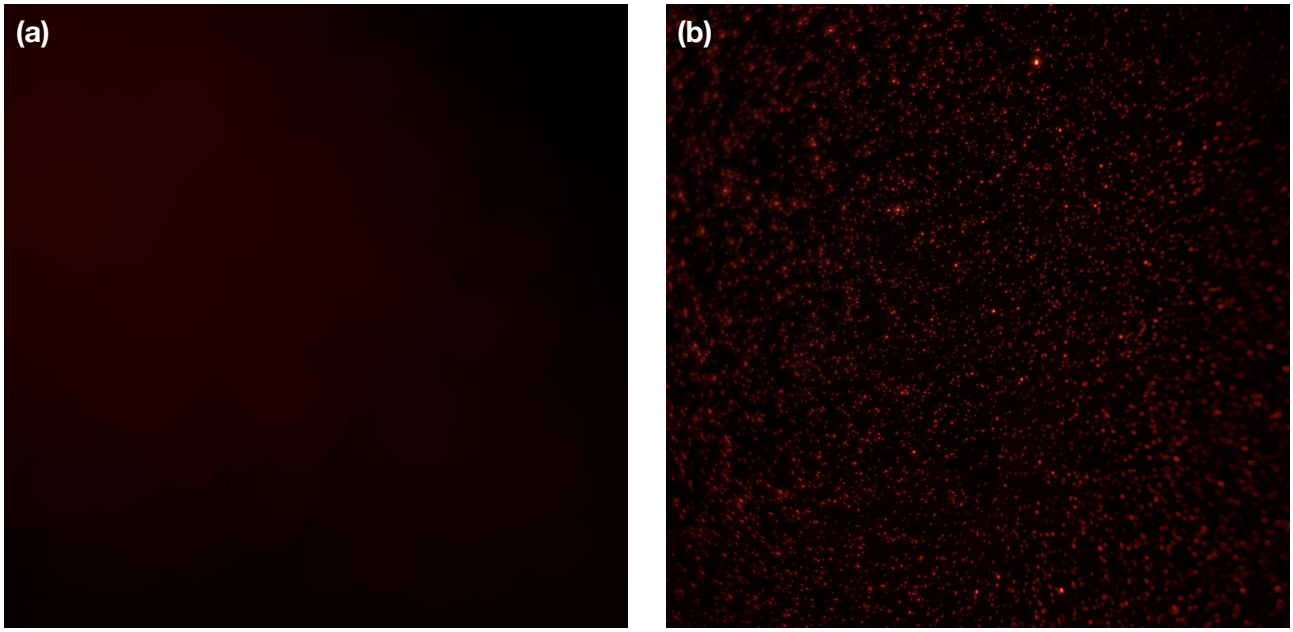

Figure 5-7. (a) Background illumination profile of the image in figure 5-6 estimated with morphological opening of the image. (b) uniformly illuminated fluorescent image obtained after removal of background from the original image.

scales. In all the experiments, I chose K to be a flat circular element with a diameter of 200 pixels. Therefore the variable y in equations 5.1 and 5.2 is bounded as $1 \leq y \leq 200$. Figure 5-7 (a) shows the estimated background of the image in figure 5-6. It can be seen that the estimated background is more intense near the center and decreases in intensity near the edges. On subtraction of the estimated background with the original image, an image with near uniform illumination across the image is obtained, as shown in figure 5-7 (b). Please note that, this is a pixel wise subtraction i.e. (figure 5-7(b)) = (figure 5-6) - (figure 5-7(a)).

5.4.2 Thresholding and NMS

The output of background removal is thresholded in a similar way as that for micrometer sized particles. Since the f-MNPs used in this study fluoresce red in color, most of the intensity of the image is in the red channel of the image. The red channel is normalized to have a value between a minimum of 0 and a maximum of 1. A threshold is applied to discard noise and peaks corresponding to the individual particles are obtained. I used a modest threshold of 0.25 in all experiments with fluorescent images. Finally, the candidate locations of the f-MNPs are filtered via non-maximal suppression which was explained in section 5.2.4. This removes duplicates and false positives. The resulting locations are identified as the locations of f-MNPs.

Figure 5-8 shows the outputs of these two steps. As shown in figure 5-8 (b), most of the f-MNPs in the image are correctly identified. In total, 3,628 f-MNPs were identified in the image shown. However, f-MNPs near the right edge of the image which have very low illumination were not identified. Although no algorithm can perform perfectly for all possible images, the algorithm outlined in this section performs quite well for the images of fluorescent magnetic nanoparticles obtained from a smartphone. Since the parameters such as threshold and kernel size are kept constant across all experiments, any errors arising due to limitation of the algorithm are systemic errors and are constant for all experiments.

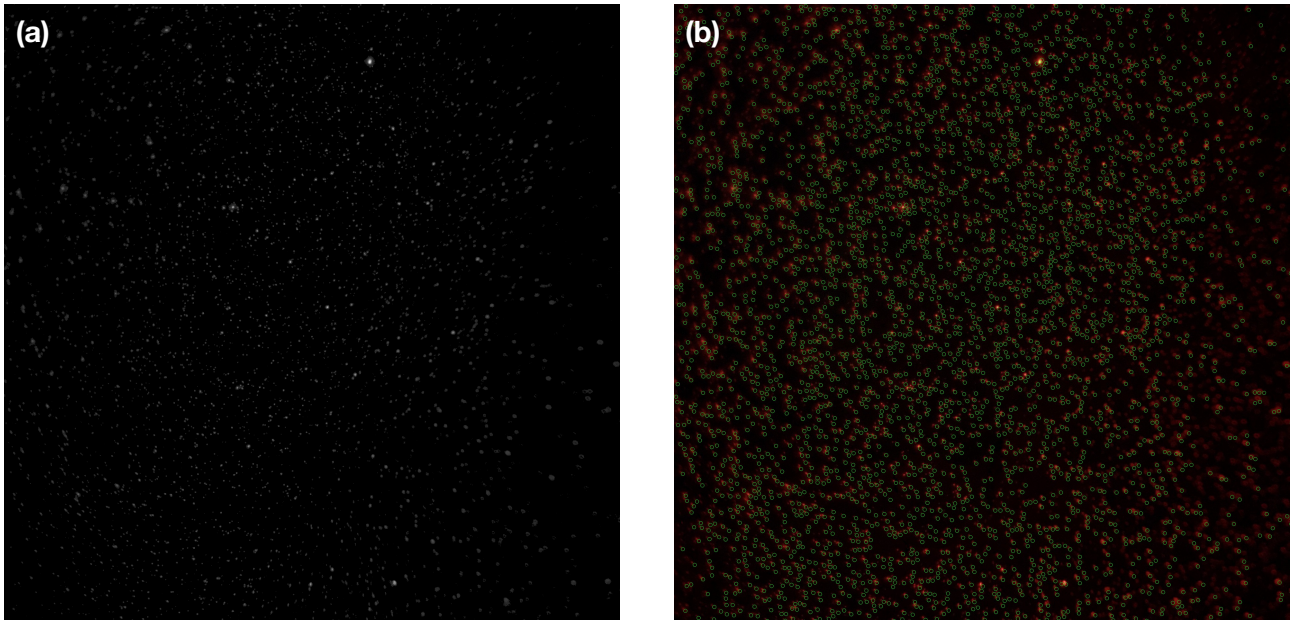

Figure 5-8. (a) Candidate locations of f-MNPs identified after thresholding (b) Locations of f-MNPs identified after non maximal suppression in (a)

5.5 Optical tracking algorithm

In the previous section, I explained the process of identification of locations of magnetic particles in an image. A sequence of images, as that present in a video, can provide additional information about the motion of the particles and has advantages for biosensing.

5.5.1 Advantages of tracking

Figure 5-9 shows a schematic of a typical magnetic particle based biosensing protocol. The protocol contains two steps. In the first step, the particles are actuated with a suitable force which induces their interactions with the a designated sensing area. The surface is assumed to be functionalized with antibodies and the surface of magnetic particles are assumed to be functionalized with the complimentary antigens. In figure 5-9(a), I assume that images of the sensing area are obtained at the beginning and end of the protocol and some final state is observed. In this case, all the information regarding the dynamics of the particles during the process is lost. Alternatively, in figure 5-9 (b), I assume that a video of the process is recorded and optical tracking is performed to reveal information about the dynamics of the particles. Three types of particle motions are relevant to biosensing:

(a) Particles which are actuated, move away from their initial positions and are then captured in the sensing area can be identified by tracking. Their initial motion and subsequent capture suggests a strong possibility that the interactions of these particles with the surface are specific i.e. biological in nature.
(b) Particles which are in the sensing area in the final state after the protocol, but are moving are clearly not stuck to the surface even though they are located in the sensing area. These particles can be identified and ignored while counting the number of particles interacting with the surface.
(c) Particles which never move throughout the process are more likely to be stuck to the surface due to non-specific interactions. These particles can be optionally ignored during calculation of number of particles interacting biologically with the surface.

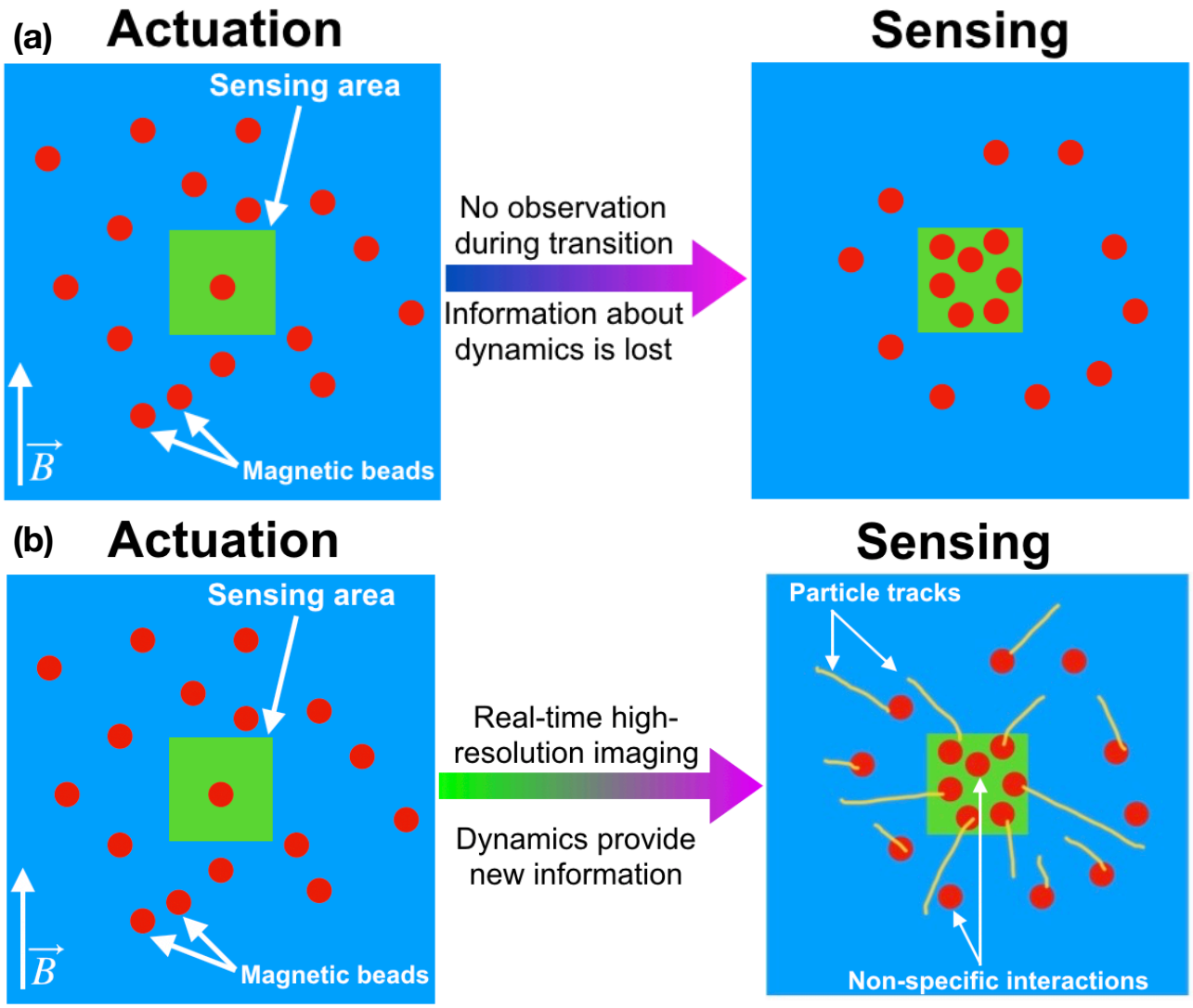

Figure 5-9. Schematic of a magnetic particle based biosensing protocol showing the advantages of optical tracking (a) In this case, I assume that images of the sensing area are obtained in the beginning and end of the protocol, (b) This shows the case when a video of the whole process is recorded and optical tracking is performed to reveal information about the dynamics of all the particles.

In biosensing literature based on imaging of magnetic particles, the nature of interactions of magnetic particles are difficult to infer. Thus, various protocols involving washing of non-specifically interacting particles from the sensing area have been proposed[4-6]. However, obtaining information about the dynamics of particles allows us to identify non-interacting and non-specifically interacting particles without the need for washing.

5.5.2 Limitations of existing approaches

Tracking the locations of objects in the presence of noisy measurements has very broad applications ranging from pedestrian avoidance in self driving cars[7] to control of air traffic[8]. Thus, algorithms for estimation of positions and velocities of objects have been developed in control theory and statistics. Tracking of particles in ‘stacks’ of time-lapse microscopic images has been used to study the dynamic processes occurring in living cells by light microscopy as well as fluorescent microscopy[9]. Similarly, tracking of magnetic particles in dark field images has been proposed as a method for studying the dynamics of particles with a functionalized surface[10], called tethered particle motion

(TPM). In principle, the algorithms[11] developed for particle tracking by these researchers can be applied for tracking of particles in a video obtained from a smartphone. However, there are two differences compared to the data analyzed with these approaches:

- As mentioned in Chapter 3, the sensing area of the actuator designed in this study is 560 µm x 560 µm. This is a large area and the resulting video contains a large number of particles, typically 8,000 to 10,000 particles.
- The type of motion studied in a large body of literature is limited to either brownian motion or motion with constant velocity and the tracking algorithms make explicit assumptions about the motion of particles. As discussed in Chapter 3, magnetic particles in the actuator perform harmonic oscillations. Thus, assumptions about constant velocity of Brownian motion are not valid.

For example, a recent thorough review[12] of various particle tracking methods considered linear motion with constant velocity throughout the video as the most challenging scenario for benchmarking the performance of various tracking algorithms developed in literature. These assumptions make already available particle tracking tools unsuitable for performing particle tracking in smartphone videos.

For example, **our videos are over 2 times longer (240 frames v/s 100 frames), contain 10 times the number of particles (≈ 10,000 v/s ≈1,000), and contain 31 times more data (2160x3840 pixels v/s 512x512 pixels) in each frame than the most challenging scenario used by [12] (Table 2 of [12])**. Thus, open source tools such as the well known ImageJ[13] software, which implement these algorithms were found to be unsuitable for our experiments. Thus, I developed my own software to address these challenges.

5.5.3 Kalman filter based motion model

Particle tracking involves two steps:

(a) Detection of locations of particles in a frame (spatial localization), and

(b) Linking the position of each particle in the frame to its position in the previous frame (temporal association).

Spatial localization has already been discussed in sections 5.2 and 5.3. Here, I discuss the algorithm for temporal association of trajectories of particles across frames. I have solved the problem of temporal association by modeling the motion of each particle in the video with a 4-state Kalman filter. Kalman filter is a well-known algorithm for estimating quantities based on noisy measurements and a control model. Mathematically, the Kalman filter is described by the following system of equations:

$$X = \begin{bmatrix} p_x \\ p_y \\ v_x \\ v_y \end{bmatrix} \tag{5.4}$$

$$X_{t|t-1} = FX_{t-1} + Bu_t + \nu \tag{5.5}$$

$$z_t = HX_t + \omega \tag{5.6}$$

The notation and explanation of all these quantities is given in the table 1. The state transition matrix, F takes the form

$$F = \begin{bmatrix} 1 & 0 & \Delta t & 0 \\ 0 & 1 & 0 & \Delta t \\ 0 & 0 & 1 & 0 \\ 0 & 0 & 0 & 1 \end{bmatrix} \qquad (5.7)$$

where Δt is the time interval between observations. The videos are recorded at 24 frames per second. Thus, $\Delta t = 1/FPS = 1/24s$. The control input model matrix is assumed to be zero to simplify the estimation of state transition. During measurements, the entire state may not be observable. For example, in our case, the measurements correspond to the position of a particle but the velocity of the particle is not directly measured. Thus, only a part of the state is observed in measurements and the observation model takes the form

$$H = \begin{bmatrix} 1 & 0 & 0 & 0 \\ 0 & 1 & 0 & 0 \end{bmatrix} \qquad (5.8)$$

The noise variables ν and ω are assumed to be drawn from multi-variate gaussian distributions with zero mean and respective covariance matrices. Specifically, $\nu \sim N(0,Q)$ and $\omega \sim N(0,R)$. The values of Q and R are empirically determined and kept constant across all experiments.

The motion model of the particle described above is used in the following way. At each time step, for a given particle, we predict its position using equation 5.5. A nearest neighbor search is carried out in the spatial location centered around the predicted position. The bead position obtained by spatial localization step which is closest to the predicted position is assigned as the position of the particle in the current frame. The position of the particle predicted by the model is usually not exactly the same as that observed by spatial localization. The difference between the two is called residual error and is used to update the velocity estimated by the model for the next time step. The update is controlled by a weighing factor called Kalman gain. The whole algorithm can thus be divided into two parts:

Prediction step:

$$X_{t|t-1} = FX_{t-1} + Bu_t + \nu \qquad (5.5)$$

$$P_{t|t-1} = FP_{t-1|t-1}F^T + Q \qquad (5.9)$$

Update step:

$$y = z - HX_{t|t-1} \qquad (5.10)$$

$$S_t = HP_{t|t-1}H^T + R \qquad (5.11)$$

$$K = P_{t|t-1}H^T S^{-1} \qquad (5.12)$$

$$X_{t|t} = X_{t|t-1} + Ky \qquad (5.13)$$

$$P_{t|t} = (I - KH)P_{t|t-1} \qquad (5.14)$$

Table 1. Notations used in Kalman filter

Symbol	Name of quantity	Explanation
X	State vector	The state vector at time t contains the positions and velocities of the particle in x and y at that time step.
$X_{t\|t-1}$	Estimated state vector	The analytical estimate of state vector at time t, before the measurement is taken into account.
$X_{t\|t}$	Updated state vector	The updated state vector after the measurement from spatial localization step is taken into account.

Symbol	Name of quantity	Explanation
F	State transition matrix	The state transition matrix maps the previous state X_{t-1} to the next state X_t.
B	Control input model	The control input model maps the control vector u to the state X and is assumed to be zero in our case.
u_t	Control vector	The control vector represents the external force applied to the magnetic particle.
ν	Process noise covariance matrix	Process noise covariance matrix represents the uncertainty in prediction of the state by eq. 5.5.
z_t	Measurement	The measurement obtained from a sensor, in our case the output of the spatial localization step.
H	Observation model	The observation model maps the full state X to the measurement z.
ω	Measurement noise	Measurement noise represents the noise in the output of the sensor. In our case, this is due to the noise in the image sensor.
y	Residual error	The vector representing the error in the position predicted by the model and that observed by spatial localization.
S	prior residual covariance	This is a intermediate variable used in the calculation of Kalman gain.
P	posterior residual covariance	This is also an intermediate variable used to calculate Kalman gain.
K	Kalman gain	The Kalman gain weighs how much the velocity should be updated based on measurements. If Δt is small the state transition model is trusted more than the measurements and vice versa.

The calculation of Kalman gain requires a few intermediate variables. First the residual error is calculated from equation 5.10. Two intermediate variables called prior residual covariance and posterior residual covariance are calculated. The prior residual covariance is calculated before the calculation of the Kalman gain as in 5.11 whereas the posterior covariance is calculated after the Kalman gain has been updated with the results of measurements as in 5.14. Equation 5.12 shows the calculation of the Kalman gain. Once the Kalman gain has been calculated, the state vector X is updated with the residual error weighted by the Kalman gain as in equation 5.13. This operation updates the estimate of velocity in the model, and the model can keep up with the changing velocity of the magnetic particle at each time step. The derivation of equations presented in this section is outside the scope of this thesis and is available in the paper by Rudolf Kalman[14], in which he proposed this algorithm.

A schematic of the complete tracking algorithm including the steps involved in spatial localization of particles in an image as well as temporal association of trajectories of particles across frames is shown in figure 5-10.

5.5.4 Implementation details

The tracking algorithm outlined in the previous section was implemented in Python programming language. Images and videos were handled using the well known OpenCV

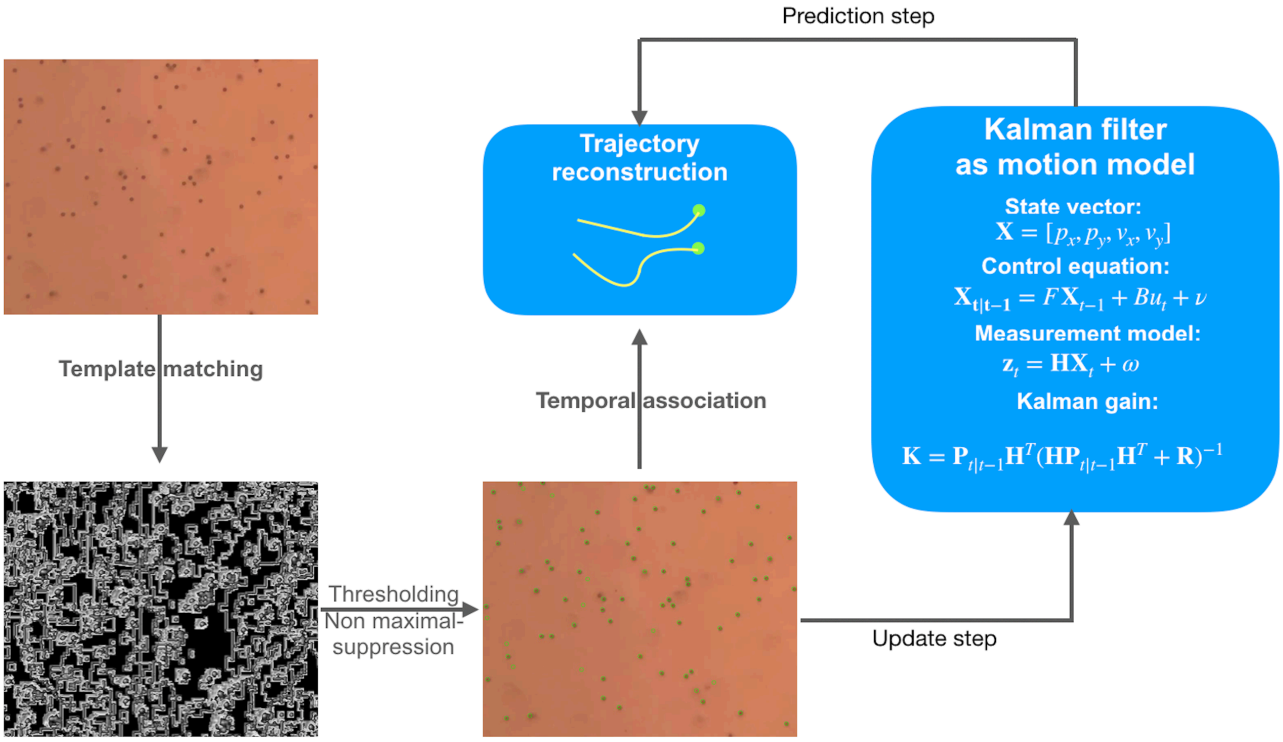

Figure 5-10. Schematic of the tracking algorithm used in this study. Template matching is used to calculate the probability of a particle being present for each pixel in the image. Locations with low probability are discarded by thresholding and non-maximal suppression (NMS) is used to eliminate duplicates. A motion model based on Kalman filter predicts the location of the particle in this frame. A nearest neighbor search in the locations identified by NMS is used to associate the particle to its location in the current frame. The location of the particles thus associated is used to update the parameters of the motion model corresponding to the particle. This process is repeated iteratively for each frame of the video for each particle in the frame. The end result is a reconstruction of the trajectory of each particle across the duration of the video.

[15] library developed by Intel for computer vision applications. The following details make our implementation fast and memory efficient:

- Some parts of the program involving array operations were written in Cython language which was then translated into an equivalent program in the C programming language and compiled into a binary file. The compiled binary functions run efficiently on any hardware.
- The program reads video frame sequentially from the video and only one frame is kept in memory (RAM of the computer) at any time. Thus, large 4K videos can be analyzed with a small memory footprint.
- The program takes advantage of GPU acceleration to perform matrix operations such as template matching and particle association.
- The process noise covariance and measurement noise covariance matrices (Q and R from section 5.4.3) are dependent on the image sensor and are the same for all particles. Thus, in our implementation the Q and R matrices corresponding to models for all the particles share the same physical memory address, which reduces memory consumption.

Writing the program took a lot of time and effort. In order to reduce the burden for other researchers working in this field, I developed a graphical user interface (GUI) so that

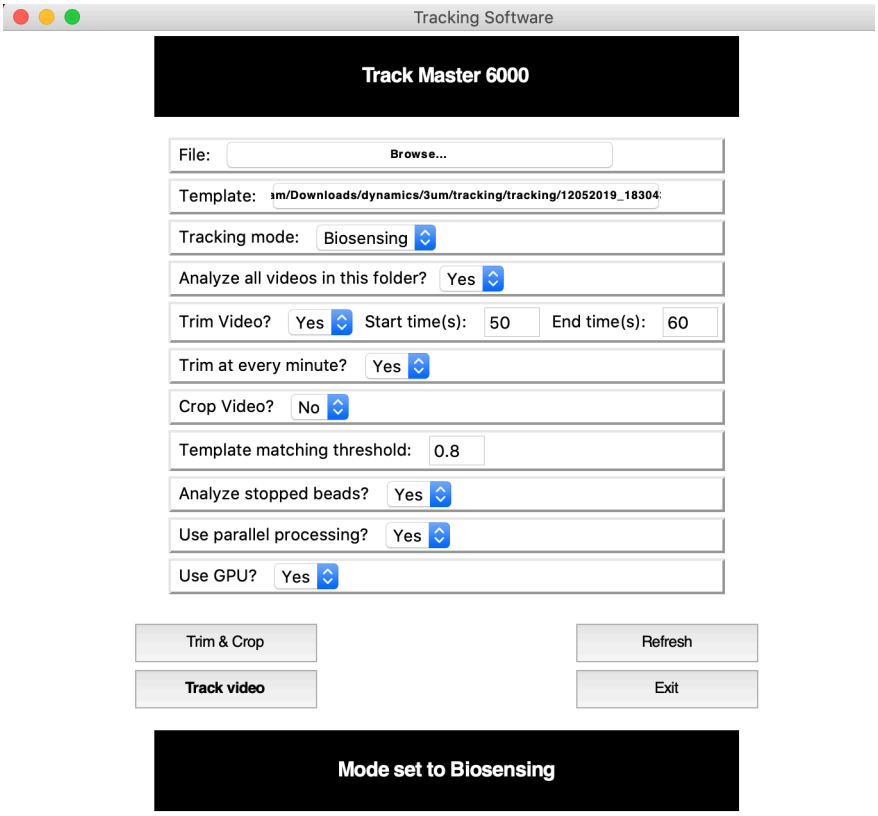

Figure 5-11. A screenshot of the graphical user interface developed to allow use of the tracking program without knowledge of programming.

others may use the program without requiring any experience in programming. A screenshot of the GUI is shown in figure 5-11. The user can choose the video to be analyzed, the template for template matching step and set the threshold for filtering out noise from the output of template matching. In addition, the software can optionally crop and trim the video as per the parameters set by the user. GPU acceleration and parallel processing are used to speed up the tracking of the video. It should be noted that both the python programming language and OpenCV library are available free of cost, even for commercial use. Thus, the program developed in this research may be deployed commercially without incurring any licensing cost. To motivate further research in particle tracking based biosensing, we plan to release the tracking software publicly on an open source platform in the near future.

5.6 The originality of the algorithms presented

Computer vision is a vast area of research which seeks to develop algorithms to let machines ‘see’ and make meaningful inferences about the real world. There is a large body of research in the fields of signal processing, image processing and robotics which was available to me in order to automate data analysis, as I set out to do. However, most of these fields are far removed from the domain of biosensing. Thus, the large body of research in computer vision focuses on processing images of everyday objects such as people, cars, chairs, streets, trees etc. There is very little research specifically on processing images or videos of magnetic particles obtained with a microscope. As described earlier, the small volume of research on particle tracking also focuses only on

fluorescent tags which exhibit very simple types of motion and was insufficient for my use. The algorithms described in this chapter were not invented by me. My contribution is to apply existing algorithms from various domains such as self driving cars, robotics and statistics to point of care biosensing. I scanned a large body of literature in computer vision, analyzed various algorithms in their applicability for analyzing images and videos of magnetic particles and implemented them in an efficient software which can be used by anyone and further which is integrated with a cloud computer, so that data can be uploaded and results obtained without having to understand the algorithmic details. Some specific examples of well known algorithms are:

- **Template matching** is a popular signal processing method used in a wide range of applications, from image processing to the detection of gravitational waves by LIGO[16]. This algorithm was used in the analysis of micrometer sized particles as the particles have uniform properties, so that they all look alike.
- **Non-maximal suppression** (NMS) is one of the most fundamental algorithms used in computer vision to eliminate duplicates in software processing. The use of NMS made sure that a magnetic particle is not counted multiple times.
- **Morphological erosion** and dilation are algorithms used for varied applications such as analysis of social media networks as well as that of three dimensional magnetic resonance imaging scans of the human brain[17]. Morphological opening was used to estimate background of the illumination in fluorescent images, so that imperfections in the optical setup do not lead to erroneous estimation of the number of fluorescent particles in the image.
- **Kalman filter** is the most ubiquitous algorithm in statistics and control theory and is used for applications ranging from tracking location of a GPS receiver to tracking pedestrians in a self driving car and robotics[18, 19]. The Kalman filter algorithm was applied to track particles across frames of video. This is mathematically equivalent to the ‘data association’ problem faced by a robot as it moves through it surroundings.

In summary, I have applied pre existing algorithms from various disciplines of mathematics and computer science to the problem of point of care diagnostics. The resulting software based on these algorithms successfully automates the task of data processing and is integral to the point of care diagnostics systems described in the following two chapters.

5.7 Examples of particle trajectories

Here, I show some examples of trajectories of particles obtained after actuation as described in Chapter 3 and tracking as described in the previous section. The experimental setup described in the previous chapter was used. A 3 μL solution containing dynabeads (diameter 2.8 μm) were dropped onto a substrate and sinusoidal currents of amplitude 30 mA were applied in both arms of the actuator with a phase difference of $\pi/2$ between the two. The resulting video was analyzed using the algorithm outlined in section 5.4. Figure 5-12 shows a small area of the full 4K frame showing the trajectories of several particles 10 seconds after the start of application of current. From this figure, it is observed that most particles show regular, periodic oscillations about a mean position. Two particles labelled as P and Q show different types of motions. While particle Q shows regular, sinusoidal motion as expected from theoretical simulations, particle P is seen to remain localized to a point. Thus, it can be inferred that the particle P is attached to the surface whereas particle Q is not attached to the surface after 10 seconds. Here, I again emphasize that this inference is only possible due to the knowledge about the dynamics of both particles provided by particle tracking. A single image the substrate surface taken 10 seconds after the start of application of current would not allow us to draw this conclusion.

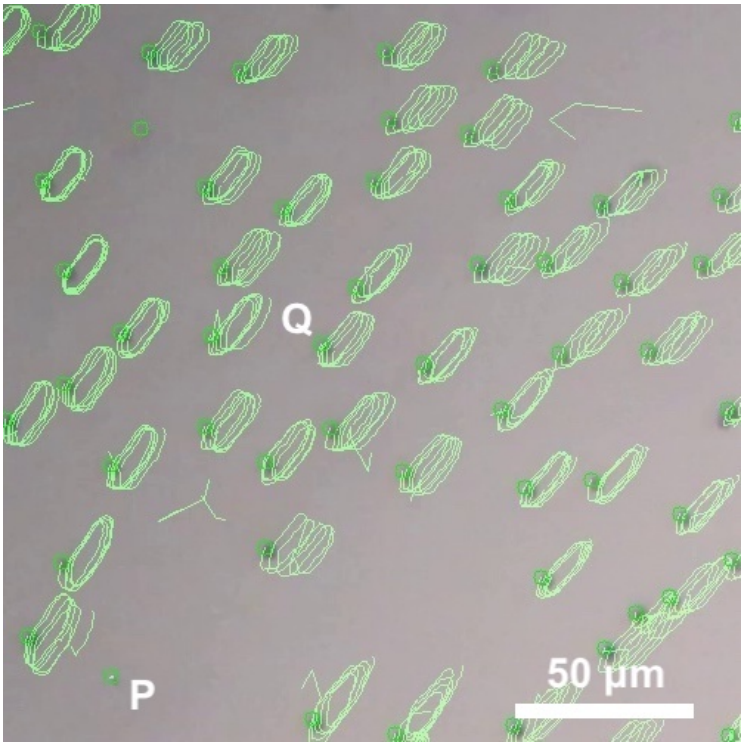

Figure 5-12. Motion of magnetic particles observed after applying current for 10 seconds. The trajectories of particles are shown in green color and were obtained after tracking. It is noteworthy that the trajectory of point P is found to be localized a point while Q is one of the many particles exhibiting harmonic oscillations.

Further information about the oscillations of these particles can be obtained from figure 5-13 (a) showing the position of both particles with time for 60 seconds. It is seen that the trajectory of particle Q is sinusoidal in nature. The amplitude of the motion of particle P is about 5 µm. However, the particle P does not appear to move at all. The variations in the position of particle P are of the order of a single pixel and the mean position drifts by a few pixels over the duration of a minute. However, the standard deviation in the motion of the particle over 10 seconds is ≈ 0.32 pixels. The fast fourier transform (FFT) of the trajectories shown in figure 5-13(a) is shown in figure 5-13 (b). Specifically the normalized amplitude of the FFT as a function of the frequency is shown on a logarithmic scale. The FFT for particle Q shows a strong peak at a frequency of 0.5 Hz, confirming that the particles exhibit harmonic oscillations at the frequency of the applied electric field.

5.8 Summary

In this chapter, I introduced methods for automated optical detection of magnetic beads in smartphone camera images with software. Detection of micrometer sized magnetic particles, and that of nanometer sized fluorescent magnetic nanoparticles were discussed separately since fluorescent images have different characteristics from images of micro meter sized particles obtained by light microscopy. The detection of particle positions in an image was then extended to sequences of images i.e. videos. A particle tracking algorithm was developed which involves detection of particle locations as well as temporal association of trajectories of particles across the frames of a video. I then described some implementation details which make our algorithm fast and memory efficient and finally provided an example of trajectories of particles obtained after harmonic oscillation and tracking.

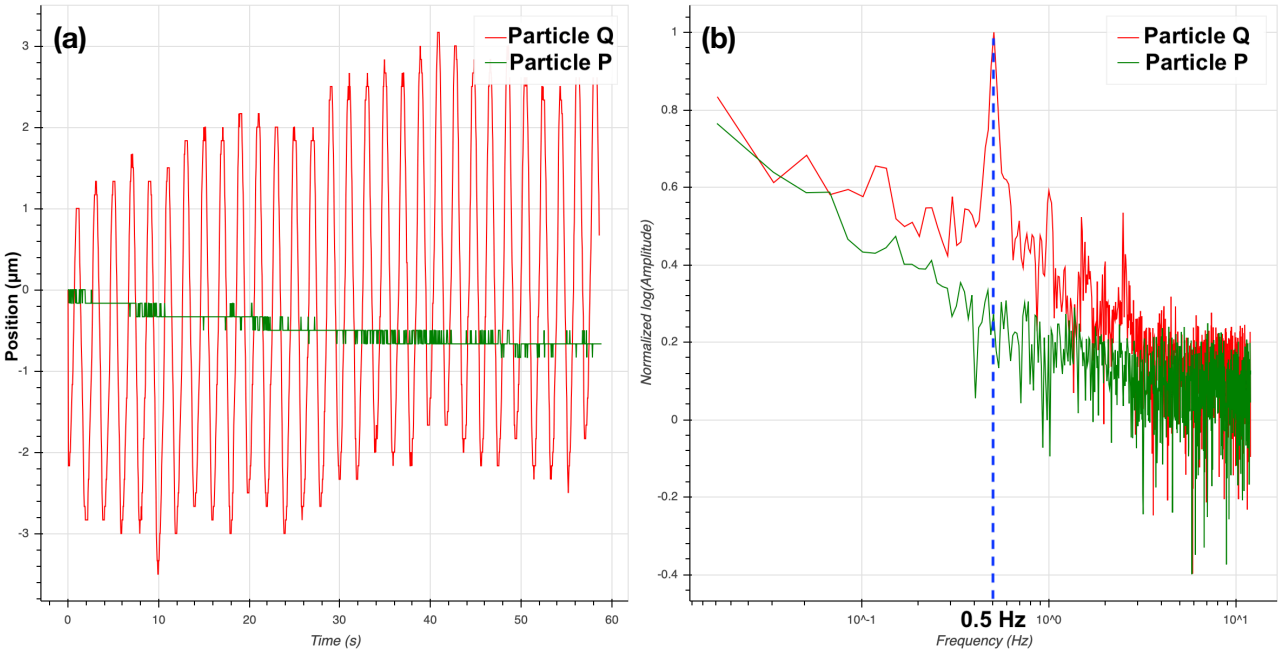

Figure 5-13. A graph of the y-position of particles P and Q for 60 seconds. (a) Position v/s time for both particles. P is shown in green color whereas Q is shown in red. (b) The normalized amplitude of the fourier transform (FFT) v/s frequency are shown on a log-log scale. The FFT for particle Q shows a strong peak at 0.5 Hz confirming that the particles exhibit harmonic oscillations at the frequency of the applied field.

5.9 References

[1] Szeliski, R., 2010. Computer vision: algorithms and applications. Springer Science & Business Media.

[2] Efford, N., 2000. Digital image processing: a practical introduction using java (with CD-ROM). Addison-Wesley Longman Publishing Co., Inc..

[3] Gonzales, R.C. and Woods, R.E., 2002. Digital image processing.

[4] Pollet, J., Delport, F., Janssen, K.P., Jans, K., Maes, G., Pfeiffer, H., Wevers, M. and Lammertyn, J., 2009. Fiber optic SPR biosensing of DNA hybridization and DNA–protein interactions. *Biosensors and Bioelectronics*, *25*(4), pp.864-869.

[5] Liu, C., De Palma, R., Reekmans, G., Laureyn, W., Stakenborg, T. and Lagae, L., 2009. Discrimination of specific and non-specific bindings by dielectrophoretic repulsion in on-chip magnetic bio-assays. *Biosensors and Bioelectronics*, *24*(7), pp.2294-2297.

[6] Pamme, N., 2006. Magnetism and microfluidics. *Lab on a Chip*, *6*(1), pp.24-38.

[7] Sarcinelli, R., Guidolini, R., Cardoso, V.B., Paixão, T.M., Berriel, R.F., Azevedo, P., De Souza, A.F., Badue, C. and Oliveira-Santos, T., 2019. Handling pedestrians in self-driving cars using image tracking and alternative path generation with Frenét frames. *Computers & Graphics*, *84*, pp.173-184.

[8] Air traffic control technology, https://en.wikipedia.org/wiki/Air_traffic_control#Technology

[9] Stephens, D.J. and Allan, V.J., 2003. Light microscopy techniques for live cell imaging. *science*, *300*(5616), pp.82-86.

[10] Visser, E.W., van IJzendoorn, L.J. and Prins, M.W., 2016. Particle motion analysis reveals nanoscale bond characteristics and enhances dynamic range for biosensing. *ACS nano*, *10*(3), pp.3093-3101.

[11] Meijering, E., Dzyubachyk, O. and Smal, I., 2012. Methods for cell and particle tracking. In *Methods in enzymology* (Vol. 504, pp. 183-200). Academic Press.

[12] Chenouard, N., Smal, I., De Chaumont, F., Maška, M., Sbalzarini, I.F., Gong, Y., Cardinale, J., Carthel, C., Coraluppi, S., Winter, M. and Cohen, A.R., 2014. Objective comparison of particle tracking methods. *Nature methods*, *11*(3), p.281.

[13] Rasband, W.S., ImageJ, U. S. National Institutes of Health, Bethesda, Maryland, USA, https://imagej.nih.gov/ij/, 1997-2018.

[14] Kalman, R.E., 1960. A new approach to linear filtering and prediction problems. *Journal of basic Engineering*, *82*(1), pp.35-45.

[15] Bradski, G. and Kaehler, A., 2000. OpenCV. *Dr. Dobb's journal of software tools*, *3*.

[16] Gabbard, H., Williams, M., Hayes, F. and Messenger, C., 2018. Matching matched filtering with deep networks for gravitational-wave astronomy. *Physical review letters*, *120*(14), p.141103.

[17] Gezimati, M., Rushambwa, M.C. and Jeeva, J.B., 2019. Brain Tumor Detection and Classification of MRI Brain Images Using Morphological Operations. In *ICTMI 2017* (pp. 137-149). Springer, Singapore.

[18] An intro to Kalman Filters for Autonomous Vehicles, https://towardsdatascience.com/an-intro-to-kalman-filters-for-autonomous-vehicles-f43dd2e2004b

[19] Simulataneous localization and mapping with the extended Kalman filter, https://jinyongjeong.github.io/images/post/SLAM/lec05_EKF_SLAM/EKF.pdf

6. Results and Discussion: Smartphone based point of care diagnostics system with fluorescent magnetic nanoparticles

6.1 Introduction

Fluorescent magnetic nanoparticles (f-MNPs) have several advantages as labels for detection of biomarkers. Specifically, the advantages are

(a) high surface area to volume ratio,
(b) ability to be actuated by magnetic fields, and
(c) fluorescent properties which enables their observation with smartphones.

I would like to emphasize here that the low magnetic moment of nanometer sized magnetic particles makes it difficult to detect MNPs with magnetic sensors such as GMR and Hall sensors[1, 2]. Thus, fluorescence is the critical property which enables optical detection of f-MNPs with fluorescence microscopy. In recent years, smartphone cameras have greatly improved in sensitivity to low light conditions. As I showed in chapter 5, smartphone cameras can resolve single or a few f-MNPs with weak fluorescence intensity in still images. I have built upon this capability of smartphone cameras to develop a smartphone based point of care (POCT) diagnostics system which utilizes f-MNPs as magnetic labels. The proposed biosensing protocol is specifically designed to enable sharing of diagnostics information in scenarios such as outbreak of epidemics in remote locations, where along with rapid diagnosis, real-time reporting of the status of individuals can enable the public health resources to be targeted to individuals and regions where help is most needed. We demonstrate the effectiveness of this system by demonstrating the detection with prostate specific antigen (PSA) with a smartphone.

I first provide a brief overview of the biosensing protocol which contains three key components. I then explain the importance of making measurements in dry conditions for real world scenarios, the experimental methods and the results obtained. Finally, I discuss the advantages and limitations of the biosensing protocol presented in this chapter.

6.2 Real world scenario: An epidemic

The biosensing system described in this chapter is motivated by the real world scenario: There is a possibility of an epidemic outbreak in a rural village in Africa or India. Public health workers need to conduct tests on hundreds or even thousands of people in a few hours and relay the information to doctors located remotely, so that they can determine whether this village has been affected by the epidemic outbreak.

What would be the requirements from a point of care testing system used in this scenario?

There are a few requirements based on our previous discussion:

- The system should offer results quickly, in a few minutes.

- Since multiple workers need to conduct tests, it would be highly beneficial if the protocol could be broken down into steps which could be conducted by different people. For example, one person could be only mixing solutions, while another person could be only washing sensing chips while another person could be only taking images.
- Data analysis should be automated.
- Results should be conveyed to the patients and remotely located doctors quickly, in near real time.
- Spatial map of the results should be created and be visible to public health officials, so that the outbreak can be prevented quickly.

The point of care testing system presented in this chapter fulfills all these requirements. The system is based on fluorescent magnetic nanoparticles and smartphone. The whole protocol takes less than 3 minutes to complete. It can be broken down into steps which are mutually decoupled from each other. Thus, different people could be processing multiple samples simultaneously i.e. one person does not have to perform the whole biosensing procedure for a given sample, it can be done by different people. This is enabled by dry measurements described below. The algorithm for analyzing fluorescent images described in Chapter 5 is implemented on a cloud computer, so that images obtained by the smartphone are synced to the cloud and analyzed automatically without the healthcare worker having to upload images manually. The cloud based image analysis system can also extract location metadata embedded in the images sent to correlate the results of the tests with the location of the patient. Thus, a spatial 'heat map' of the disease outbreak can be created.

6.3 Overview of the POCT system

The proposed POCT system consists of three key components

- A protocol for detection of PSA by fluorescent imaging of f-MNPs.
- A digital image processing algorithm for determining the concentration of PSA via fluorescent images of f-MNPs obtained with a smartphone.
- A shared 'cloud server' platform for performing the analysis and communicating the results to designated users.

A schematic of the POCT system is shown in figure 6-1.

6.3.1 Importance of dry measurements

As we have discussed in chapters 2 and 3, heterogenous medical diagnostics protocols involving the interaction of magnetic particles with a solid substrate usually follow three basic steps.

- First, beads are introduced on a substrate surface functionalized with biomolecules complimentary to the surface functionalization of the beads themselves.
- Next, interactions of magnetic particles with the surface are promoted by magnetic actuation of the particles and extraneous particles, attached to the surface by non-specific interactions are removed from the sensing area by means of some form of washing.
- Finally, the magnetic particles remaining on the substrate are detected with either magnetic or optical sensors to obtain a quantitative estimate for the biomolecule of interest.

In protocols involving magnetic field sensors, such as magnetoresistive sensors[3, 4], all the steps outlined in the previous sub-section are carried under 'wet conditions' i.e. while the biomolecular reaction is occurring on the sensing area. Various biosensing

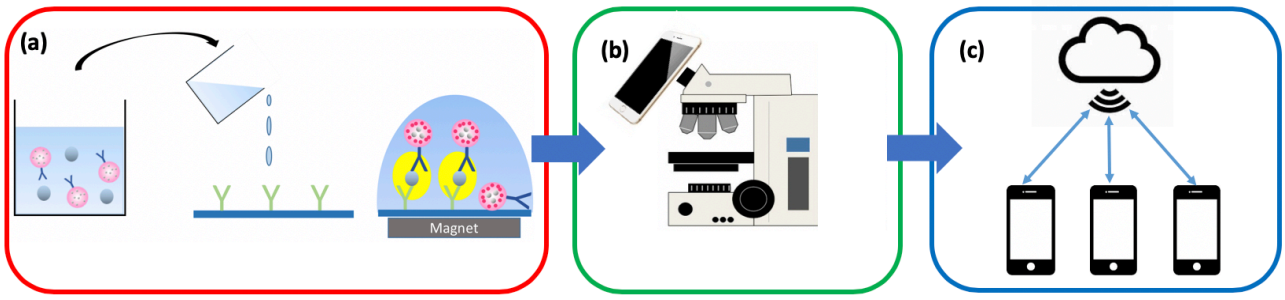

Figure 6-1. Schematic fo the proposed POCT system consisting of three steps (a) f-MNPs functionalized with antibodies are introduced on a substrate and a magnetic field is applied for 30 seconds. The substrate is subsequently washed and is then said to be in a dry state. (b) The substrate is imaged with a smartphone mounted on a fluorescent microscope. (c) The images of fluorescent magnetic nanoparticles are uploaded to a central server and analyzed remotely. The results re available within 1 minute and are communicated to the relevant people.

protocols proposed stress the importance of obtaining real-time information on the interaction of the particles with the surface[5, 6]. While such wet measurements can provide detailed information about the time scale of interaction of magnetic particles with the surface, there are several advantages for decoupling the steps outlined above, so that measurements and analysis can be performed independently of the actuation and washing steps.

Thus, we propose a biosensing system where the measurement step is decoupled from actuation and washing step. The measurements can be performed long after the biomolecular reaction occurring on the substrate surface has concluded. We call this state, when the biomolecular reactions occurring on the sensing surface has ceased, as **dry state**. A biosensing protocol allowing measurements to be performed in dry state simplifies the workflow for healthcare professionals in real-world scenarios where a large number of patients may have to be tested, so that different people may perform different steps. The protocol for biomolecular detection involving dry measurements forms a part of the proposed POCT system. The analysis of images obtained is completely automated so that once the measurements have been performed, data is uploaded to the cloud server and analysis is performed automatically, without requiring any intervention from the user.

6.3.2 Protocol for detection of PSA

The detection of PSA is carried out with a sandwich bioassay as follows:

- First, silicon substrates are functionalized with PSA antibodies (also commonly known as anti-PSA in literature). The concentration of antibodies was kept constant across all experiments at 6.9 μM.
- Second, f-MNPs are functionalized with PSA. The concentration of the antigens was varied across experiments. This step is to be carried out just before the particles are introduced on the substrate.
- The functionalized f-MNPs are introduced onto the substrate and a vertical magnetic field of 100 gauss (1 gauss = $1x10^{-4}$ Tesla) is applied for 30 seconds to promote the interaction of the f-MNPs with the substrate surface.
- Next, the substrate is washing thrice in a solution of phosphate-buffered saline and deionized water to remove non-specifically bound particles from the substrate.
- After washing, the substrate is considered to be in a dry state i.e. all biomolecular reactions are deemed to have been concluded.

Figure 6-2 shows a schematic of the protocol described above.

In the next sub-sections we describe the protocols for functionalization of substrate as well as for fluorescent magnetic nanoparticles.

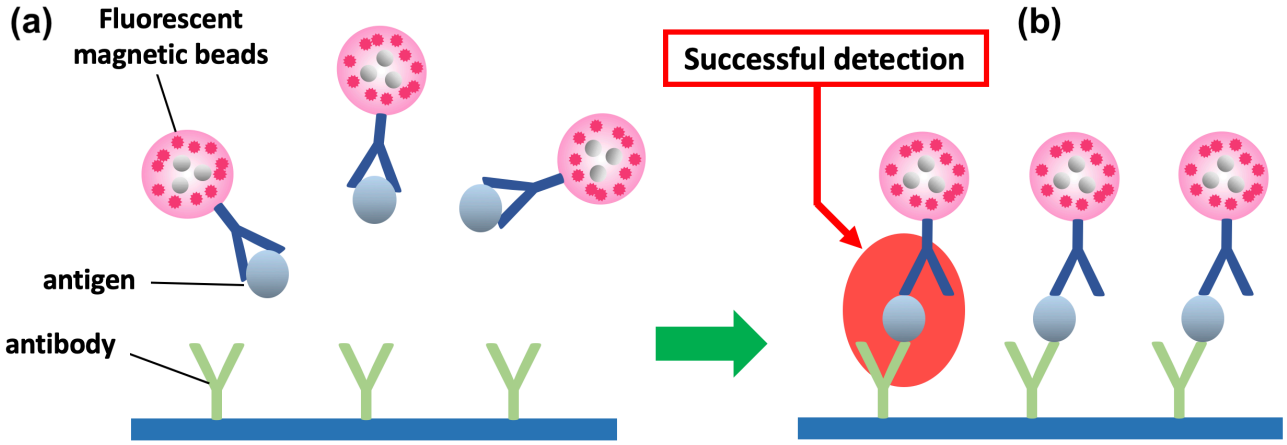

Figure 6-2. Schematic of PSA detection protocol (a) Antibodies are functionalized onto the substrate and f-MNPs functionalized with complimentary antigens interact with the substrate (b) The antigens get sandwiched between the two antibodies and the fluorescence of the f-MNPs is detected with a smartphone.

6.3.3 Functionalization of substrate surface

Silicon substrates were cleaned with acetone and ethanol and rinsed with deionized water for 5 minutes. The substrate surface was made hydrophilic by treatment with oxygen plasma for 2 minutes. The hydrophilic substrate was immersed in a solution of PSA antibodies for 30 minutes. The concentration of the antibody solution was 6.9 μM. After this step, there may be unreacted hydroxyl bonds on the surface of the substrate, which may lead to non-specific interactions later on. These excess bonds were capped with a solution of PEG5000 (diluted in deionized water to 50% by weight). This concludes the functionalization of PSA antibodies on the substrate. In the next section, we show that this protocol leads to functionalization of PSA antibodies on the substrate as verified by Electron Spectroscopy for Chemical Analysis (ESCA or XPS).

6.3.4 Functionalization of f-MNPs

The f-MNPs obtained from the manufacturer (Tamagawa Seiki Co. Ltd.) were already functionalized with PSA antibodies. Thus, the functionalization of f-MNPs with PSA antigens could be performed in a single step. We prepared a buffer solution containing PSA antigens along with 0.05% Tween 20, 0.4% bovine serum albumin (BSA), 0.4% BlockAce and 0.05% ProClin150 in Tris-buffered saline solvent. The buffer solution containing PSA antigens was mixed with another solution containing f-MNPs in 1:1 volumetric ratio. The PSA antibody antigen interaction occurs in the solution, leading to the functionalization of antigens on the surface of f-MNPs. The blocking agents BSA and BlockAce bond to unoccupied sites on the f-MNPs to prevent the possibility of non-specific interaction of the surface with other molecules in the solution. The surface of the f-MNPs are hydrophobic and thus, f-MNPs may aggregate due to hydrophobic interactions. Thus, Tween 20 is used to reduce hydrophobic interaction between f-MNPs which can lead to the formation of clusters of particles. Moreover, to reduce the time available for hydrophobic interactions among nanoparticles, the f-MNPs were functionalized with PSA antigens just before their introduction onto the surface of the substrate.

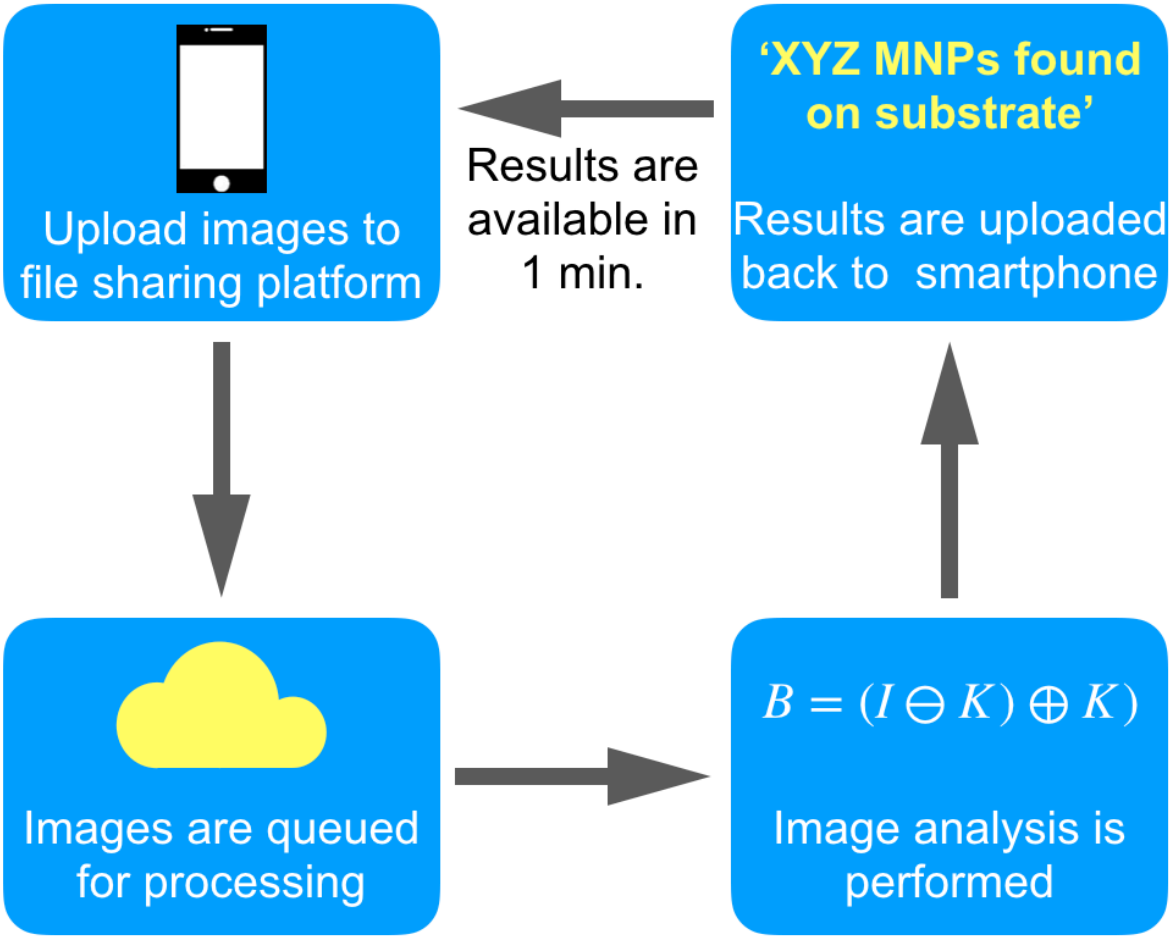

Figure 6-3. Schematic of the image processing pipeline on a cloud computer. The user uploads the fluorescent images to a central file sharing platform. A service running on the cloud server automatically detects new images and performs analysis to determine the number of f-MNPs in the image. The results are made available to the user within 1 minute and may also be shared with other people if necessary.

6.3.5 Image processing and integration with cloud computer

The images of the substrate obtained by the smartphone were analyzed using the algorithm described in section 5.3. The objective lens used for these measurements had a magnification of 40 x and a numerical aperture of 0.60. Thus, the diffraction limited resolution of the optical setup was

$$\Delta x = \frac{0.61\lambda}{N.A.} = \frac{0.61 \times 0.6\mu m}{0.6} = 0.61\mu m \qquad (6.1)$$

The algorithm was implemented to run on a cloud server to which the smartphone can connect to upload data and receive results of the analysis. The processing pipeline carried out on the cloud computer is shown in figure 6-3. The user uploads the images on to the cloud computer. Several users may upload their data simultaneously. A program running on the server detects requests for analysis made by users and all images received from various users are queued for processing. Each image in the queue is analyzed and the results are obtained. The results are then communicated back to the user and optionally email alerts are sent to people who have the access privilege to the results of the analysis.

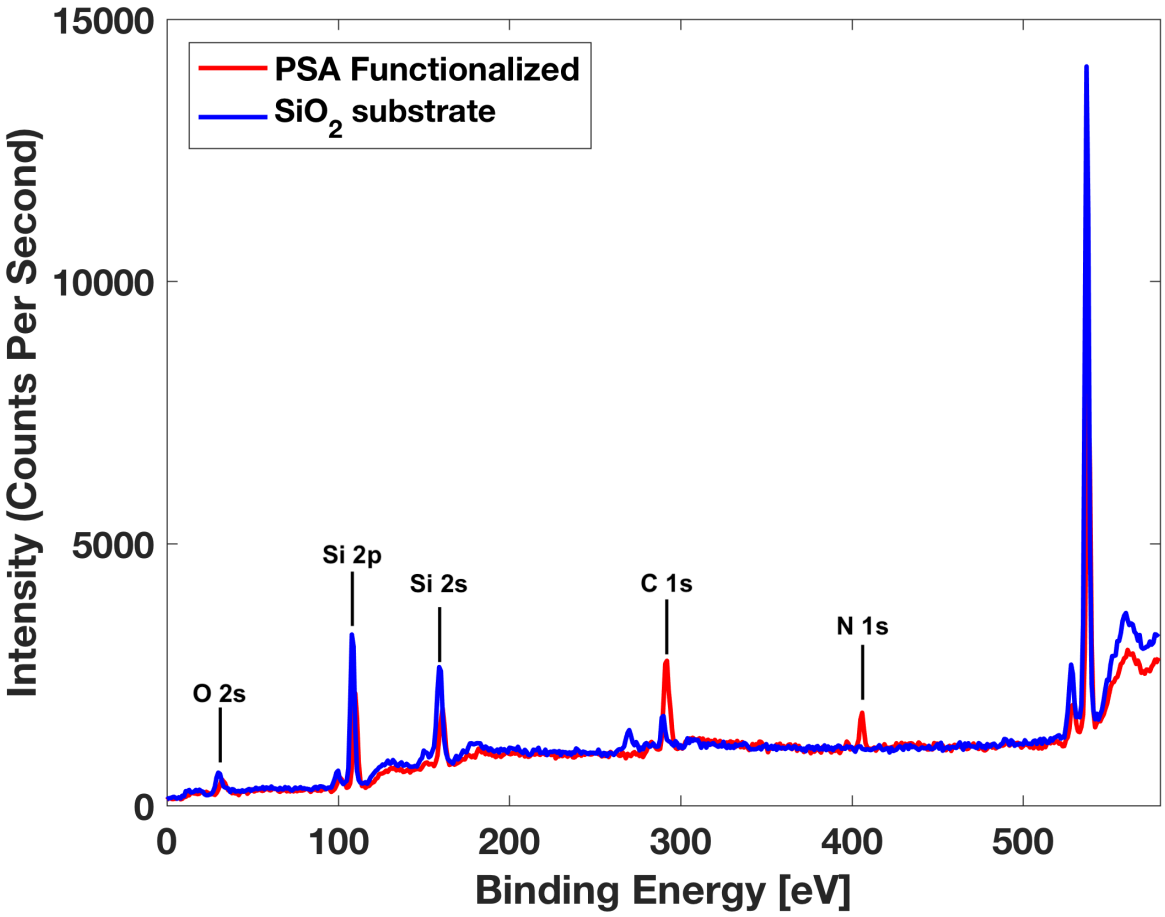

Figure 6-4. ESCA spectra of pure silicon dioxide substrate as well as the one with PSA functionalization protocol performed on it. It can be seen that the substrate with PSA functionalized on it has peaks corresponding to carbon and nitrogen.

6.4 Experimental results

We will present the results of the experiments in two parts. First, we will show that the protocol outlined in section 6.2.3 results in functionalization of PSA antibodies on the substrate surface. Then, we will present the results of quantitative estimation of PSA antigens with a smartphone using cloud computing.

6.4.1 Functionalization of PSA on substrate

An aluminium X-ray source with accelerating voltage of 10 kV and filament current 10 mA was used in the measurements presented here. ESCA spectra of two substrates, one with functionalization protocol performed on it and another without the functionalization protocol (control) were measured and compared. Figure 6-4 shows the ESCA spectra of the two substrates. The spectra shown have been corrected for the charging of the substrate by referencing the position of carbon 1s to 284.8 eV. The substrate which has the functionalization protocol performed on it displays distinctly sharper peaks corresponding to carbon 1s and nitrogen 1s than the control. Even after care taken during sample preparation and analysis, an adventitious carbon layer was formed on the control substrate which leads to a peak corresponding to carbon. However, this peak was much smaller than that for the substrate with PSA on it. The peaks corresponding to silicon 2s and 2p were higher for the control substrate. This shows that

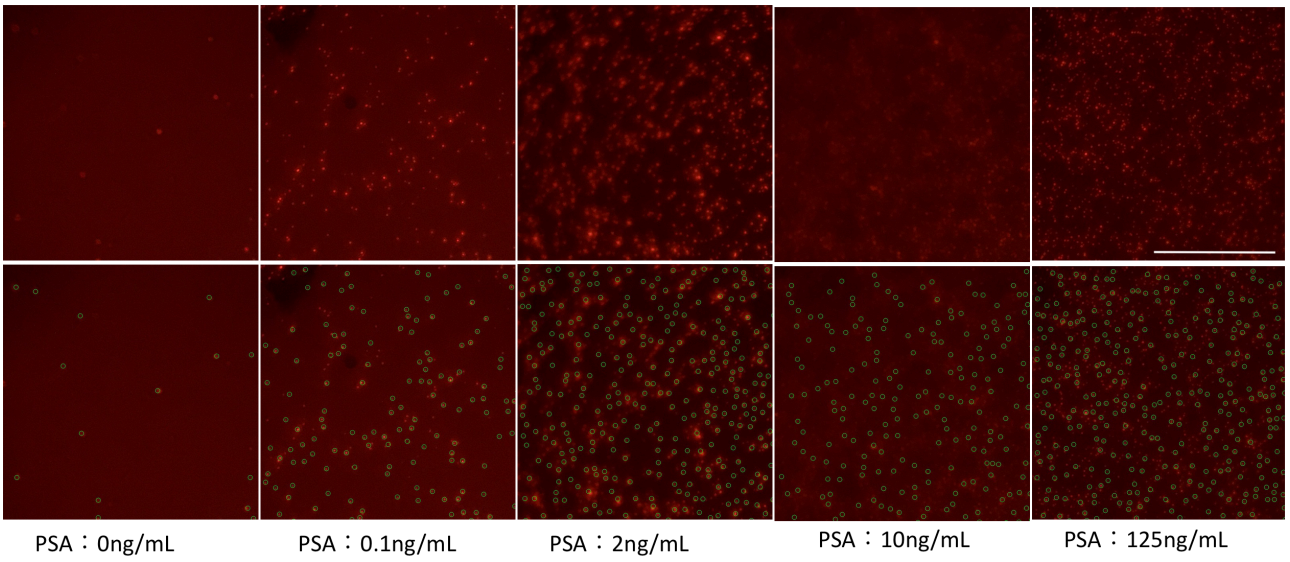

Figure 6-5. Images of the sensing surface obtained from the smartphone for the concentration of PSA antigens shown in the figure. The raw images obtained from the smartphone are shown in the top row and the results of analysis performed on cloud server are shown in the bottom row. The scale bar shown in the rightmost image in the top row corresponds to 50 μm. The scale is the same for all images.

the substrate with PSA functionalization protocol performed on it has a layer of compounds of nitrogen and carbon on silicon dioxide layer. The ratios of C/Si and N/Si were calculated and are shown in table 1.

Table 1. C/Si and N/Si ratios for the two types of substrates

Substrate type	C/Si	N/Si
Silicon oxide	0.19	0
PSA functionalized	0.49	0.48

Our results are in agreement with previous reports[7, 8] on functionalization of antibodies and show that the carbon to silicon and nitrogen to silicon ratio for the substrate on which functionalization protocol was performed was much higher than the control substrate. Thus, we conclude that the antibodies are successfully functionalized on the antibodies on the substrate following the protocol described in section 6.2.3.

6.4.2 Quantitative detection of PSA with smartphone

The experiments for quantitative detection of PSA were performed for five concentrations of PSA antigens: control (0 ng/mL), 0.1 ng/mL, 2.0 ng/mL, 10 ng/mL and 125 ng/mL. The images taken for each of these five concentrations from the smartphone are shown in figure 6-5. The top row in the figure shows the images taken from the smartphone while the bottom row shows the locations of particles identified by the cloud based image processing pipeline. We see that for the control sample i.e. when antigens are not present in the solution (0 ng/mL) very few particles are observed on the substrate. For 0.1 ng/mL the number of particles observed on the substrate is much larger than that that for control sample. This is reflected in the results of the analysis. For 2 ng/mL, the number of particles increases even more. However, on going from 2 ng/mL to 125 ng/mL we visually observe that the number of particles does not change significantly, implying

that a saturation of the particle density is observed for antigen concentrations above 2 ng/mL.

We quantify the results obtained in the above figure by taking 50 square windows in the images centered at random locations. Each window has an area 100 μm x 100 μm. We perform statistical inferences about the number of particles in a 100 μm x 100 μm area from these 50 estimates. The results are shown in figure 6-6. As expected from figure 6-5, the density of f-MNPs increases up to a concentration of 2.0 ng/mL and saturates thereafter. The blue dashed line shows the level 3 standard deviations below the mean value for 0.1 ng/mL. In literature, a commonly used metric[9] for calculation of limit of detection of a protocol is the level $\mu + 3\sigma$ for the mean, μ and standard deviation σ of the

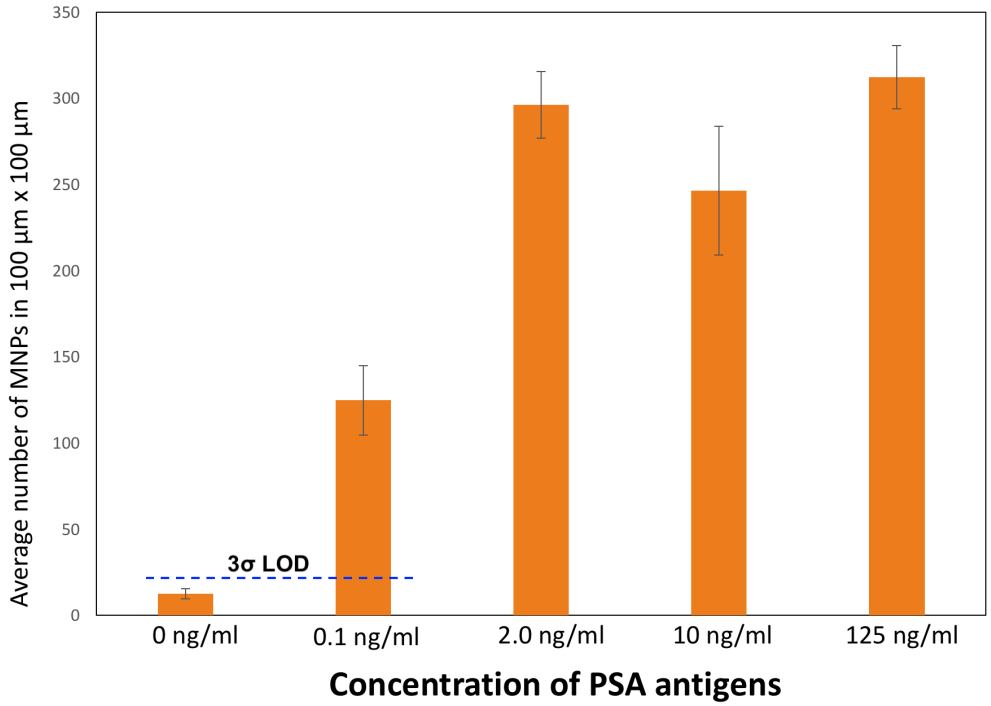

Figure 6-6. Calibration curve for PSA biomarker obtained from smartphone images shown in figure 6-5. The dashed blue line shows the level 3 standard deviations below the mean for 0.1 ng/mL. Since the blue line is above the number of particles estimated for control, we conclude that the limit of detection of this method is 0.1 ng/mL.

control sample. Since the corresponding level for a concentration of 0.1 ng/mL (100 pg/mL) is well above that for the control sample, we conclude that the limit of detection for the PSA detection protocol is 100 pg/mL. The limit of detection of PSA obtained is an order of magnitude lower than other approaches in literature using for example, localized surface plasmon effect in gold nanoparticles[10]. Moreover, while previously proposed protocols for detection of PSA require bulky and sophisticated equipment, our approach uses a smartphone and cloud computing for the detection. To the best of our knowledge, this is the first report of detection of PSA with a smartphone in less than 3 minutes while previously reported smartphone based protocols take about 20 minutes[11].

Patients with concentrations of PSA below 4.0 ng/mL are considered to be healthy whereas those with higher concentrations are deemed to be at elevated risk of prostate cancer. Since the limit of detection of the proposed protocol is well below this limit, the POCT medical diagnostics system introduced in this chapter comprising a smartphone, dry measurement technique and cloud based digital image processing is clinically relevant.

6.5 Advantages and limitations of the proposed system

The POCT system introduced in this chapter has the following advantages:

- The actuation step takes 30 seconds while the washing step takes about 1 minute.
- Measurements of fluorescence images can be performed independently of the washing and actuation steps in dry state after the biomolecular reaction has concluded.
- Fluorescent images are obtained with a smartphone and thus, bulky equipment is not required.
- Analysis is performed in an automated way, remotely on a cloud computer, thereby freeing the user from the task of doing the analysis.
- The results are available in just a minute on an average.
- The results are communicated to the user immediately and can also be shared with other public health officials to aggregate real time statistics on the spread of diseases in a region.
- The protocol for detection of biomarkers achieves a very low limit of detection of 100 pg/mL which is an order of magnitude lower than that required for clinically relevant detections.

However, in spite of the advantages mentioned above, the system suffers from the following limitations

- The washing step performed in this protocol is performed manually. This can limit the reproducibility of results across users as the washing procedure may be subjective.
- The integration of the method with a cloud computer implicitly assumes that internet is always available in the locations where analysis is being performed. This is not always true for remote locations and may limit the applicability of the proposed approach in POCT medical diagnosis.

6.5 Summary

In this chapter, we introduced a point of care medical diagnostics system for detection of prostate specific antigen using fluorescent magnetic nanoparticles as labels. The POCT system is based on obtaining high resolution fluorescent images from a smartphone and utilizes the camera as well as network communication capabilities of the smartphone to send data for analysis and receive results. The analysis is performed remotely on a cloud computer and the results can be shared in real time with many people. The proposed approach achieves clinically relevant limit of detection of 100 pg/mL for PSA.

6.7 References

[1] Wang, S.X. and Li, G., 2008. Advances in giant magnetoresistance biosensors with magnetic nanoparticle tags: Review and outlook. *IEEE transactions on Magnetics*, *44*(7), pp.1687-1702.

[2] Sandhu, A., Sanbonsugi, H., Shibasaki, I., Abe, M. and Handa, H., 2004. High sensitivity InSb ultra-thin film micro-hall sensors for bioscreening applications. *Japanese journal of applied physics*, *43*(7A), p.L868.

[3] Gaster, R.S., Xu, L., Han, S.J., Wilson, R.J., Hall, D.A., Osterfeld, S.J., Yu, H. and Wang, S.X., 2011. Quantification of protein interactions and solution transport using high-density GMR sensor arrays. *Nature nanotechnology*, *6*(5), p.314.

[4] Cardoso, S., Leitao, D.C., Dias, T.M., Valadeiro, J., Silva, M.D., Chicharo, A., Silverio, V., Gaspar, J. and Freitas, P.P., 2017. Challenges and trends in magnetic sensor integration with microfluidics for biomedical applications. *Journal of Physics D: Applied Physics*, *50*(21), p.213001.

[5] Chicharo, A., Cardoso, F., Cardoso, S. and Freitas, P.P., 2014. Dynamical detection of magnetic nanoparticles in paper microfluidics with spin valve sensors for point-of-care applications. *IEEE Transactions on Magnetics*, *50*(11), pp.1-4.

[6] Chicharo, A., Cardoso, F., Cardoso, S. and Freitas, P.J., 2015. Real-Time Monitoring of Magnetic Nanoparticles Diffusion in Lateral Flow Microporous Membrane Using Spin Valve Sensors. *IEEE Transactions on Magnetics*, *51*(1), pp.1-4.

[7] Williams, E.H., Davydov, A.V., Motayed, A., Sundaresan, S.G., Bocchini, P., Richter, L.J., Stan, G., Steffens, K., Zangmeister, R., Schreifels, J.A. and Rao, M.V., 2012. Immobilization of streptavidin on 4H–SiC for biosensor development. *Applied surface science*, *258*(16), pp.6056-6063.

[8] Yalcin, A., Popat, K.C., Aldridge, J.C., Desai, T.A., Hryniewicz, J., Chbouki, N., Little, B.E., King, O., Van, V., Chu, S. and Gill, D., 2006. Optical sensing of biomolecules using microring resonators. *IEEE Journal of Selected Topics in Quantum Electronics*, *12*(1), pp.148-155.

[9] Long, K.D., Woodburn, E.V., Le, H.M., Shah, U.K., Lumetta, S.S. and Cunningham, B.T., 2017. Multimode smartphone biosensing: the transmission, reflection, and intensity spectral (TRI)-analyzer. *Lab on a Chip*, *17*(19), pp.3246-3257.

[10] Jazayeri, M.H., Amani, H., Pourfatollah, A.A., Avan, A., Ferns, G.A. and Pazoki-Toroudi, H., 2016. Enhanced detection sensitivity of prostate-specific antigen via PSA-conjugated gold nanoparticles based on localized surface plasmon resonance: GNP-coated anti-PSA/LSPR as a novel approach for the identification of prostate anomalies. *Cancer gene therapy*, *23*(10), p.365.

[11] Barbosa, A.I., Gehlot, P., Sidapra, K., Edwards, A.D. and Reis, N.M., 2015. Portable smartphone quantitation of prostate specific antigen (PSA) in a fluoropolymer microfluidic device. *Biosensors and Bioelectronics*, *70*, pp.5-14.

7. Results and Discussion: Smartphone based point of care diagnostics system with magnetic micro-particles and optical tracking

7.1 Introduction

Smartphone based medical diagnostics protocols have been under intense development[1-5] over the past decade due to the advantages of optical imaging, communication and processing offered by them. In the previous chapter, we described a point of care medical diagnostics system based on fluorescent magnetic nanoparticles and smartphone. In addition to magnetic nanoparticles, magnetic micro-particles are widely used as labels for biosensing applications and have particular advantages for integration with smartphones. In particular, magnetic particles with size of the order of a micro meter can easily be resolved with conventional light microscopy with a high signal to noise ratio.

The high signal to noise ratio allows us to use a low exposure time for taking images and thus enables us to take series of images of the particles in quick succession. A series of images, namely a video, enables us to perform inferences regarding the dynamics of the particles and thus about their interaction with the sensing surface. In this chapter we show that information about the dynamics of particles allows us to develop a point of care diagnostics system for highly sensitive quantitatively detection of biomolecules. We present an overview of the various components of the proposed POCT system. Our method eliminates the need for a separate washing step which was one of the weaknesses of the fluorescent magnetic nanoparticle based system introduced in the previous chapter. Promotion of specific interactions and elimination of non-specific interactions are performed simultaneously by three dimensional electromagnetic actuation of magnetic particles. Optical tracking of the dynamics of thousands of particles over a large area (560 μm x 560 μm) with sub-micron resolution allows us to make statistically significant inferences about the interaction of particles with the surface. We benchmark the proposed approach with a streptavidin-biotin based competitive bioassay and experimentally demonstrate a limit of detection of 1 nM with the smartphone. This limit of detection is achieved within 2 minutes of application of electromagnetic actuation. Thus, the proposed biosensing protocol is highly suitable for POCT applications.

7.2 Overview of the POCT system

The proposed POCT system has two key components:

(a) Actuation of magnetic particles with three dimensional electromagnetic forces and video recording.
(b) High resolution optical tracking of magnetic particles in the video

Figure 7-1 shows a schematic of the proposed POCT system. As shown in figure 7-1 (a), the system consists of an electromagnetic actuator fabricated on a silicon nitride substrate. Antigens are functionalized on to the substrate surface. Magnetic particles (Dynabeads MyOne, diameter 1µm) are functionalized with complimentary antibodies. The particles have been incubated in solutions with varying concentrations of complimentary antigens. Thus, the antibody sites on the surface of the particles occupied with antigens are not available for interacting with the substrate. These 'free' antigens thus compete with the surface for interaction with magnetic particles. The concentration of free antibodies in the solution is varied across experiments while the concentration of antigens on the substrate surface is kept constant. Vertical magnetic field (50 Gauss) promotes the interaction of the particles with the surface while horizontal dielectrophoretic forces dislodge loosely attached non-specifically bound particles from the surface. As shown in figure 7-1 (b), optical tracking reveals information about the dynamics of particles and the number of particles bound to the surface after a certain time of actuation are counted. The percentage of particles bound to the surface is indicative of the concentration of free antigens in the solution. *The antibodies used for demonstrating the proposed POCT system are streptavidin and antigens are biotin.*

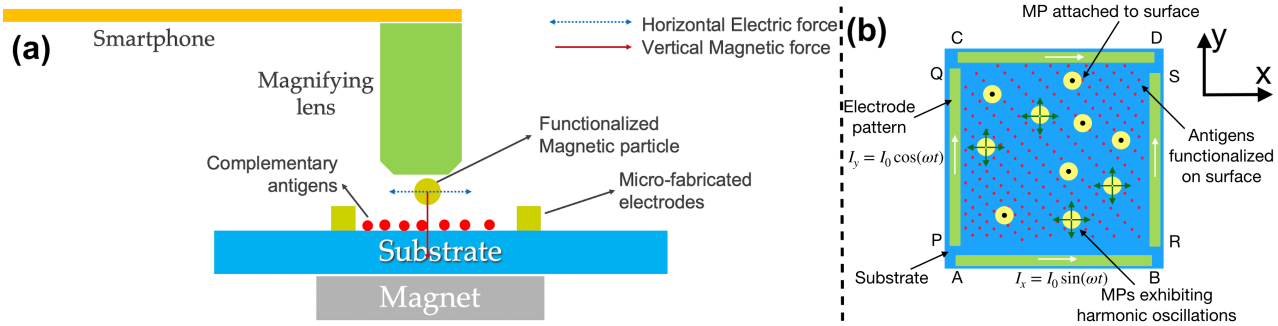

Figure 7-1. Schematic of the proposed POCT system. (a) The system consists of an electromagnetic actuator fabricated on a silicon nitride substrate. Antigens are functionalized on to the substrate and magnetic particles functionalized with complimentary antibodies are introduced on the substrate. 'Free' antigens in the solution compete with the surface for interaction with magnetic particles (competitive assay). Vertical magnetic force promotes interaction of the particles with the surface while horizontal dielectrophoretic forces dislodge loosely attached non-specifically bound particles from the surface. (b) Optical tracking reveals information about the dynamics of particles and the number of particles bound to the surface are counted. The percentage of particles bound to the surface is indicative of the concentration of free antigens in the solution.

7.2.1 Definition of the sensing area

The magnetic particles are actuated with a combination of vertical magnetic forces and horizontal dielectrophoretic forces. The design of the actuator is as presented in chapter 3. Figure 7-2 shows an image of the actuator obtained with a smartphone mounted on a microscope objective (magnification 20x, numerical aperture 0.45, please refer to section 4.5 for more details). The four straight line electrodes are clearly seen and their ends are marked as points A to D and P to S corresponding with the notation used in the schematic in figure 7-1 (b). Vertical magnetic field was applied to bring the magnetic particles to the substrate. However, horizontal forces were not applied while taking this image. We observe several thousand 1 µm particles uniformly distributed across the surface. The square region defined by the points AB-RS-DC-QP is considered as the

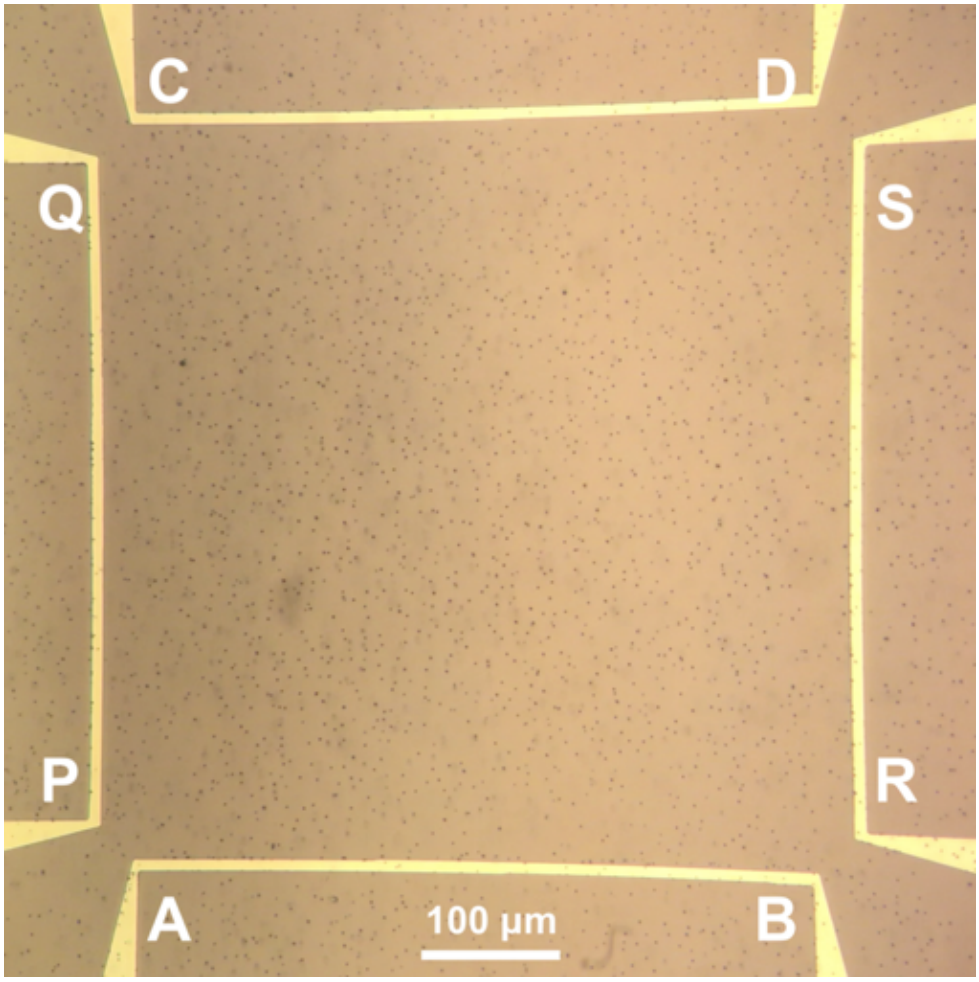

Figure 7-2. An image of the actuator and magnetic particles taken from a smartphone in the absence of electric fields. Magnetic particles of diameter 1 µm are found to be uniformly distributed across the substrate. Points A to D and P to S correspond to the schematic shown in figure 7-1 (b).

sensing area since the forces for particles within this region are nearly uniform, except at the very edges of the sensing area. *Magnetic particles outside the square sensing area are excluded from the analysis and are not counted towards the signal.* The sensing area is **560 µm x 560 µm**. This is three orders of magnitude larger than the sensing area reported for magnetic force[6] based biosensors (at equivalent currents) and an order of magnitude larger than that reported for high density magnetoresistive sensors[7]

7.2.2 Functionalization of substrate

The surface of silicon nitride can be functionalized similarly to silicon dioxide surface[8]. The substrate surface was cleaned by sonication in acetone and ethanol and was subsequently rinsed with deionized water. The surface was made hydrophilic by treating it with ozone plasma for 2 minutes. A polydimethyl siloxane (PDMS) reaction well (described in chapter 4) with a hydrophilic surface was prepared by plasma treatment as well. The reaction well was placed onto the substrate and both of them were heated at 120℃ for 10 minutes. This led to adhesion of the reaction well onto the substrate. The substrate with PDMS well attached onto it was then placed in a solution of ethanol containing 0.05% 3-Aminopropyl)triethoxysilane (APTES) by volume for 10 minutes. This was followed by baking the substrate for 15 minutes. After baking, the substrate was allowed to cool down for a few minutes and then immersed into a solution of dimethyl

sulfoxide (DMSO) solvent containing 1μM N-hydroxy-succinamide (NHS)-biotin for 1 hour. After an hour was finished, the substrate was washed twice with deionized water to remove any excess NHS-biotin not attached to the substrate.

7.2.3 Functionalization of magnetic particles

The magnetic particles provided by the manufacturer were already functionalized with streptavidin. We prepared four types of solutions of magnetic particles with varying concentrations of biotin in the solution. First, a solution, A of magnetic particles with a concentration of 2% particles by volume was prepared in deionized water. Four solutions B, C, D and E containing 20 μM, 200 nM, 2 nM and 0 nM (control) concentrations of biotin respectively were prepared. The solution A was mixed with equal volumes of B,C, D and E. Thus, 500 μL of A and 500 μL of B results in a solution with 1% streptavidin coated magnetic particles by volume and 10 μM concentration of free biotin. Similarly, for solutions C, D and E. Thus, we obtained four solutions, each containing 1% magnetic particles and 10 μM, 100 nM, 1 nM and 0 nM concentrations of free biotin. The solutions obtained were incubated in a refrigerator for 12 hours to allow the interaction of biotin with streptavidin sites on the surfaces of magnetic particles.

7.2.4 Application of current and video recording

Once the substrate was functionalized and magnetic particle solutions were prepared, the substrate was connected to a current source with the printed circuit board (PCB) and its holder as described in section 4.4. A 3 μL solution of magnetic particles was introduced into the reaction well. The PDMS reaction well was covered with a thin cover slip. Sinusoidal currents were then applied to induce forces along the x and y directions. The axis notation is as shown in figure 7-1 (b). Note that as described in chapter 3, currents applied along electrodes PQ and RS result in a force along the x direction while currents applied along electrodes AB and CD result in forces along y direction. Also, please note that the points B and C are electrically connected to each other via the PCB, with traces of very low resistance so that points B and C have almost no potential difference between them. Similarly, points Q and R are connected to each other. We applied a current of amplitude 30 mA (peak to peak amplitude 60 mA, root mean square (r.m.s.) amplitude 21 mA) at a frequency of 0.5 Hz. The currents along x and y axes had a phase difference of 90° between them. Video recording and application of currents were started simultaneously. The videos were recorded at 24 frames per second at a resolution of 2160 pixels x 3840 pixels (4K). The experiment was performed for 5 minutes.

Table 1. Splitting of experimental video

Start time ~ end time (mm:ss)	Duration (seconds)	Label
00:50 ~ 01:00	10	1m
01:50 ~ 02:00	10	2m
02:50 ~ 03:00	10	3m
03:50 ~ 04:00	10	4m
04:50 ~ 05:00	10	5m

7.2.5 Video analysis

The experimental video obtained after the previous step is 5 minutes long. Although eyehole video can be analyzed as well, experimentally we found that analyzing a few

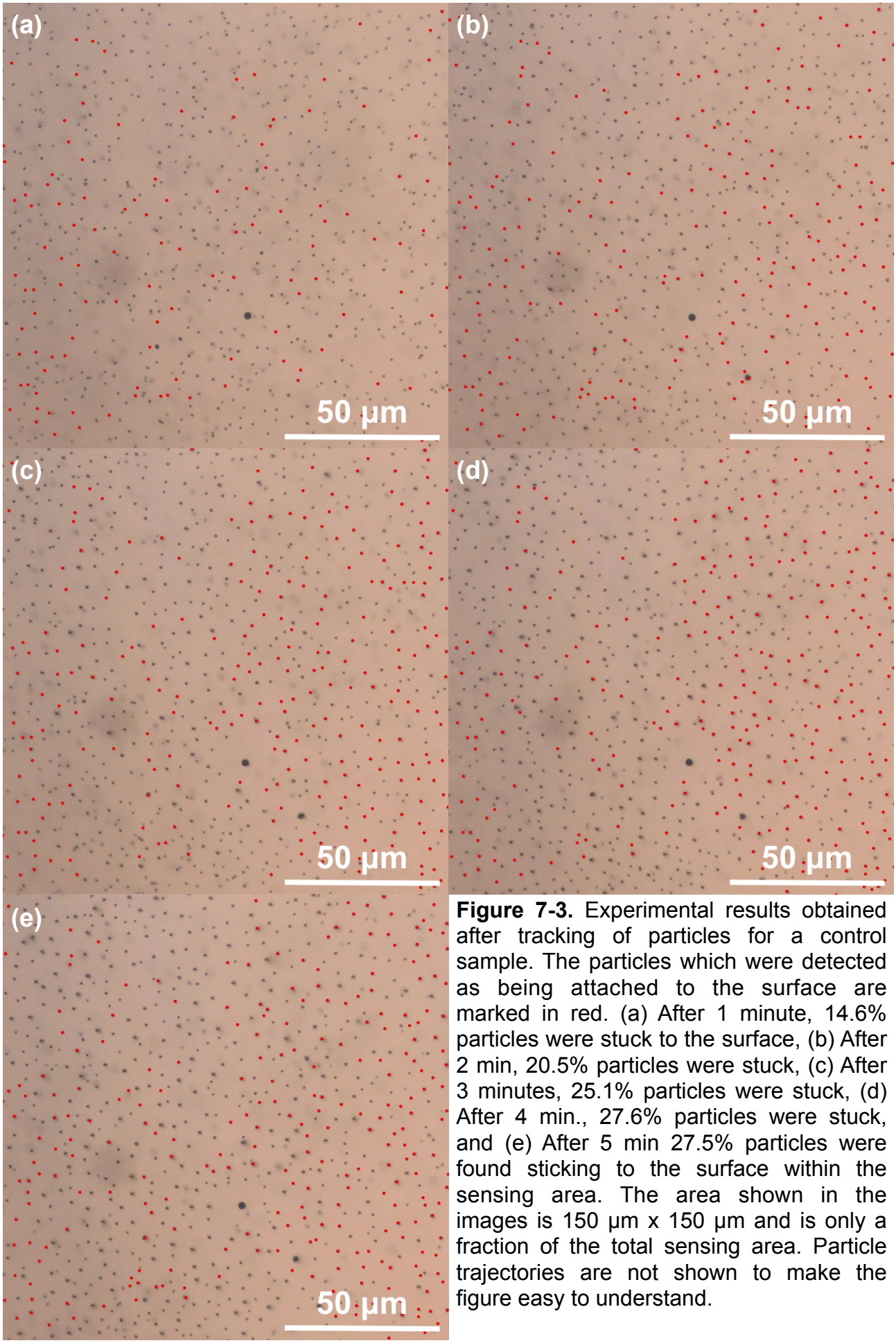

Figure 7-3. Experimental results obtained after tracking of particles for a control sample. The particles which were detected as being attached to the surface are marked in red. (a) After 1 minute, 14.6% particles were stuck to the surface, (b) After 2 min, 20.5% particles were stuck, (c) After 3 minutes, 25.1% particles were stuck, (d) After 4 min., 27.6% particles were stuck, and (e) After 5 min 27.5% particles were found sticking to the surface within the sensing area. The area shown in the images is 150 µm x 150 µm and is only a fraction of the total sensing area. Particle trajectories are not shown to make the figure easy to understand.

seconds worth of data every minute was sufficient to derive quantitative estimates of number of particles interacting with the surface. Thus, we split the video into five parts, each of duration 10 seconds as shown in table 1. The video from 50 seconds to 1 minute is labelled as '1m' and so on. The rest of the data is not used for analysis. The particles and their trajectories are then estimated by the particle tracking algorithm described in chapter 5 and the percentage of particles which stick to the surface are calculated. This is the signal used for estimating the concentration of free biotin present the solution of magnetic particles.

7.3 Quantitative detection of biotin with smartphone

The experimental steps described in the previous section led to a quantitative estimation of the fraction of magnetic particles attached to the sensing area.

Figure 7-3 shows the results obtained for the control sample (no free biotin). The entire sensing area is too large to be shown fully. If figures of the whole sensing area or the whole 4K video frames are inserted into this document, the display (or printer) will downscale the image automatically to make it compatible with the resolution of the display

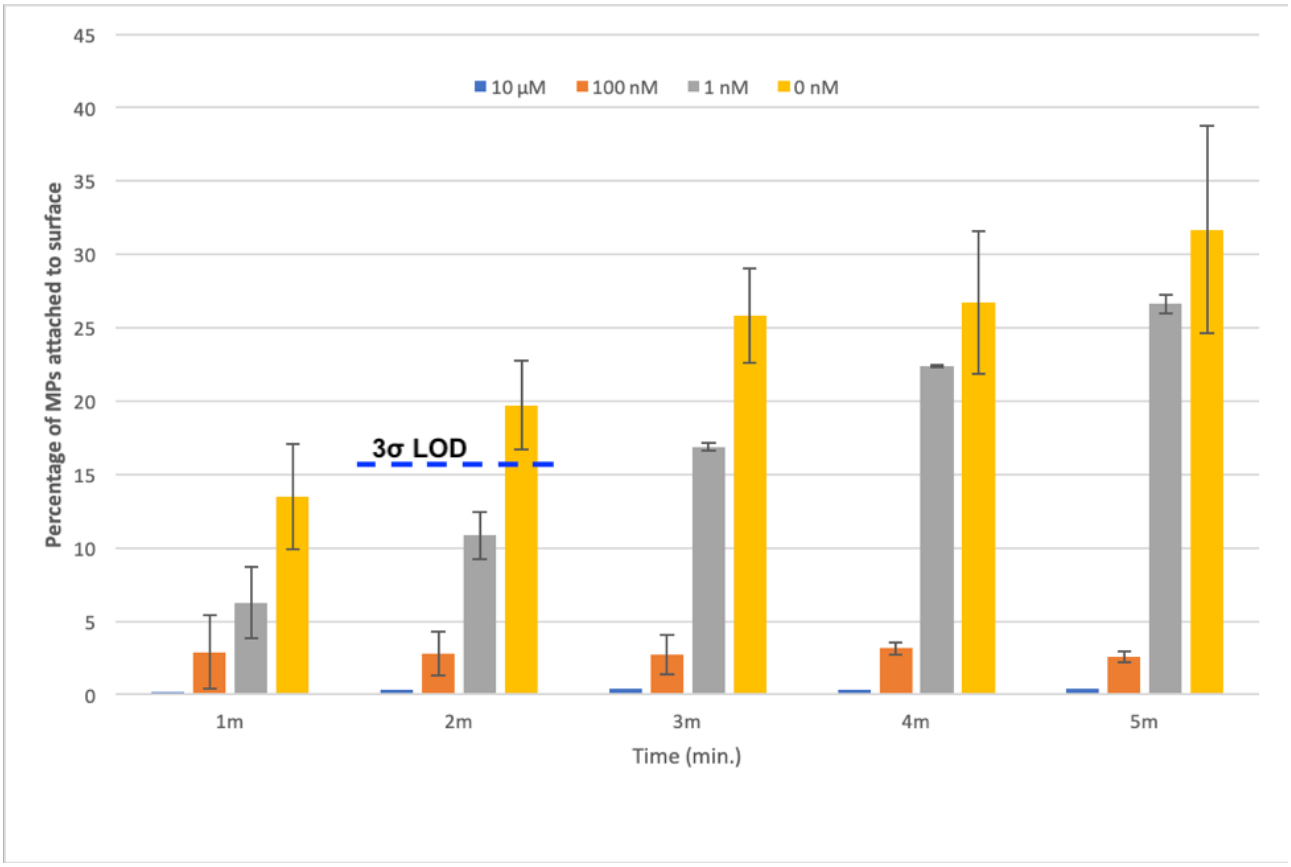

Figure 7-4. Calibration curves for detection of free biotin via a competitive assay at various times from 1 minute to 5 minutes. The vertical axis shows the percentage of particles attached to the substrate within the sensing area. Standard deviations are shown for n=3 trials. For 1 minute, the averages are close enough that the confidence intervals overlap. For 2 minutes, we see that the averages are clearly separated. The blue dashed line represents the level 3 standard deviations above the mean for 1 nM. Since this level is below the mean of the control sample, we conclude that the proposed protocol has a limit of detection of 1 nM.

(or the dots per inch of the printer). This will lead to loss of detail and make the figures difficult to understand.

Thus, we present high resolution images of the same region in the sensing area from 1 minute to 5 minutes from figure 7-3(a) to 7-3 (e). The area shown is 150 µm x 150 µm. The particles which are identified as being stuck to the surface are marked in red. It can be visually observed that the number of particles stuck to the surface increases from figure 7-3 (a) to 7-3 (b) and from 7-3 (b) to 7-3 (c). However, the particles stuck to the surface do not change significantly from figure 7-3 (c) to 7-3(e). The percentage of particles attached to the surface determined by the tracking program is 14.6% after 1 min., 20.5% after 2 min., 25.1% after 3 min, 27.6% after 4 min. and 27.5% after 5 minutes (figure 7-3(a)-(e) respectively).

This procedure was performed for all the concentration of free biotin used in this study. The resulting calibration curve for biotin detection is shown in figure 7-4. The

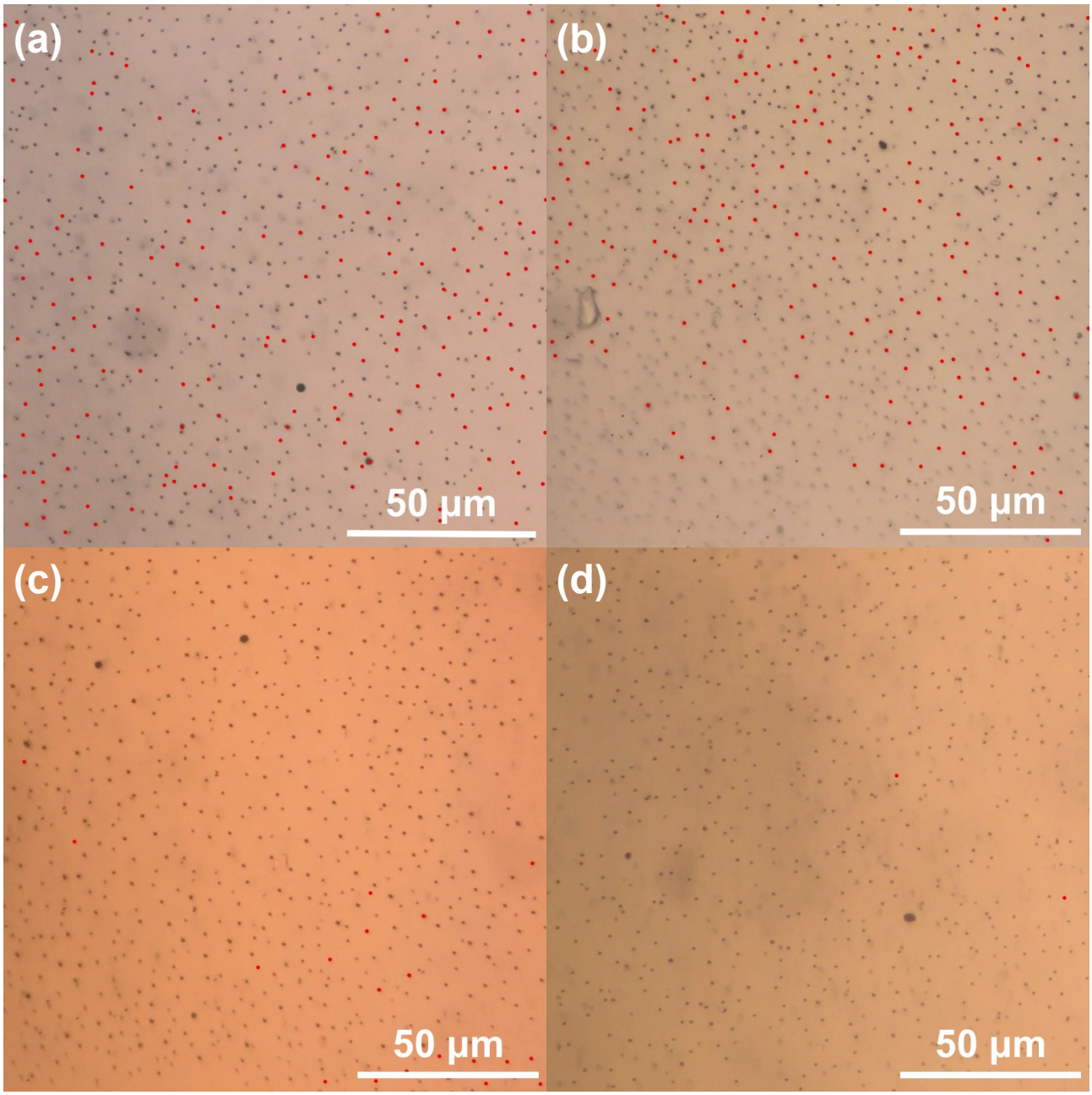

Figure 7-5. Experimental results obtained by tracking for different concentrations of free biotin (a) For control 0 nM, (b) for 1 nM, (c) for 100 nM and (d) for 10 µM. A part of the sensing area 150 µm x 150 µm is shown. Particles stuck to the surface are marked red.

standard deviations are shown for 3 trials. We note that the average percentage of particles stuck to the surface within the sensing area after 1 minute are not markedly different between 10 μM, 100 nM and 1 nM, so that confidence intervals overlap. However, after 2 minutes, we find that the averages are well separated and the confidence intervals do not overlap. The calculation of limit of detection is performed by considering 3 standard deviations away from the mean of the minimum sample concentration other than control. Since this is a competitive assay, the control sample has maximum signal as opposed to sandwich assays where the control has the minimum signal. Thus, we consider the level $\mu + 3\sigma$ for the 1nM curve. As shown by the blue dashed line in figure 7-4, the level 3 standard deviations away from the mean is below the mean for the control sample, as well as the level one standard deviation below the mean of the control sample. Thus, we conclude that the limit of detection of the proposed protocol is 1 nM for biotin and is achieved after 2 minutes of actuation of magnetic particles. Figure 7-5 shows images of the sensing area after tracking has been completed and particles stuck to the surface have been identified. These images correspond to the state of the sensing area after 2 minutes. From figure 7-5 (a) we see that a large number of particles are stuck to the surface which decreases as we move to 7-5(d). Although it is difficult to visually distinguish the difference between figure 7-5 (a) and (b) (especially since only a small part of the sensing area is shown in the figure), quantitative analysis over the complete sensing area shows that for control sample, 20.5% particles were found attached to the surface whereas for 1 nM sample, 11.8% particles were found stuck to the surface.

Thus, we have experimentally demonstrated detection of free biotin with a competitive assay by three dimensional actuation of magnetic particles over a sensing area of 560 μm x 560 μm within 2 minutes of actuation by particle tracking. In practice, the time required for tracking of videos should also be included in the procedure. When tracking is performed on a mid range computer (8 core CPU, 16 GB RAM), it takes 7 minutes to track each video of 10 seconds. Thus, the time required for obtaining the results from the beginning of the protocol is about 9 minutes. While higher sensitivities have been reported in literature up to several hundred femto molar concentrations, these sensitivities were only achievable with highly expensive and bulky equipment such as superconducting quantum interference device (SQUID) or magneto resistive sensors not optimized for point of care sensing[9].

7.4 Advantages and limitations of the proposed approach

The particle tracking based point of care testing system introduced in sections 7.1 to 7.3 has the following advantages:

- Magnetic field accelerates the interaction of the particles with the sensing surface.
- Horizontal dielectrophoretic forces applied to magnetic particles reduce their non-specific interactions with the substrate.
- Tracking of particles provides information about the nature of their interaction with the surface.
- Inference is carried out for thousands of particles and thus the results obtained are statistically significant.
- The proposed method utilizes a smartphone camera. Hence, bulky and expensive equipment is not required.
- The proposed biosensing protocol achieves a limit of detection of 1 nM in just 9 minutes which is much faster than conventional technology which may require many hours.

However, particle tracking based approaches may suffer from some limitations:

- An external magnetic field is required in this protocol. Permanent magnets need to be accurately positioned in order to apply the field of 50 gauss. Therefore, careful mechanical alignment of the substrate with an external magnet is required.
- The image quality during recording of the video should be uniformly good in order to enable accurate tracking. This presents constraints in the experimental procedure as out of focus frames or sudden mechanical motion of the camera can completely disorient the tracking program and produce inaccurate results.
- The time required for tracking of each video of 10 seconds is about 7 minutes. Thus, there is a delay in obtaining the results which may be unsuitable in many POCT scenarios where results may be needed as soon as possible.

7.5 Alternate biosensing protocols

The concept of tracking of particles in a solution can be extended to design other types of biosensing protocols. Here, we briefly introduce two other types of protocols which also use particle tracking but are different from the one described in the previous sections of this chapter.

7.5.1 Brownian motion based biosensing

It is well known that magnetic particles suspended in a liquid show brownian motion, as described analytically in chapter 3. In the previous section we discussed that particle tracking can be used to distinguish between particles exhibiting harmonic oscillations from those attached to the surface. However, the same methods can be used to distinguish particles exhibiting browning motion from those stuck to the surface. Moreover, if the particles are large in size, they tend to interact with the surface by gravitational force alone and thus a vertical magnetic force is not necessary. Thus, we propose an alternative protocol in which no actuation from either magnetic or electrostatic

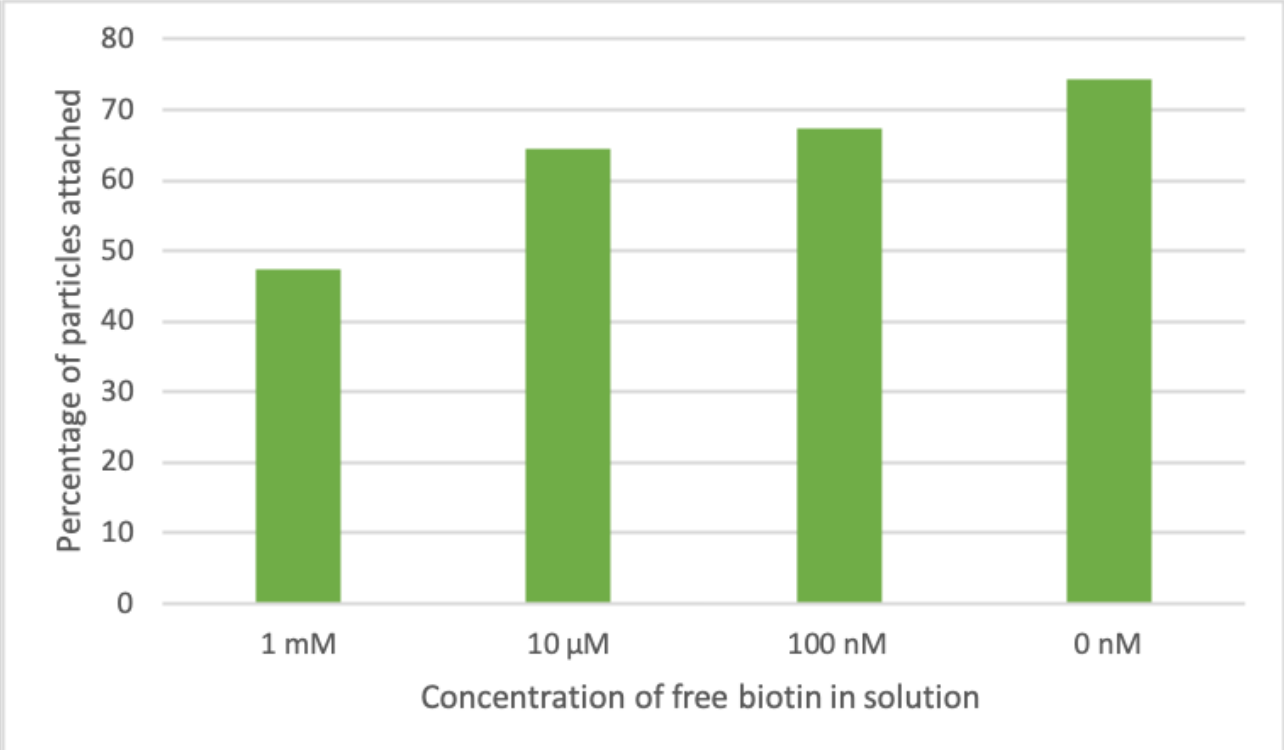

Figure 7-6. Calibration curve for streptavidin and biotin obtained from distinguishing particles showing brownian motion from particles attached to the surface.

forces is applied. The substrate is functionalized with antigens and the particles are functionalized with antibodies on which varying amounts of antigens have been functionalized, as in the previous protocol. The particles (2.8 μm) are introduced onto the substrate and are drawn to the substrate surface due to gravitational forces and interact with the substrate via specific antibody antigen interactions. A video of the substrate is recorded for 1 minute and the percentage of particles which stop exhibiting brownian motion after 1 minute are identified. This is a simple biosensing protocol as it does not require fabrication of actuators, nor a magnetic field. The particles are large and thus easy to image and track. However, since there is no mechanism for removal of non-specifically interacting particles from the substrate, this method is expected to have a much lower limit of detection than the protocol involving three dimensional electromagnetic actuation.

We performed an experiment to test this protocol for streptavidin and biotin. The particles used were Dynabeads M-280 Streptavidin. Silicon nitride substrates were functionalized with NHS-biotin (100 μM) as described in section 7.2.2, while the streptavidin coated particles were incubated with varying concentrations of biotin in order to produce a competitive effect. Particles were introduced onto the surface and allowed to interact with the surface due to gravity. No currents or magnetic fields were applied. A video of the substrate was taken for 1 minute, the motion of the particles was analyzed and the percentage of particles stuck to the surface was calculated. Some preliminary results are shown in figure 7-6. As we can see, when the concentration of free biotin is very high, about 47% particles get stuck to the surface after 1 minute. However, as the concentration of the free biotin decreases, more and more particles get attached to the surface. These results show that this method has potential to be used in cases where a binary yes/no result is required and accurate quantitative estimation of concentration of biomolecules is not required. However, these are preliminary results and more experiments need to be performed in order to ascertain the reproducibility of this method.

7.5.2 Homogenous biosensing

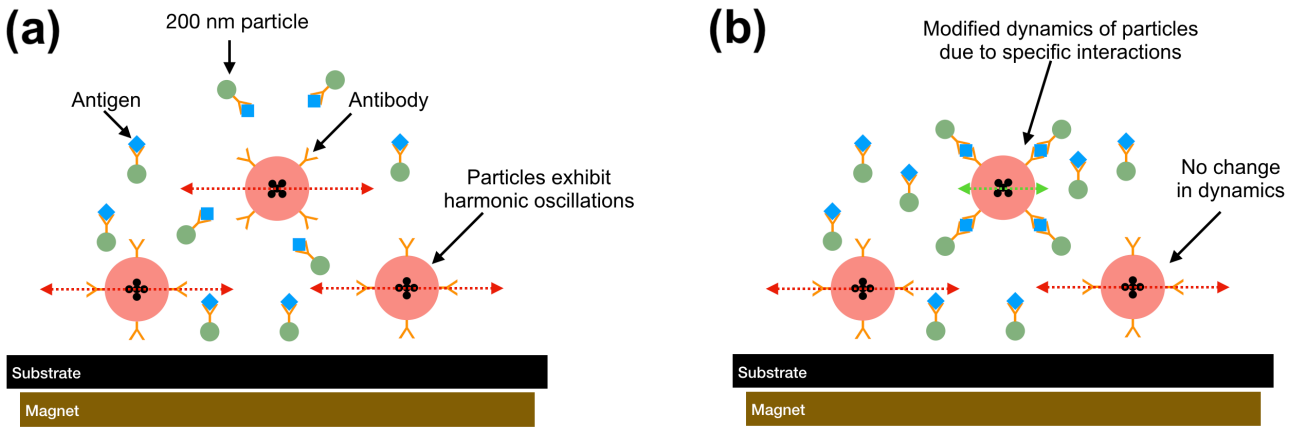

Figure 7-7. Schematic of the proposed homogenous biosensing protocol. (a) Large 1μm beads and small 200 nm beads are actuated under the influence of horizontal dielectrophoretic forces and vertical magnetic field. The particle surfaces are functionalized with complimentary antibody-antigen pairs (b) Micro meter sized particles which interact with nanometer sized particles are expected to show a change in their dynamics, such as a reduced amplitude of motion, which can be detected by optical tracking.

Homogenous biosensing protocols[10, 11] do not involve functionalization of substrates and the reaction occurs completely within a liquid solution. This simplifies the process of biosensing as the steps requiring functionalization of the substrate as well as

washing are eliminated. We build upon the discussion on particle tracking to propose a homogenous biosensing protocol based on particle tracking.

I have worked with Mr. Taisuke Ono from our research group to develop a homogenous biosensing protocol which has the following major advantages:

- Surface functionalization is not required. This considerably decreases the complexity of sample preparation and sample refrigeration.
- A vertical magnetic field is not used for actuation and only on-chip dielectrophoretic forces are used. Thus, this biosensing protocol can potentially be used with non-magnetic polystyrene particles, which have much lower cost than their magnetic counterparts.

The proposed biosensing protocol involves two sets of particles: large particles (say, 1 µm in size) functionalized with antibodies as well as small particles (say, 200 nm in size) functionalized with complimentary antigens. A solution containing both these particles is introduced onto an actuator as described in chapter 3 and dielectrophoretic forces are used to actuate the particles. The surface is not functionalized. The relative motion of the particles is expected to induce interactions between them and thus, when a biomolecular reaction occurs, the motion of the combined assembly of large and small particles is

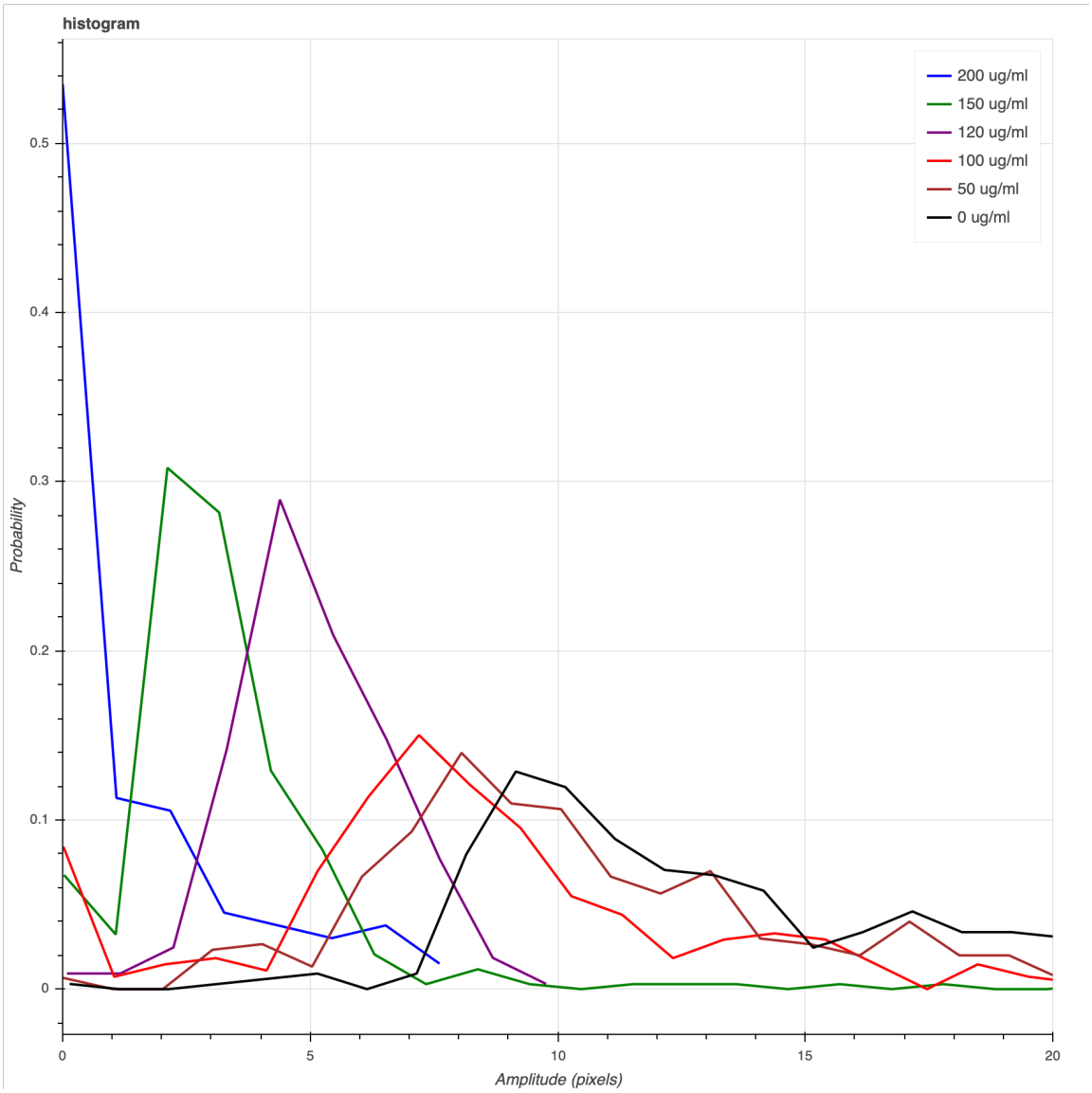

Figure 7-8. Histogram of particle amplitudes for varying concentrations of 200 nm amine particles from 0 to 200 µg/mL.

expected to have different motion characteristics from those of the large particles which do not have any interaction with complimentary biomolecules on the smaller particles. The change in the dynamics of the particles may be detected by optical tracking and may be used for quantitative detection of antigens. Figure 7-7 shows a schematic of the proposed homogenous biosensing protocol. We tested this method with 1 μm carboxyl (COOH) and 200 nm amine (NH_2) coated particles. The amine particles were not visible in an optical image whereas the carboxyl particles were clearly visible and their motion was analyzed with optical tracking software described in the previous chapter. The concentration of carboxyl particles was kept constant while the concentration of amine particles was varied from 0 to 200 μg/mL in the aqueous solution. The amplitude of motion of particles in the sensing area was obtained by curve fitting. The amplitudes of particles which were found to be oscillating were determined and the distribution of such amplitudes (histogram) was plotted. The results are shown in figure 7-8. When the concentration of complementary amine particles in the solution is low, the carboxyl particles oscillate at a high amplitude of about 9 pixels. As the concentration of mine particles increases, more and more amine particles get attached onto the surface of carboxyl particles. Thus the amplitude of motion of these particles decreases. Although these are preliminary results, homogenous biosensing protocol is much more suitable for real world applications than heterogenous biosensing protocol presented in this chapter. Thus, at our lab, we are actively developing this method at the moment.

7.6 Summary

In this chapter we introduced a point of care medical diagnostics system based on tracking the motions of thousands of magnetic particles over a large sensing area. The proposed system consists of a three dimensional actuation mechanism consisting of a vertical magnetic field (50 gauss) which accelerates the interaction of the magnetic particles with the sensing surface, and a planar actuator which applies horizontal dielectrophoretic forces to reduce non-specific interactions of the particles with the surface. We described the procedure for functionalization of the surface of the actuator, application of currents, recording of the video and analysis of the motion. We experimentally demonstrated a limit of detection of 1 nM biotin with this system in 9 minutes (2 minutes for actuation and 7 minutes for analysis of the video). Finally, we described some alternative biosensing protocols based on optical tracking of magnetic particles.

7.7 References

[1] Long, K.D., Woodburn, E.V., Le, H.M., Shah, U.K., Lumetta, S.S. and Cunningham, B.T., 2017. Multimode smartphone biosensing: the transmission, reflection, and intensity spectral (TRI)-analyzer. *Lab on a Chip*, *17*(19), pp.3246-3257.

[2] Lee, S.A. and Yang, C., 2014. A smartphone-based chip-scale microscope using ambient illumination. *Lab on a Chip*, *14*(16), pp.3056-3063.

[3] Yu, H., Tan, Y. and Cunningham, B.T., 2014. Smartphone fluorescence spectroscopy. *Analytical chemistry*, *86*(17), pp.8805-8813.

[4] Hossain, M.A., Canning, J., Ast, S., Cook, K., Rutledge, P.J. and Jamalipour, A., 2015. Combined “dual” absorption and fluorescence smartphone spectrometers. *Optics letters*, *40*(8), pp.1737-1740.

[5] Long, K.D., Yu, H. and Cunningham, B.T., 2014. Smartphone instrument for portable enzyme-linked immunosorbent assays. *Biomedical optics express*, *5*(11), pp.3792-3806.

[6] Sharma, J., Ishizawa, S., Yukino, R., Takamura, T., Hanyu, N., Yasuno, H., Handa, H. and Sandhu, A., 2016. Fast and sensitive medical diagnostic protocol based on integrating circular current lines for magnetic washing and optical detection of fluorescent magnetic nanobeads. *Sensing and bio-sensing research*, *9*, pp.7-12.

[7] Gaster, R.S., Xu, L., Han, S.J., Wilson, R.J., Hall, D.A., Osterfeld, S.J., Yu, H. and Wang, S.X., 2011. Quantification of protein interactions and solution transport using high-density GMR sensor arrays. *Nature nanotechnology*, *6*(5), p.314.

[8] Williams, E.H., Schreifels, J.A., Rao, M.V., Davydov, A.V., Oleshko, V.P., Lin, N.J., Steffens, K.L., Krylyuk, S., Bertness, K.A., Manocchi, A.K. and Koshka, Y., 2013. Selective streptavidin bioconjugation on silicon and silicon carbide nanowires for biosensor applications. *Journal of Materials Research*, *28*(1), pp.68-77.

[9] Bhuiya, A.K., Asai, M., Watanabe, H., Hirata, T., Higuchi, Y., Yoshida, T. and Enpuku, K., 2012. Characterization of magnetic markers and sensors for liquid-phase immunoassays using Brownian relaxation. *IEEE Transactions on Magnetics*, *48*(11), pp.2838-2841.

[10] Park, S.Y., Handa, H. and Sandhu, A., 2009. Magneto-optical biosensing platform based on light scattering from self-assembled chains of functionalized rotating magnetic beads. *Nano letters*, *10*(2), pp.446-451.

[11] Schrittwieser, S., Pelaz, B., Parak, W.J., Lentijo-Mozo, S., Soulantica, K., Dieckhoff, J., Ludwig, F., Guenther, A., Tschöpe, A. and Schotter, J., 2016. Homogeneous biosensing based on magnetic particle labels. *Sensors*, *16*(6), p.828.

8. Conclusion and future work

8.1 Contributions of this research

In this work, we reported the development of smartphone based point of care medical diagnostics systems utilizing magnetic particles as labels. Our work takes advantage of the tremendous improvements in smartphone cameras over the past decade driven by trends in consumer photography which have made modern smartphones capable of detecting micrometer and nanometer sized particles via light microscopy and fluorescence microscopy respectively. We build upon these capabilities fo smartphones and develop methods for actuation of magnetic particles over a large area as well as their accurate detection and tracking. In particular, we proposed two types of point of care (POCT) diagnostics systems:

8.1.1 Fluorescent magnetic particles based POCT system

Fluorescent magnetic nanoparticles (f-MNPs) are promising labels for biosensors due to their high surface area to volume ratio, magnetic and fluorescence properties. The POCT system based on f-MNPs as labels consists of three key components:

- A protocol for detection of prostate specific antigen (PSA) by fluorescent imaging of f-MNPs.
- A digital image processing algorithm for determining the concentration of PSA via fluorescent images of f-MNPs obtained with a smartphone.
- A shared ‘cloud server’ platform for performing the analysis and communicating the results to designated users.

The proposed method allowed us to achieve a limit of detection of 100 pg/mL in 2.5 minutes (30 seconds for actuation, 1 minute for washing and about 1 minute for data analysis). This is the first reported detection of PSA by a smartphone based biosensing system in less than 3 minutes.

8.1.2 Magnetic micro particles based POCT system

Magnetic micro-particles are well resolved in images obtained by light microscopy. Thus a series of images of the substrate surface taken in quick succession contains information about the dynamics of each particle which can reveal information about the interaction of particles with the sensing area. We proposed a POCT biosensing system based on magnetic micro-particles with two key components:

- A three dimensional actuation mechanism for magnetic particles which promote specific interactions and inhibits non-specific interactions simultaneously. The actuator is based on application of dielectrophoretic forces on particles, due to which the particles exhibit harmonic oscillations.
- An algorithm for high resolution optical tracking of magnetic particles in a video taken from a smartphone. The optical tracking algorithm is based on template matching for spatial localization of particles and a Kalman filter based motion model for accurate temporal association of particle trajectories across the frames of the video.

The proposed method allowed us to achieve a limit of detection of 1 nM for biotin in 9 minutes (2 minutes for actuation and 7 minutes for optical tracking). This is the first smartphone based biosensing protocol using optical tracking of magnetic particles.

8.2 Advantages and limitations of this research

Here, we present the advantages and limitation of our work for point of care testing applications.

8.2.1 Fluorescent magnetic particles based POCT system

The proposed fluorescent magnetic nanoparticle based POCT medical diagnostics system has the following advantages:

- The actuation step takes 30 seconds while the washing step takes about 1 minute. This is much faster than conventional methods and is suitable for POCT diagnostics.
- Measurements of fluorescence images can be performed independently of the washing and actuation steps in dry state after the biomolecular reaction has concluded.
- Fluorescent images are obtained with a smartphone and thus, bulky equipment is not required.
- Analysis is performed in an automated way, remotely on a cloud computer, thereby freeing the user from the task of doing the analysis.
- The results are available in about a minute on an average.
- The results are communicated to the user immediately and can also be shared with other public health officials to aggregate real time statistics on the spread of diseases in a region.
- The protocol for detection of biomarkers achieves a very low limit of detection of 100 pg/mL which is an order of magnitude lower than that required for clinically relevant detections and is comparable with other reports on detection of PSA which are not suitable for POCT applications.

However, in spite of the advantages mentioned above, the system suffers from the following limitations:

- The washing step performed in this protocol is performed manually. This can limit the reproducibility of results across users as the washing procedure may be subjective.
- The integration of the method with a cloud computer implicitly assumes that internet is always available in the locations where analysis is being performed. This is not always true for remote locations and may limit the applicability of the proposed approach in POCT medical diagnosis.

8.2.2 Magnetic micro particles based POCT system

The proposed particle tracking based point of care testing system has the following advantages:

- Magnetic field accelerates the interaction of the particles with the sensing surface.
- Horizontal dielectrophoretic forces applied to magnetic particles reduce their non-specific interactions with the substrate, thereby enhancing sensitivity of the method.
- Tracking of particles provides information about the nature of their interaction with the surface.
- Inference is carried out for thousands of particles and thus the results obtained are statistically significant.
- The proposed method utilizes a smartphone camera. Hence, bulky and expensive equipment is not required.

- The proposed biosensing protocol achieves a limit of detection of 1 nM in just 9 minutes, which is much faster than conventional technology such as ELISA which may require many hours for detection.

However, particle tracking based approaches suffers from some limitations:

- An external magnetic field is required in this protocol. Permanent magnets need to be accurately positioned in order to apply the field of 50 gauss. Therefore, careful mechanical alignment of the substrate with an external magnet is required.
- The image quality during recording of the video should be uniformly good in order to enable accurate tracking. This presents constraints in the experimental procedure as out of focus frames or sudden mechanical motion of the camera can completely disorient the tracking program and produce inaccurate results.
- The time required for tracking of each video of 10 seconds is about 7 minutes. Thus, there is a delay in obtaining the results which may be unsuitable in many POCT scenarios where results may be needed as soon as possible.

8.3 Future work

8.3.1 Near term

In the near term, the key areas of focus are the following:

- The proposed biosensing protocols need to be verified with other antibody antigen pairs than those presented in this work.
- Currently, only one type of biomolecular detection test can be performed with either of the proposed biosensing systems. However, for practical applications it is desirable to perform tests for several antibody-antigen interactions at the same time. Thus, the proposed systems need to be extended to allow multiple detections simultaneously.
- We have developed a homogenous biosensing protocol which removes the need for functionalizing surfaces as well as the need for magnetic particles. These features make the homogenous biosensing protocol very attractive for real-world use. A major focus of our research in the near term will be to further develop the homogenous biosensing protocol and verify its functioning with biomarkers of clinical relevance.

8.3.2 Intermediate to long term

In the intermediate and long term, two keywords become important, namely, A**rtificial Intelligence (AI)** and **Internet of Things (IoT)**. In the future, I envisage that most of the algorithms introduced in this work will be replaced by AI based algorithms which can process data for different protocols and account for variations among smartphone cameras resulting from a large scale deployment of the POCT systems proposed in this work. Enhanced connectivity by fifth generation (5G) mobile communication technology will enable Internet of Things (IoT) and the biosensors developed may be available to the user as an IoT device. Figure 8-1 shows the schematic of a futuristic point of care diagnostics system. The system encapsulates the biosensor as an Internet of Things (IoT) device. The IoT sensor is connected to a cloud based analysis system by high speed 5G communication. The cloud analysis system contains an Artificial Intelligence (AI) based algorithm which performs the analysis and keeps a record of the results. The results are also shared with a doctor or other healthcare professionals, as

needed. As AI based algorithms become better at analyzing data, additional features may be enabled by such systems without replacement or modification of the sensor hardware, which will become available to the user as a software upgrade, much like app updates are available for smartphones today.

I hope that the research presented in this thesis will play a role in realizing this future.

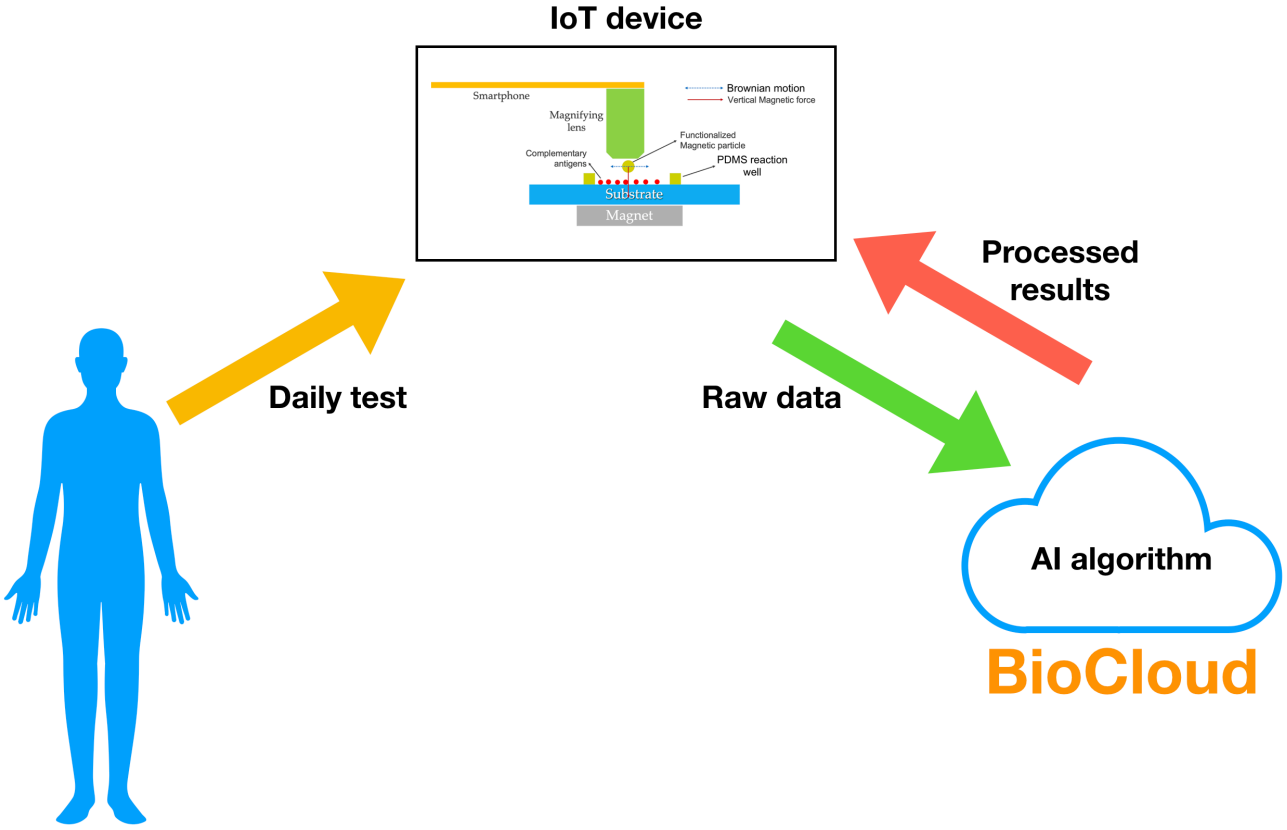

Figure 8-1. A schematic of a futuristic medical diagnostics system which encapsulates the biosensor as an Internet of Things (IoT) device. The IoT sensor is connected to a cloud based analysis system by high speed 5G communication. The cloud analysis system contains an Artificial Intelligence (AI) based algorithm which performs the analysis and keeps a record of the results. The results are also shared with a doctor or other healthcare professionals.

8.4 A library of diagnostic protocols

In this thesis, I have focused on two diagnostic protocols described in chapters 6 and 7. However, towards the end of chapter 7, I introduced two new diagnostic protocols, both based on particle tracking. Thus, overall, I have introduced four point of care diagnostic protocols based on:

- Fluorescent magnetic nanoparticles and mechanical washing (Chapter 6).
- Heterogenous biosensing method using magnetic micro particles and harmonic motion (substrate surface functionalized, sections 7.2 and 7.3)
- Potentially non-magnetic micro particles, non-magnetic nanoparticles and harmonic motion (homogenous method, section 7.5.2)
- Non-magnetic micro particle (large size) exhibiting brownian motion on a functionalized surface (brownian motion method, section 7.5.1)

Each of these methods have their strengths and limitations and together they form a 'library' of point of care diagnostic protocols which can all be performed on a smartphone. For a given real diagnostic scenario, the choice of the protocol would depend on the requirements from the test. The strengths and weaknesses of the four diagnostic protocols presented in this thesis are summarized graphically in figure 8-2.

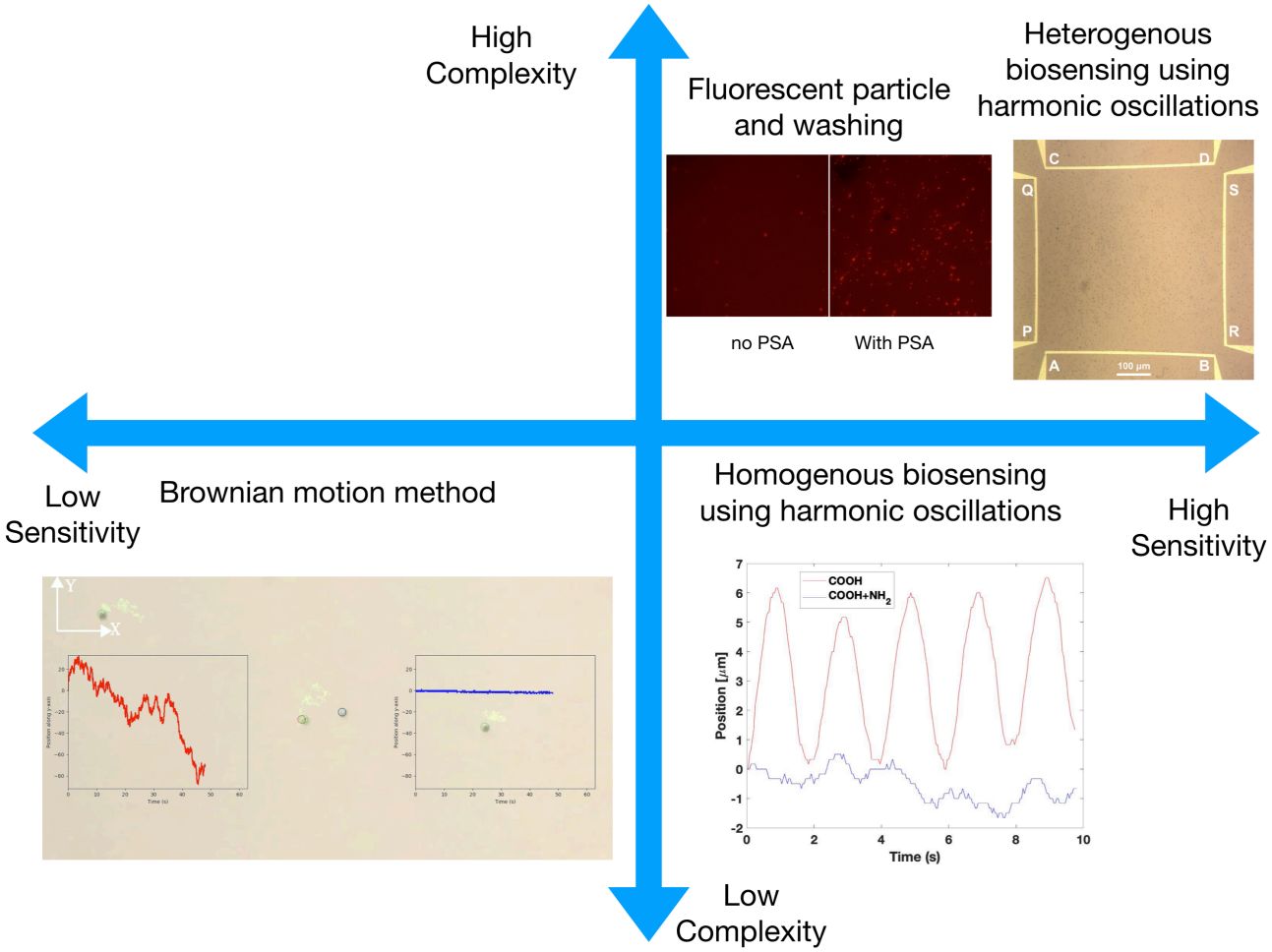

Figure 8-2. A graphical representation of the strengths and weaknesses of the four diagnostics protocols presented in this thesis

The simplest method among the four is that based on brownian motion since it does not require any electronics for actuating the particles. Large particles attach to the substrate due to gravitational force acting on the particles. However, this method is expected to have a low sensitivity. Thus, it may be suitable for simple cases where just a Yes/No result is required.

The second simplest method is one of homogenous biosensing which does not require functionalization of the substrate but does require electronics for actuation. Although more experiments are currently being performed, initial results show that this method is expected to have a high sensitivity.

The protocol using fluorescent particles and manual washing has a higher complexity than either of the above two approaches since it requires functionalization of the substrate as well as a magnet for actuation of particles. There is some added complexity arising due to the use of fluorescent particles since these particles aggregate and form clusters due to their ferromagnetic properties. However, in spite of some complexity, this protocol has very good sensitivity with a limit of detection of 100 pg/mL for PSA.

Finally, the heterogenous biosensing protocol based on harmonic oscillation of magnetic particles, described in chapter 7 has high complexity since it requires functionalization as well as electronics for actuation. This protocol also has high sensitivity.

It is important to note that although I have used the term ‘high complexity’ to describe some of these protocols, these are relative classifications and all of these protocols are much easier to use than conventional bioassays.

8.5 A new parameter for evaluating POCT technologies

Throughout this thesis and in a multitude of research papers published in the field of point of care diagnostics, the aim is to develop low-cost and portable medical diagnostics systems which can be used by unskilled personnel. The parameters researchers use to determine the suitability of a POCT technology are: limit of detection, time of assay and cost. Are these parameters enough?

Consider the following real world scenario. A POCT device is being used in a village in India by a public health worker (AWC worker introduced in Chapter 1), who is treating several children. A mature POCT device which has been proven to work in clinical settings may still fail in the hands of this worker due to the following reasons:

- The biosensing chip may fall onto the floor making the surface dirty.
- Dust may settle on the chip if it is placed in open environment even for a few minutes.
- A piece of foreign contaminant such as a piece of PDMS (polymer) may get stuck onto the sensing area of the biosensing chip.
- A magnet may be placed nearby which may not be visible in a cluttered environment.

The scenarios described above are very realistic based on my own experience as a patient at public health centers in India. When a POCT technology is deployed into the real world, many more potential sources of error will come up which researchers cannot anticipate at the moment. These sources of error are broadly of two types (a) errors due to wrong handling by the user, and (b) errors due to the harshness of the environment.

Researchers are well aware of the reasons why the errors listed above would result in unreliable measurements and that such substrates should not be used for clinical tests. However, it may not be possible to train all public health workers equally on the various ways in which such extrinsic errors may creep into the measurements and why these errors adversely affect diagnostic measurements. Conventional medical diagnostic technologies such as ELISA and SPR avoid such extrinsic errors because they are operated by professionals with years of training and because rigorous quality control standards are enforced by federal regulatory agencies on pathology laboratories. Such rigorous quality control cannot be enforced on illiterate and uneducated public health workers. Research on adoption of new innovations has shown that a lot of new technologies that offer objective benefits over older technologies fail during the early stages (of the so called ’S curve’ of technology adoption[1]) because users do not understand the nuances associated with them. For example, an intensive two-year campaign in the village of Los Molinos in Peru to convince villagers to boil water before drinking failed because villagers could not understand the concept of germs[2]. They wondered “If germs are so small that they cannot be seen or felt, how can they hurt a grown person?”. This is not an isolated case and research on diffusion of technology is filled with may such case studies. In a world where something as simple as the importance of boiling water is difficult to communicate to rural, uneducated people, can we really expect to educate public health workers coming from these backgrounds on the various

ways in which a POCT device may give erroneous results? Thus, in future, researchers working on POCT will eventually have to ask the question:

If a village woman performs a complex bioassay with our POCT device, can her results be trusted for making decisions about life and death of a patient?

I believe that the user of the device cannot be trusted to find her own errors and thus, a POCT device must be able to detect such errors *on its own in an automated fashion*. Such requirements from POCT technologies are not discussed in research papers today. However, they should be taken into account early on during the design of the technology to avoid POCT technologies from falling into the 'valley of death' after having achieved a high technology readiness level (TRL)[3]. Thus, **I propose that one of the most important parameters for evaluating a POCT technology should be whether extrinsic errors can be automatically detected**, apart from the usual parameters like sensitivity, limit of detection, time of assay and cost currently used in literature.

In this context, it is noteworthy that several leading contenders of POCT technology fall short on this parameter. Technologies such as magnetoresistive (GMR) sensors, surface plasmon resonance (SPR) sensors and diffraction grating sensors provide only a single number as their result. GMR sensors provide voltage reading, SPR and diffraction based sensors provide only reflectance curve and peak shift as output. The actual state of the sensing area which is producing those results is not directly known but is inferred from the results. Thus, out of the four realistic error scenarios listed above, GMR sensors can detect only one error when a magnet is present nearby. Other sources such as dust or polymers do not have magnetic signature and will not be detected. Similarly, SPR and diffraction grating based sensors, will not be able to detect these errors since dust particles and polymer contaminants (being several microns) are much larger than the wavelength of light being used to probe the surface.

The POCT system I have presented in Chapter 7, which involves recording a video of the sensing area directly and analyzing the dynamics of magnetic particles for several seconds, performs significantly better on this front. Any contaminant such as dust, polymer or other types of foreign substances from the environment would be directly visible in the video and thus be detected. An unwanted magnet nearby would cause a change in the dynamics of the magnetic particles from the expected harmonic oscillations and thus could also be detected. Notably, all of these detections can be automated in the cloud using object detection, semantic segmentation and anomaly detection algorithms (discussed in more detail in the next section) which are at the forefront of artificial intelligence today.

While I do not claim that all possible extrinsic errors can be detected by this system (mostly because all possible sources of such errors are not known at this stage), **the POCT diagnostics system presented in this thesis is much more suitable for real-world application than many other competing technologies** as discussed earlier. My system has this advantage because I adopted a different approach to developing POCT diagnostics by building the system around innate strengths of a smartphone rather than by miniaturizing an existing system based on conventional technology to interface with a smartphone.

8.6 The Role of Artificial Intelligence in point of care diagnostics

In chapter 5, I explained the importance of automation in point of care diagnostics. There are two ways in which automation will improve diagnostics in the future. The first way is to augment the functionality of hardware with software so that data obtained from

low cost hardware can be processed in such a way as to approximate what would have been obtained if more expensive hardware were used. A good example of this is the so called ‘super resolution’ problem in computer vision. A low cost microscope is unable to produce high quality, aberration free images like a state of the art microscope. However, if examples of images are collected from both microscopes, one can train Artificial Intelligence (AI) algorithms to produce an approximation for a high quality image from a low quality image. Thus, once such an algorithm has been trained, one can obtain high quality images from potentially very low cost microscopes. The second way in which automation, and more specifically AI can improve diagnostics is by finding statistical correlations between quantities which human experts have not found yet.

8.6.1 AI based tracking algorithm

In chapter 5, I presented an algorithm for large scale tracking of particles in a 4K video. This algorithm is based on so called ‘classical’ computer vision algorithms. There are a few limitations of classical algorithms. One of the well known limitations is that of generalization. The algorithm uses a template to identify particles in an image. When this algorithm is deployed on a large scale for many smartphones with different camera quality, a few problems will have to be resolved:

- Should we use different templates for different smartphone cameras?
- If the video is not well focused, can we still use it?
- If contaminants are present on the sensing area, can we trust that measurement?

These problems cannot be fully solved with classical computer vision algorithms as the combinations of all these factors are too numerous to be programmed individually into a system. Thus, a program which learns to adapt to cameras of varying quality, different focus levels, and which detects possible errors is required. AI algorithms are best suited to match this challenge. Here, I will present a solution which addresses the first two problems: that of different smartphones and unfocused video.

An algorithm which can detect particles from a number of different smartphones and even in unfocused videos was developed. It consists of an artificial neural network, more specifically a convolutional neural network (CNN) which performs the task of semantic segmentation[4]. **A 4K video frame is provided as input to the algorithm and it outputs a probability map of a particle distribution in the video frame**. Each pixel of the probability map has a value between 0 and 1 where 1 represents that the model is completely certain that a the pixel contains a particle. A 0 at a certain pixel position denotes that the model is certain that no particle is present at at pixel.

A 4K video frame of size 2160x3840x3 is broken down into 64 patches of size 270x480x3. This patch is padded with zeros along the first axis to create a 272x480x3 tensor. This tensor is an RGB image which is passed through a convolutional neural network whose architecture is shown in figure 8-3.

The CNN applies four convolutional layers with increasing number of filters in each layer and with a stride of 2x2 which results in downscaling of the image at each successive layer. After four convolutional layers, the tensor size is 17x30x256. From here on, I apply transposed convolution also known as devolution layers[5], with decreasing number of deconvolution filters and with a stride of 2x2, which results in upscaling of the tensor. Inspired from U-Net architecture[6], I concatenate tensors in the latter half of the network with those in the first half of the network and compatible shapes. The last deconvolution layer has 2 filters and thus outputs a 272x480x2 tensor. The first channel of this tensor is

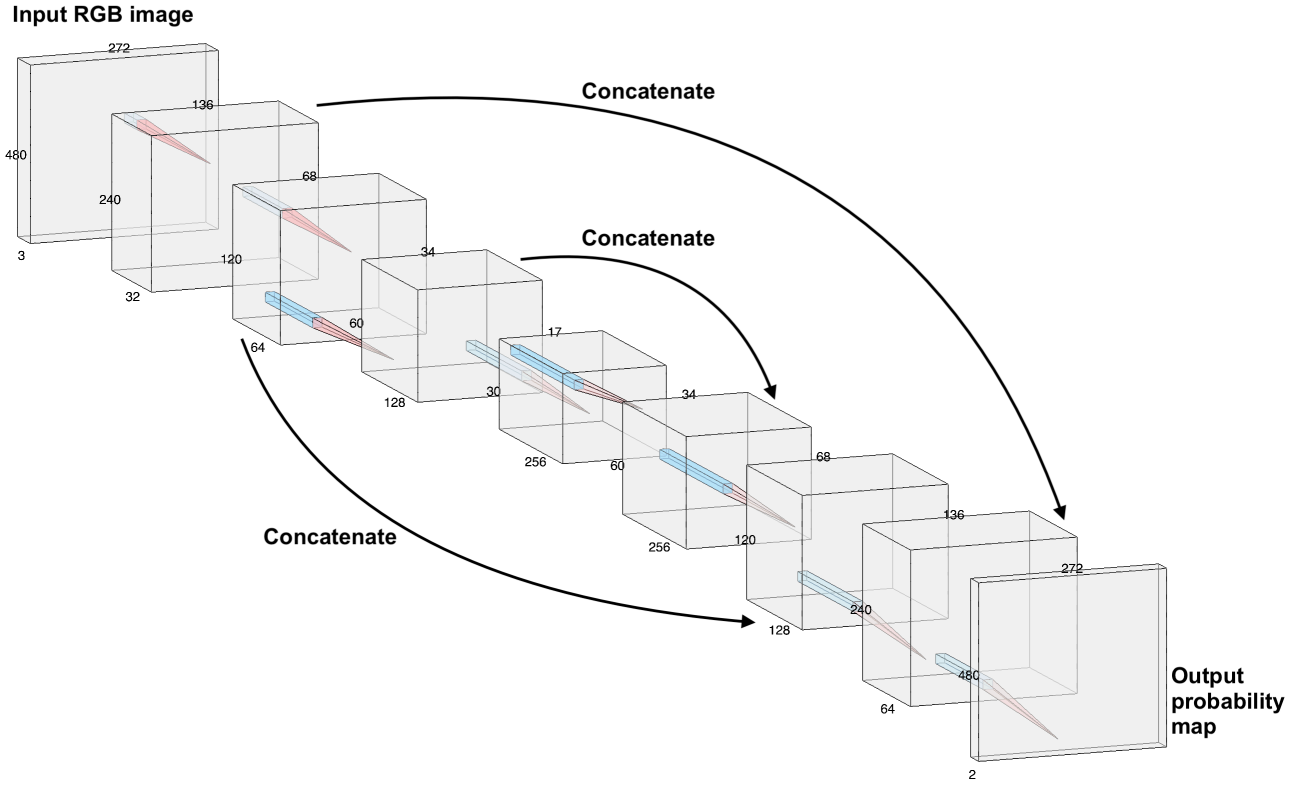

Figure 8-3. Architecture of semantic segmentation model used to detect particles in a video.

the probability that the pixel is background while the second channel is the probability that the pixel has a particle in it. Both these probabilities sum to 1 for each pixel. Depth wise separable convolutions[7] were used in the first half of the network to reduce computational cost of the network. At each layer, the x and y positions of each pixel are concatenated with the input tensor, in order to provide the network with more information about the position of the pixels. This approach is known as CoordConv[8] and has been shown to improve accuracy and intersection over union (IOU) scores for semantic segmentation models such as Faster-RCNN. The convolution and deconvolution kernels have the size 3x3 for all layers. Batch normalization[9] is used at all layers. For deconvolution layers, the batch norm is applied after concatenation. Leaky ReLu[10] activation function (with α=0.3) is used at all layers except at the last one where pixel-wise softmax is used. At the output, softmax cross-entropy loss is calculated and Adam optimizer[11] is used to train the model using the standard back-propagation algorithm. The learning rate starts initially at $5x10^{-5}$ and decays at each epoch by a factor of 2 in order to accelerate convergence of the optimizer.

Modern CNN models require vast datasets containing hundreds of thousands of images to be trained. In most domains of computer vision, large, open datasets are available to train and benchmark new algorithms[12]. However, as stated in Chapter 5, there is almost no research on computer vision algorithms for magnetic particles. Thus, the biggest hurdle in getting the AI algorithm to train is that there is no data (examples of image and corresponding probability map) to train the above neural network on. I achieved a breakthrough in this by **generating a synthetic dataset**. I extracted templates of magnetic particles from experimental data and superimposed them on frames of empty substrates which did not have any particles on them. Since the superimposition was done in software, the exact position of the particle was known. Based on this information, I generated the corresponding probability map for the image. This is a computationally expensive process. Thus, generation of synthetic data was implemented in Cython and

compiled to C code to improve the speed of execution. I used this procedure to generate about 370,000 synthetic frame patches and their corresponding probability maps. This training data was used to train the network described earlier for 5 epochs.

This method of using synthetic data works extremely well in practice. Figure 8-4 shows a synthetic frame and its corresponding probability map generated by this program. It can be seen that the synthetic frame has sharp boundaries at the edges of magnetic particles and it is clear to human observers that this is not a naturally occurring image.

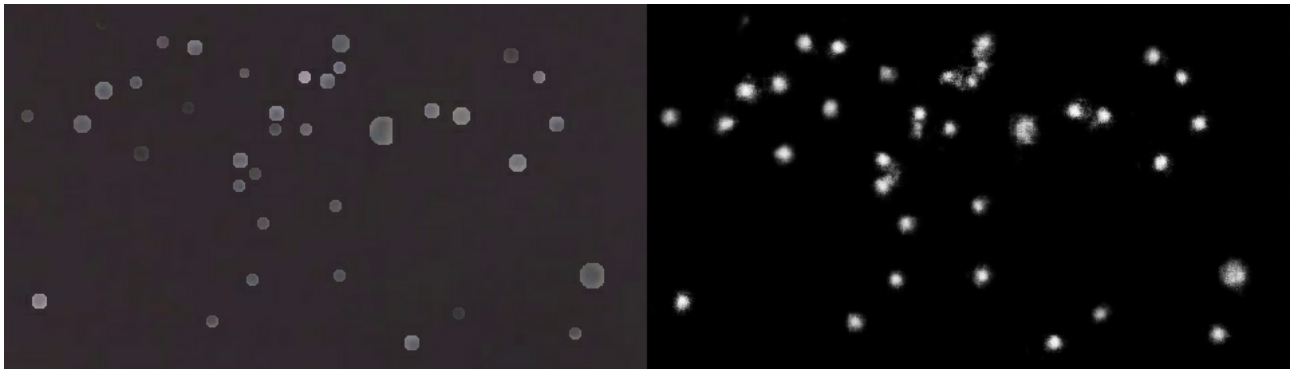

Figure 8-4 A synthetic frame patch (left) and its corresponding probability map (right) generated to train the neural network shown in figure 8-3. (bright represents high probability that a particle is present)

Even though the data used for training is artificial, the resulting trained network works very well on real videos obtained from smartphones. Figure 8-5 shows the results on some real images obtained with a smartphone. In figure 8-5 (a), a polymer contaminant in the image is ignored by the algorithm as shown in figure 8-5(b) (the output at the corresponding position is very low or dark). In figure 8-5(c), all the particles in the image are successfully detected in the output of the network shown in figure 8-5 (d). In figure 8-5(e), a prominent gold pattern is present on the substrate. This pattern is ignored by the network (figure 8-5(f)) as it has learnt from synthetic data that the presence of gold pattern does not necessarily signify the presence of magnetic particles. The particles on or near the pattern are successfully detected. There are a few important things to note from the above discussion:

- The output of the network is much cleaner than the output of the template matching algorithm (a representative example of the latter is shown in figure 5-3). Thus, a maximum a posteriori threshold of 0.5 can be used for inference in all videos regardless of the smartphone camera or image quality.
- Although in the example above, there is only one type of particle, this algorithm can easily be modified to detect several different types of particles and to automatically identify them as being different from each other. This may be useful in the future.
- The key breakthrough here is that from the perspective of the researcher, very few real images are required to train a robust segmentation network. A few frames of 4K videos contain several thousand particles which can be extracted automatically and superimposed on images of empty substrates to create several orders of magnitude more training data than what one started out with. This effectively solves the problem of lack of datasets which has hampered research into computer vision algorithms for magnetic particle research.
- As more smartphones are used for research, only a few ‘seed images’ will be required to be taken from newer smartphones to generate more training data and creating a software which adapts to a variety of smartphones and sensor characteristics.

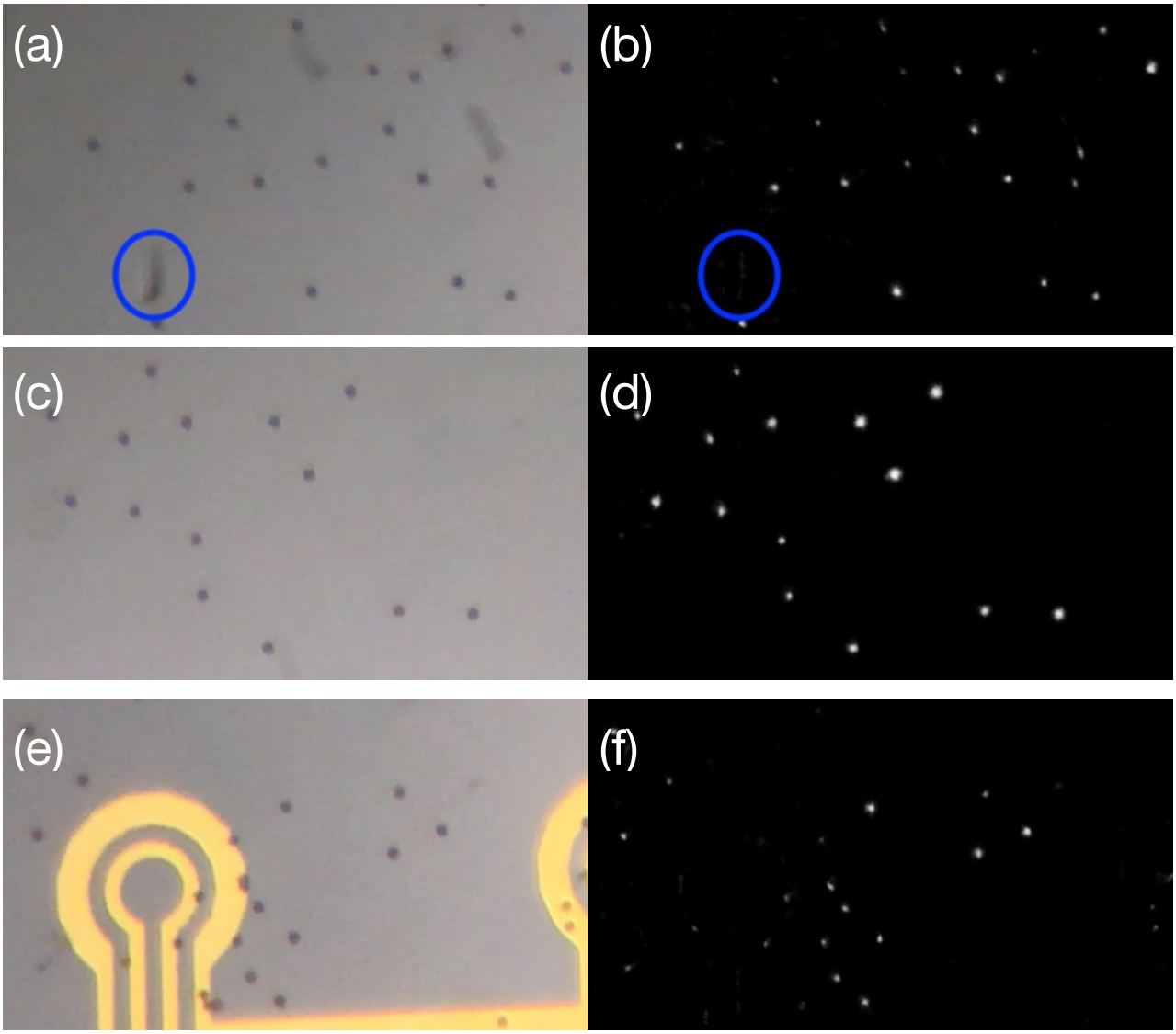

Figure 8-5. Examples of output of the neural network trained on synthetic data on real images. Left images are the inputs and right images are the predicted probability maps (bright represents high probability that a particle is present). The network has successfully learnt to distinguish noise in the images, such as the region in blue circle in (a), which commonly lead to false positives with traditional computer vision algorithms. This is one of the many advantages of deep neural networks.

As stated earlier, one of the biggest strengths of the diagnostics protocols presented in this thesis is that contaminants of any size shape and magnetic property can be detected. If enough training data is present, the semantic segmentation network can also be trained to look for such objects in the sensing area.

Although the above discussion does not include a quantitative comparison between classical algorithms and the new semantic segmentation algorithm, it serves as a starting point for training more capable AI algorithms which can handle a large number of variable conditions which are bound to occur in real-world applications. I have uploaded the program implementing the neural network described above to a repository on GitHub[13]. This code is currently private and may be open sourced in the future.

8.6.2 Looking into the eyes to find heart diseases

The rise of artificial intelligence has led to some startling discoveries in the field of medical diagnostics. Google has been working to implement AI in medical diagnostics through its life sciences division, Verily. People suffering from diabetes are at risk of going blind due to diabetic retinopathy (DR). The diagnosis for DR is usually performed by ophthalmologists (eye doctors). An image of the eye's retina, taken from a specialized camera can enable ophthalmologists to identify diseased individuals. Working with Aravind Medical Research Foundation in India, researchers at Google collected a large dataset of retinal images from a large number of patients and had them graded by ophthalmologists by severity of disease. They then used those examples to train an AI algorithm to predict the severity of the disease given the image. A convolutional neural network trained on this data achieved a high accuracy of prediction for severity of the disease and even surpassed several professional doctors[14].

Based on what I have just discussed in the previous sub-section, this is not a very surprising result on its own. However, what happened next is very interesting and holds great lessons for the future of AI in point of care diagnostics.

A young engineer joined the research team working on DR. In order to let her get familiarized with the dataset and machine learning algorithms, her supervisor gave her a toy problem of teaching an AI algorithm to predict the gender of the patient from an image of their eye. There is no research anywhere in medical literature suggesting that male and female retinas are different and thus, they expected that any algorithm would achieve a 50% accuracy (obtained by random 'male' or 'female' prediction). However, to their surprise, an AI algorithm trained on this dataset picked up small differences between the retinal images of males and females, such as, small differences between the width of veins in the retina. Rather than 50% expected by the researchers, the AI algorithm achieved an accuracy of 97%! It is important to understand the significance of this development. Throughout the history of medical research, human experts with years of training had missed some patterns among male and female retinas, which could be discovered only with the help of AI *when enough data became available to train a good algorithm*.

Eventually, the team started looking for other possible metrics which could be predicted with these retinal images. They found that they could reliably predict not only gender but also age, blood pressure, smoking status (smoker/non-smoker) and whether the patient had suffered any major cardiac events in the past. Putting all these things together, these researchers showed that it was possible to predict cardiovascular risk factors just from the images of eyes[15]. Why were these researchers able to predict such seemingly unrelated metrics from retinal images and what lessons does this hold for the future of point of care diagnostics?

From the perspective of systems biology, complex biological systems such as human bodies are extremely complicated networks of gene expressions and proteins. Within these complicated networks, it is very difficult to find causality for a given effect. However, correlations exist in plenty. Thus, the field of proteomics (the study of proteins) generally involves large scale statistical study of gene expressions (for example figure 6 of [16]) to find statistical correlations between expressions of different genes. What the researchers at Google discovered was probably a large scale manifestation of correlations between genes involved in diabetes and eye function and those involved in cardiovascular diseases.

This has important lessons for POCT. A POCT device deployed on a large scale will not only help in diagnosing diseases in people at an early stage, but also become tools for collection of so called ***big data*** about the health of large populations. Once such large scale data is collected, researchers could begin to uncover previously unanticipated correlations. For example, although biotin is not considered a serious biomarker for diseases today, it is well known that biotin deficiency in humans causes hair loss, anemia, birth defects and fungal infections[17], implying that the level of biotin in human body is correlated with these health issues although it does not have a causal relationship with these diseases. These correlative relationships have not been discovered yet since there is no large scale dataset on the level of biotin in humans and their other health parameters. The Google researchers collected data from about 280,000 patients. In future, POCT devices could enable such *large scale data collection* for biotin deficiency and the levels of biotin from such a large population could tell us more about different diseases that we cannot anticipate at the moment. Thus, just like Google researchers demonstrated testing of heart diseases from retinal images, **it might become possible one day to test for seemingly unrelated health conditions by measuring the level of biotin in a person**. I have used biotin as an example since in the previous chapter, I have presented results for detection of biotin, but, of course, such correlations could be discovered for other biomarkers as well. Such *diagnosis of correlative factors* could be the performed much more quickly than *diagnosis of causative factors*.

To summarize, in the future, point of care diagnostics will benefit significantly from advances in artificial intelligence algorithms. In turn, point of care diagnostics could accelerate the development of artificial intelligence algorithms for healthcare by enabling the curation of large datasets necessary to discover previously unanticipated correlations between various health factors.

8.7 References

[1] Christensen, C.M., 1992. Exploring the limits of the technology S-curve. Part I: component technologies. *Production and operations management*, *1*(4), pp.334-357.

[2] Rogers, E.M., 2010. Diffusion of innovations. Simon and Schuster. Chapter 1, Elements of Diffusion.

[3] The Innovation Challenge and the Valley of Death, https://www.uk-cpi.com/blog/the-innovation-challenge-and-the-valley-of-death

[4] Garcia-Garcia, A., Orts-Escolano, S., Oprea, S., Villena-Martinez, V. and Garcia-Rodriguez, J., 2017. A review on deep learning techniques applied to semantic segmentation. *arXiv preprint arXiv:1704.06857*.

[5] Dumoulin, V. and Visin, F., 2016. A guide to convolution arithmetic for deep learning. *arXiv preprint arXiv:1603.07285*.

[6] Ronneberger, O., Fischer, P. and Brox, T., 2015, October. U-net: Convolutional networks for biomedical image segmentation. In *International Conference on Medical image computing and computer-assisted intervention* (pp. 234-241). Springer, Cham.

[7] Chollet, F., 2017. Xception: Deep learning with depthwise separable convolutions. In *Proceedings of the IEEE conference on computer vision and pattern recognition* (pp. 1251-1258).

[8] Liu, R., Lehman, J., Molino, P., Such, F.P., Frank, E., Sergeev, A. and Yosinski, J., 2018. An intriguing failing of convolutional neural networks and the coordconv solution. In *Advances in Neural Information Processing Systems* (pp. 9605-9616).

[9] Ioffe, S. and Szegedy, C., 2015. Batch normalization: Accelerating deep network training by reducing internal covariate shift. *arXiv preprint arXiv:1502.03167*.

[10] Xu, B., Wang, N., Chen, T. and Li, M., 2015. Empirical evaluation of rectified activations in convolutional network. *arXiv preprint arXiv:1505.00853*.

[11] Kingma, D.P. and Ba, J., 2014. Adam: A method for stochastic optimization. *arXiv preprint arXiv:1412.6980*.

[12] Awesome Public Datasets, https://github.com/awesomedata/awesome-public-datasets

[13] Detecting magnetic beads in microscopic images, https://github.com/dataplayer12/bead_detection

[14] Gulshan, V., Peng, L., Coram, M., Stumpe, M.C., Wu, D., Narayanaswamy, A., Venugopalan, S., Widner, K., Madams, T., Cuadros, J. and Kim, R., 2016. Development and validation of a deep learning algorithm for detection of diabetic retinopathy in retinal fundus photographs. *Jama*, *316*(22), pp.2402-2410.

[15] Poplin, R., Varadarajan, A.V., Blumer, K., Liu, Y., McConnell, M.V., Corrado, G.S., Peng, L. and Webster, D.R., 2018. Prediction of cardiovascular risk factors from retinal fundus photographs via deep learning. *Nature Biomedical Engineering*, *2*(3), p.158.

[16] Hedhli, J., Konopka, C.J., Schuh, S., Bouvin, H., Cole, J.A., Huntsman, H.D., Kilian, K.A., Dobrucki, I.T., Boppart, M.D. and Dobrucki, L.W., 2017. Multimodal assessment of mesenchymal stem cell therapy for diabetic vascular complications. *Theranostics*, *7*(16), p.3876.

[17] Biotin deficiency, https://en.wikipedia.org/wiki/Biotin_deficiency#Signs_and_symptoms

Acknowledgements

I would like to acknowledge the support and guidance I received from various people, without whom this work would not have been possible.

First of all, I would like to extend my sincerest thanks to **Professor Adarsh Sandhu** under whom this research was done. Professor Sandhu provided me the opportunity to come to Japan as a graduate student, first at Toyohashi University of Technology and later on at UEC. Throughout this research, he shared his time liberally with me to brainstorm ideas, discuss strategies for future work and suggest ideas for improvement when experiments did not go well.

Next, I would like to thank Mr. Ryoji Yukino, who is an excellent friend and colleague. His knowledge of chemical aspects of functionalization helped me immensely in learning the functionalization protocols described in chapters 6 and 7.

I would like to thank colleagues, present and past: Mr. Hideki Miyashita, Mr. Taisuke Ono with whom the homogenous biosensing protocol is still being developed, Miss Kato with whom I learnt more about the dynamics of particles, especially rotating chains in a magnetic field.

I would like to extend my special thanks to Assistant Prof. Tsukasa Takamura who often went out of his way to help me when I was new to Japan and struggling with the language (which I still do).

Several people helped me while I was a student at Toyohashi University of Technology (TUT). In particular, I would like to thank Professor Makoto Ishida, who created the International Master's Program, which I entered in. I owe a debt of gratitude to Prof. Hiroshi Okada, who provided valuable insights towards the end of my Master's course. I would also like to thank Mr. Shunji Ishizawa, who went out of his way to get me acquainted with the equipment in the clean room at TUT.

Finally, I would like to extend my thanks to the staff at UEC, International student's office who helped me find a scholarship in the second year of my research and to Mr. Kato, the administrator of cleanroom at UEC who generously helps everyone in using and maintenance of cleanroom equipment.

February, 2020

Jaiyam Sharma

List of peer reviewed research papers and book chapters

Main papers

Sharma, J., Ono, T., Yukino, R., Miyashita, H., Hanyu, N., Handa, H. and Sandhu, A., 2019. Smartphone based platform for real-time sharing of medical diagnostics information by optical detection of functionalized fluorescent magnetic nanoparticles. *Biomedical Physics & Engineering Express*, *5*(3), p.035014.

(Corresponds to the contents described in chapters 5 and 6)

Sharma, J., Ono, T., and Sandhu, A., 2019. Smartphone enabled medical diagnostics by optically tracking electromagnetically induced harmonic oscillations of magnetic particles suspended in analytes, *Biosensors and Bioelectronics* (under review)

(Corresponds to the contents described in chapters 5 and 7)

Related papers

Takamura, T., Ko, P.J., **Sharma, J.**, Yukino, R., Ishizawa, S. and Sandhu, A., 2015. Magnetic-particle-sensing based diagnostic protocols and applications. *Sensors*, *15*(6), pp.12983-12998.

Sharma, J., Ishizawa, S., Yukino, R., Takamura, T., Hanyu, N., Yasuno, H., Handa, H. and Sandhu, A., 2016. Fast and sensitive medical diagnostic protocol based on integrating circular current lines for magnetic washing and optical detection of fluorescent magnetic nanobeads. *Sensing and bio-sensing research*, *9*, pp.7-12.

Yukino, R., **Sharma, J.**, Takamura, T., Joseph, J. and Sandhu, A., 2017. Magnetic nanoparticle-based nano-grating guided-mode resonance biosensors. *IEEE Transactions on Magnetics*, *54*(2), pp.1-6.

Yukino, R., Sahoo, P.K., **Sharma, J.**, Takamura, T., Joseph, J. and Sandhu, A., 2017. Wide wavelength range tunable one-dimensional silicon nitride nano-grating guided mode resonance filter based on azimuthal rotation. *AIP Advances*, *7*(1), p.015313.

Book chapters

1. **Sharma J.**, Noda K., Yukino R., Takamura T., and Sandhu A., 2018 “Magnetic Nanoparticles for Medical Diagnostics”, Chapter 8, 8-1-8-26, ISBN: 978-0-7503-1584-5, IOP Publishing, UK.

Presentations at International Conferences

1. **Sharma J.**, Yukino R., Takamura T. and Sandhu A., IRAGO Conference, 2015. "Design of an innovative smartphone based spectrometer for medical diagnostics", Poster presentation, Oct. 23, 2015, Tahara-shi, Japan (Abstract No. 00035)

2. **Sharma J.**, Yukino R., Takamura T. and Sandhu A., IRAGO Conference, 2016. "Biosensing by digital image processing based detection of fluorescent magnetic nanolabels and micro-current coils for reduction of non-specific interactions", Poster presentation, Nov. 2, 2016, Chofu-shi, Tokyo, Japan (Registration No. 136323).

3. **Sharma J.**, Yukino R., Sandhu A., "Simultaneous tracking of thousands of microbeads with a smartphone for biosensing applications,"The Irago Conference 2018, 1 November, 2018, Tokyo, Japan.

4. **Sharma J.**, Ono T., and Sandhu A., "Detection of biotin by tracking movements of functionalized magnetic particles in solution", The Irago Conference 2019, 29 October 2019, Tokyo, Japan

5. **Sharma J.**, Ono T., and Sandhu A., "Rapid biosensing protocol based on self-assembly of monolayers and magnetic particles", The Irago Conference 2019, 29 October 2019, Tokyo, Japan.

Patent applications

The patent applications were made to the Japanese patent office. Thus, the original titles of the patent applications in Japanese are shown.

(1)

Authors: Sandhu A., **Sharma J.**, Takamura T., Yukino R., Hanyu N., Yasuno K., Tanaka T. and Handa H.

Title: 磁性粒子を用いたバイオセンシング方法及び装置

Status: Granted (Patent Number 6155452)

(2)

Authors: Sandhu A., **Sharma J.**, Takamura T., Yukino R., Hanyu N., Yasuno K., Tanaka T. and Handa H.

Title: 基板上の粒子の検出装置

Status: Rejected (Application number 2016-026818)

(3)

Authors: Sandhu A., **Sharma J.**, Yukino R.

Title: センシングシステム、及びセンシング方法

Status: Under review (Reference number 18-058JP00)